TEXTE
130/2024

Final report

PINETI-4: Modelling and assessment of acidifying and eutrophying atmospheric deposition to terrestrial ecosystems

by:
Richard Kranenburg , Martijn Schaap, Peter Coenen
TNO, Utrecht

Markus Thürkow, Sabine Banzhaf
Freie Universität Berlin, Berlin

publisher:
German Environment Agency

German Environment Agency

Umwelt Bundesamt

TEXTE 130/2024

Ressortforschungsplan of the Federal Ministry for the Environment, Nature Conservation, Nuclear Safety and Consumer Protection

Project No. (FKZ) 3718 63 202 0

FB001419/ENG

Final report

PINETI-4: Modelling and assessment of acidifying and eutrophying atmospheric deposition to terrestrial ecosystems

by

Richard Kranenburg , Martijn Schaap, Peter Coenen
TNO, Utrecht

Markus Thürkow, Sabine Banzhaf
Freie Universität Berlin, Berlin

On behalf of the German Environment Agency

Imprint

Publisher
Umweltbundesamt
Wörlitzer Platz 1
06844 Dessau-Roßlau
Tel: +49 340-2103-0
Fax: +49 340-2103-2285
buergerservice@uba.de
Internet: www.umweltbundesamt.de

Report performed by:
TNO
Princetonlaan 6
3584 CB Utrecht
The Netherlands

Freie Universität Berlin
FB Geowissenschaften, Institut für Meteorologie
Carl-Heinrich-Becker-Weg 6-10
12165 Berlin

Report completed in:
January 2024

Edited by:
Section II 4.3 Air quality and terrestrial ecosystems
Alexander Moravek, Markus Geupel

Publication as pdf:
http://www.umweltbundesamt.de/publikationen

ISSN 1862-4359

Dessau-Roßlau, September 2024

Abstract: PINETI-4: Modelling and assessment of acidifying and eutrophying atmospheric deposition to terrestrial ecosystems

Biodiversity in Europe is strongly affected by atmospheric nitrogen and acid deposition to ecosystems. We present new quantitative estimates of the deposition of atmospheric nitrogen (N) and sulfur compounds to terrestrial ecosystems across Germany for the years 2000, 2005, 2010 and 2015 till 2019. On average, the nitrogen deposition in Germany has decreased from more than 19.5 kg N ha^{-1} yr^{-1} to about 14 kg N ha^{-1} yr^{-1} (which is from ~1400 eq ha^{-1} yr^{-1} to 1000 eq ha^{-1} yr^{-1}). The total deposition mapping combines three approaches: 1) chemistry transport modelling for the dry deposition, 2) geostatistical interpolation of observations for the wet deposition, and 3) a simple estimate for the occult deposition. To improve the assessment compared to earlier estimates from PINETI-3 the LOTOS-EUROS modelling was improved by including the latest information on emissions (most notably for the agricultural sector), by incorporation of dynamic emission time profiles and by increasing the horizontal (2x2 km^2) and vertical model resolutions. These implementations lead to better evaluation scores in comparison to observations and result, on average, in an approximately 10 % increased nitrogen deposition estimates compared to the PINETI-3 report. The latter is mainly driven by larger modelled fluxes for dry deposition, as a result of the updates in the emission information and the model's vertical resolution.

We also provide model-based estimates of the origin of N-deposition in each of the federal states for the year 2019. The importance of long-range transport is illustrated by the result that for all states more than 50 % of the N deposition was calculated to originate from emissions outside the state. Sensitivity simulations for surface and stack emissions of ammonia showed that within a distance of 20 km around the source about 20 % and 5 % of the total emission is deposited, respectively.

Kurzbeschreibung: Modellierung und Bewertung der versauernden und eutrophierenden atmosphärischen Deposition auf terrestrische Ökosysteme (PINETI-4)

Die Biodiversität in Europa wird durch die Deposition von Stickstoff (N) und versauernd wirkenden Verbindungen auf terrestrische Ökosysteme stark beeinflusst. Der Bericht stellt neue Berechnungen der atmosphärischen Deposition von Stickstoff- und Schwefelverbindungen auf terrestrische Ökosysteme in Deutschland für den Zeitraum 2000, 2005, 2010 und 2015 bis 2019 vor. Im Durchschnitt ist die Stickstoffdeposition in Deutschland von über 19,5 kg N ha^{-1} yr^{-1} im Jahr 2000 auf Werte von etwas über 14 kg N ha^{-1} yr^{-1} im Jahr 2019 gesunken (entspricht 1400 eq ha^{-1} yr^{-1} bzw. 1000 eq ha^{-1} yr^{-1}). Die Kartierung der Gesamtdeposition kombiniert drei Ansätze: 1) Chemie-Transportmodellierung für die trockene Deposition, 2) geostatistische Interpolation von Beobachtungen für die nasse Deposition und 3) eine einfache Schätzung für die okkulte Deposition. Um die Bewertung im Vergleich zu früheren Schätzungen aus PINETI-3 zu verbessern, wurde die LOTOS-EUROS Modellierung durch Einbeziehung der neuesten Emissionsdaten (insbesondere für die Landwirtschaft), durch Einbeziehung dynamischer Emissionszeitprofile und durch Erhöhung der horizontalen (2x2 km^2) und vertikalen Modellauflösung verbessert. Diese Implementierungen führen zu besseren Ergebnissen im Vergleich zu Messungen und ergeben im Durchschnitt etwa 10 % höhere Werte für den Stickstoffdeposition im Vergleich zu PINETI-3. Letzteres ist hauptsächlich auf größere Flüsse für die trockene Deposition zurück zu führen, die sich aus den aktualisierten Emissionsdaten und der vertikalen Auflösung des Modells ergeben.

Darüber hinaus präsentieren wir auch eine modellgestützte Bewertung der Herkunft der N-Deposition in jedem Bundesland für das Jahr 2019. Die Bedeutung des Ferntransports wird durch das Ergebnis illustriert, dass für alle Bundesländer mehr als 50 % der N-Deposition aus

Emissionen außerhalb des Landes stammen. Sensitivitätssimulationen für Ammoniak ergaben, dass für Oberflächenquellen bzw. hohe Schornsteine etwa 20 % bzw. 5 % der Gesamtemissionen innerhalb einer Entfernung von 20 km deponiert wird.

Table of content

List of figures

List of tables

List of abbreviations

ara	Arable land
Cl-	Chloride
CL	Critical Load
CLC	Corine Land Cover
CLRTAP	UNECE Convention on Long-range Transboundary Air Pollution, CLRTAP
cnf	Coniferous forest
crp	Permanent crops
CTM	Chemical-Transport-Model
dec	Deciduous forest
DEPAC	Deposition of Acidifying Compounds,
DWD	Deutscher Wetterdienst (German weather service)
ECMWF	European Centre for Medium-Range Weather Forecasts
EMEP	European Monitoring and Evaluation Programme (EMEP), see online on the Internet: URL: http://www.emep.int
eq	Acidification equivalent
FKZ	Research code of the UBA
FUB	Freie Universitat Berlin
grs	Grassland
ha	Hectare
HNO_3	Nitric acid
IfM	Institute für meteorology
MAPESI	Modelling Air Pollutants and Ecosystem Impact (research project)
mix	Mixed forest
N	Nitrogen
NH_3	Ammonia
NH_4	Ammonium
NH_x	Reduced nitrogen components
NO_2	Nitrogen dioxide
NO_3	Nitrate
NO_y	Oxidised nitrogen components
PAREST	Particle Reduction Strategies (research project)
PINETI	Pollutant Input and Ecosystem Impact, UBA project series
QAQC	Quality Assessment and Quality Control
RIVM	Dutch Institute for Public Health and Environment

RMSE	Root Mean Squared Error
S	Sulphur
sem	Semi natural vegetation
SIA	Secondary Inorganic Aerosol (SIA)
SMB	Simple Mass Balance method
SO_2	Sulphur dioxide
SO_4	Sulphate
SO_x	Oxidised sulphur compounds
UBA	German Environment Agency
urb	Urban land
yr	Year
wai	Inland water
wat	Sea water

Summary

1. Background and goals

The input of air pollutants into ecosystems poses a threat to biodiversity in Germany (Bobbink et al., 2022; Dise et al., 2011; Ströher et al., 2016). The main impact pathways are through eutrophication and acidification. Both impact pathways currently relate to reactive nitrogen inputs while the latter used to be controlled by sulphur compounds.

To assess the extent to which an ecosystem is at risk the critical load (CL) concept has been developed (Hettelingh et al., 1995). A critical load is defined as "a quantitative estimate of an exposure to one or more pollutants below which significant harmful effects on specified ecosystem do not occur according to present knowledge" (Nilsson, 1988). In the previous assessment on atmospheric inputs to ecosystems in Germany (PINETI-3) it was estimated that in 2015 about 68 % of the terrestrial ecosystems in Germany received more nitrogen than their respective critical loads for eutrophication (Schaap et al., 2018). The area of exceedance of the critical load for acidification was estimated to be much smaller (26 %). In short, a large proportion of the natural ecosystems in Germany is threatened by atmospheric deposition of nitrogen and sulphur containing compounds.

The critical load exceedance situation due to nitrogen and acid deposition is currently regulated at national (e.g. sustainability strategy of the German government) and international level (e.g. EU Thematic Strategy on Air Pollution). The proposal for a legislative package to adapt EU air pollution control policy presented by the EU-COM at the end of 2013 also mentions the reduction of air pollution inputs into terrestrial ecosystems as a key objective. The emission reductions required to achieve this are to be achieved, among others, through the NEC Directive (EU 2016/2284). In the German Sustainable Development Strategy 2016, it was agreed to reduce nutrient deposition to such an extent by 2030 that the area of sensitive ecosystem with critical load exceedances is to be reduced by 35 % compared to 2005 (Federal Government 2016).

These targets are ambitious and require significant investment in mitigation measures. The German Environment Agency (UBA) and the German Advisory Council on the Environment (SRU, 2015) recently recommended the development of a national, interdepartmental nitrogen strategy, which has been adopted by the Federal Government (Salomon et al., 2016). To support the setting of (emission) targets, several approaches concerning the development of an integrated nitrogen indicator (Geupel et al., 2021) informed by a national nitrogen budget (NNB) for Germany (Häußermann et al., 2021) are under development.

To verify compliance with the set environmental quality targets and to quantify the national nitrogen budget, current data on pollutant inputs are required. For the planning of measures to reduce the deposition and critical load exceedances more effectively, it is important to better identify the causes of exceedances. To be able to use deposition data and the critical load exceedances derived from them in Germany for legislative requirements (i.e. permitting practice according to TA Luft 4.8) or for reporting within the framework of the NEC Directive, the instruments for calculating pollutant inputs should correspond to the scientific state of the art.

National high-resolution maps on atmospheric deposition in Germany were constructed in a series of PINETI (Pollutant INput and EcosysTem Impact) projects for the UBA. The last available year for which PINETI-3 provided information was 2015. The overall goal of the PINETI-4 project was to extend the time series of nitrogen and sulphur deposition in Germany for the period 2015-2019, based on an improved mapping procedure, and to provide quantitative information on the contributions of federal states and local emissions to nitrogen deposition.

Figure 1: Schematic overview of deposition pathways for nitrogen.

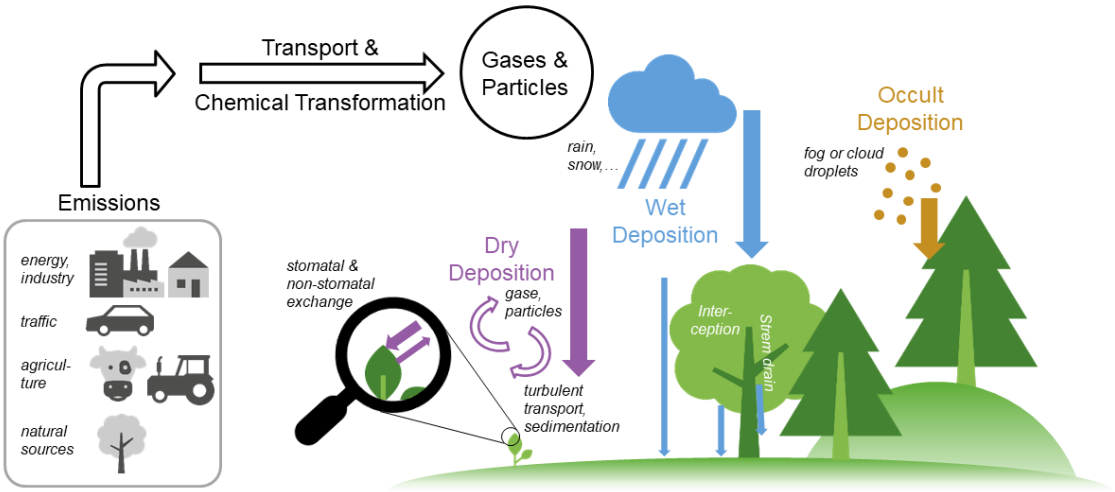

Source: German Environment Agency

To reach this goal the following objectives were defined:

1. To increase the resolution of the LOTOS-EUROS model and assess the model performance of using higher resolved meteorological data from the German Weather Service;
2. To evaluate the results of the LOTOS-EUROS model against measurements and other models;
3. To evaluate the informative value of the high-resolution results for the permitting practice for a small number of cases;
4. To quantify for each federal state the share of the nitrogen deposition caused by emissions from all federal states and neighbouring countries;
5. To extend the deposition time series for nitrogen and sulphur compounds for the years 2015 to 2019 and provide reassessments of the pillar years of 2000, 2005 and 2010 with the updated PINETII-4 methodology.

2. Methodology

The deposition of atmospheric compounds into ecosystems occurs via three pathways: dry, wet, and occult deposition. To determine the total deposition, the dry, wet and occult deposition of reduced nitrogen (NH_x), oxidized nitrogen (NO_y), and sulphur compounds (SO_x) are calculated and summed. Hence, to this end the mapping procedure consists of four calculation steps:

a) Dry deposition

Calculation of deposition and concentration fields based on meteorological data and an emission database using a chemistry transport model (Result: dry deposition for NH_x, NO_y and SO_x). Dry deposition flux measurements are currently only performed in research projects; there is no observation network for dry deposition. This means that the quantification of the dry deposition across Germany can only be performed by using a chemistry transport model. These models can be evaluated by comparing their results to e.g. observations of pollutant concentrations in air or by comparing their results to those of other models.

In this study, the LOTOS-EUROS model is used, which has a long history studying the atmospheric nitrogen and sulphur budgets. Many scientific studies have been carried out with the LOTOS-EUROS model studying secondary inorganic aerosol (Banzhaf et al., 2015;

Erisman & Schaap, 2004; Schaap et al., 2004, 2011), sea salt (Manders et al., 2010), particulate matter (Hendriks et al., 2013; Manders et al., 2009), ozone (Beltman et al., 2013; Curier et al., 2012), nitrogen dioxide (Curier et al., 2014; Schaap et al., 2013) and ammonia (Hendriks et al., 2016; Van Damme et al., 2014; Wichink Kruit et al., 2012). The model is run over Germany with a resolution of about 2x2 km^2. Crucial input data are meteorological data, land use data and the officially reported emission database. Spatial distributed emissions were provided by UBA's Gridding Emission Tool for ArcGIS (GRETA) Version 1.2.0.1 in about 1x1km^2 resolution. Meteorological data were obtained from the European Centre of Medium Range Weather Forecasting (ECMWF) as high-resolution German meteorological data are not available in a consistent manner.

b) Wet deposition

The mapping of the annual wet deposition distributions is based on observations. The interpolation of observations of measured concentrations in rain is performed using geostatistical methods, whereby the information about the spatial distribution from the chemistry transport model is also used. A wet deposition map is derived through combination with a high resolution (1x1 km^2) precipitation distribution.

c) Occult deposition

A simple approach is used to estimate occult deposition. The concentration in fog water is derived from the concentration in rainwater using empirical factors. With calculated cloud water deposition rates, the contribution of cloud water to the total deposition is calculated.

d) Total Deposition

The coarser resolution dry and occult deposition maps are projected onto the fine 1x1km^2 grid of the wet deposition. By addition of the wet, dry and occult deposition fluxes the total deposition with a spatial resolution of 1x1 km^2 is obtained.

3. Main achievements

The new estimates yield national mean total nitrogen deposition fluxes between 14 and 16.2 kg N ha^{-1} yr^{-1} (1000 and 1160 eq ha^{-1} yr^{-1}). From 2015 to 2017 total N-deposition increases from 15.1 to 16.2 kg N ha^{-1} yr^{-1} (1080 to 1160 eq ha^{-1} yr^{-1}), while the lowest values around 14 kg N ha^{-1} yr^{-1} (1000 eq ha^{-1} yr^{-1}) were estimated for 2018 and 2019. The latter is driven by lower (observed) wet deposition fluxes due to significantly less precipitation in 2018 and 2019 in comparison to earlier years and especially 2017. On average, NH_x contributes approximately 60 % to the total N deposition, while NO_y contributes for 40 %. Looking at the spatial distribution, largest depositions of nitrogen are mapped in the agricultural regions in the north-west of the country as well as in the southern part of Bavaria. For sulphur, largest values are also found in the north-west of Germany, but also regions bordering the Czech Republic have significant deposition. Sulphur deposition estimates show a similar behaviour with larger national mean values (200-225 eq ha^{-1} yr^{-1}) for 2015 to 2017 and lower values (175 eq ha^{-1} yr^{-1}) for 2018 and 2019. This is also driven by lower wet deposition. The resulting maps replace the PINETI-3 maps in the high-resolution (1x1 km^2) and nation-wide UBA GIS service.

Figure 2: Timeseries of annual average nitrogen deposition over Germany.

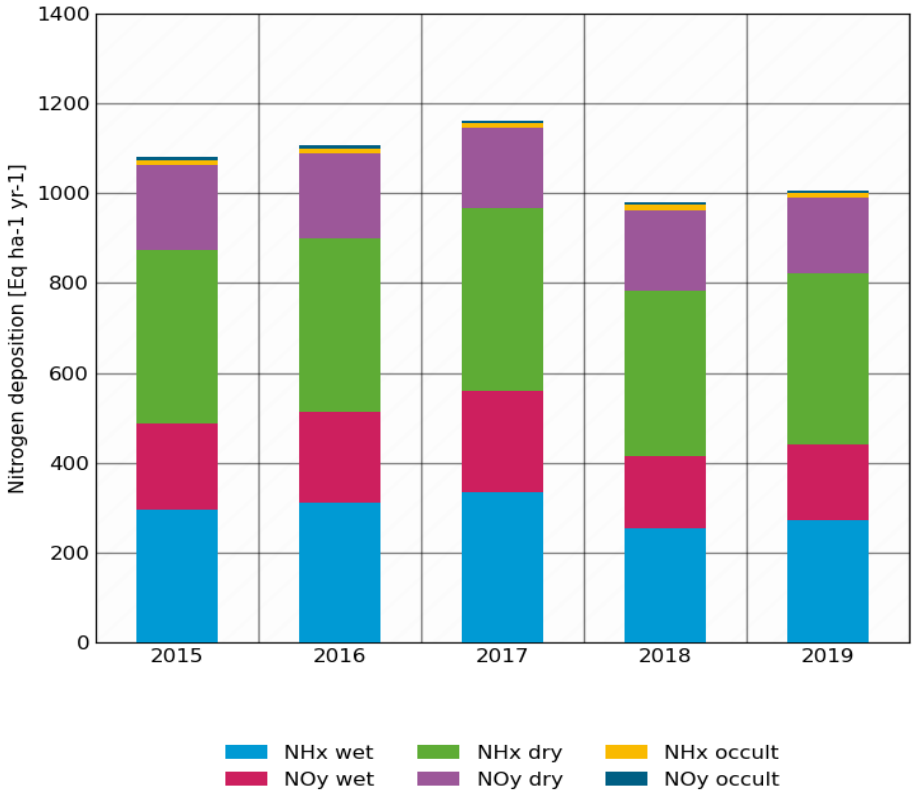

Source: This study

The mapping procedure applied in PINETI-4 was improved compared to the procedure used in PINETI-3 through updates in the LOTOS-EUROS modelling. The simulations were improved by including the newest available emission information (i.e. totals and spatial distributions; most notably for the agricultural sector), by incorporation of dynamic emission time profiles and by considerably increasing the horizontal and vertical model resolutions of the model. Due to a lack of (consistent) meteorological data at this resolution, the implementation of high-resolution meteorological data was unfortunately postponed. For 2015 it was shown that these updates have generally a positive impact on the model performance. Temporal and spatial correlations for all gaseous tracers increased or remained almost unchanged. For example, for annual mean NO_2 concentrations the spatial correlation increased from 0.57 to 0.64, whereas the average temporal correlation over all stations increased from 0.50 to 0.54. Also, the model-measurement biases and RMSE were improved for air concentrations. Largest impact was found for ozone with a mean overestimate by the model reduced from 18 µg m^{-3} to less than 5 µg m^{-3}. The systematic underestimation of wet deposition was slightly increased for NO_y and SO_x, whereas the spatial correlations increased for both. Overall, we conclude that model skill increased in comparison to PINETI-3. Nonetheless, the process of implementing and testing potential improvements of the modelling and mapping procedure is a continuous and ongoing process and ongoing activities are listed in the outlook.

Given the update in the mapping procedure, re-assessments were performed for the pillar years 2000, 2005 and 2010 using the PINETI-4 methodology and input data. On average, depositions are 12 % larger for total nitrogen and 9 % larger for total sulphur compared to the results from the previous study (PINETI-3). The differences are mainly driven by larger modelled fluxes for dry deposition, as a result of the updates in the emission information and the model's vertical resolution.

The calculation of critical load exceedances was carried out for the same years as the deposition modelling, i.e. 2000, 2005, 2010 and the years 2015 to 2019. For the critical loads, the same data as in the PINETI-3 project was used. The critical load exceedance was calculated for eutrophication using the modelled total nitrogen deposition and for acidification using the modelled total nitrogen and sulphur deposition. The course of the critical load exceedance for acidification shows the most promising trend. The area without critical load exceedance developed from around 29.6 % (2000) to around 73.9 % (2019). In the case of critical load for eutrophication, a positive trend is observed, however, the proportion of ecosystems with critical load exceedance is still high. The proportion of ecosystems without exceedances increased from around 15.7 % (2000) to around 31.5 % (2019). This means that about 68.5 % of the ecosystems analysed were still threatened by eutrophication in 2019.

By applying the source apportionment functionality of LOTOS-EUROS, we established a source attribution at state level for the first time. Hamburg and Bremen have the largest average nitrogen depositions in Germany, followed by Niedersachsen, Nordrhein-Westfalen and Schleswig-Holstein. Both Hamburg and Bremen are small city states with relatively high NO_x emission densities and are surrounded by agricultural regions. The local emissions in these states only play a limited role in the local deposition (approx. 20 %), due to their small size. Niedersachsen and Schleswig-Holstein have higher values due to their prominent agricultural sector that emits large amounts of ammonia. Even for Nordrhein-Westfalen with large emitters of nitrogen oxides deposition is dominated by NH_x. In general, an average domestic contribution of 40 % is found for these states. For all other states modelled domestic contributions are approximately 20 %. Not surprisingly, a feature with elevated contributions by neighbouring states in the east-west direction is noticed, due to preferred westerly winds. Further, considerable contributions from neighbouring countries is found, especially from countries west of Germany. The Netherlands contribute mainly in Bremen, Hamburg, Niedersachsen, Nordrhein-Westfalen and Schleswig-Holstein, while France contributes to Saarland and Baden-Wurttemberg. Contributions of Poland and Czech Republic to eastern states are more limited due to the preferential westerly winds. The result outlined above indicate that national and international efforts are required to lower the nitrogen deposition across Germany. Targeting ammonia is the most effective route to ensure domestic deposition reductions.

Figure 3: Domestic contribution to nitrogen deposition in each state in Germany. In green the domestic contribution from emissions within in the state is depicted, in blue the summed contributions from all other states and countries.

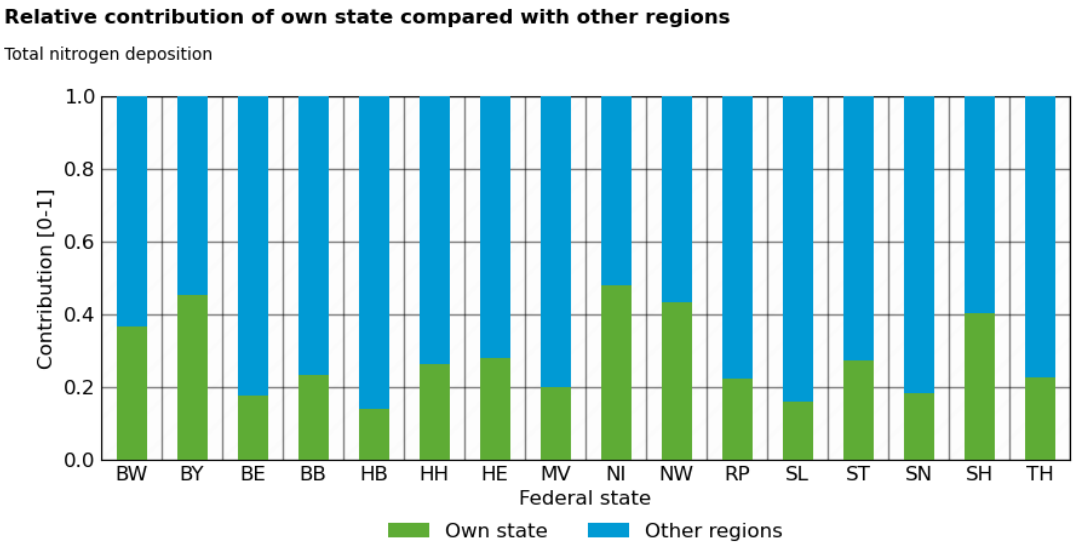

Source: This study

To assess the effect of a reduction of specific local emission sources on the modelled nitrogen deposition with the new model resolution additional scenario calculations were performed. In six counties, the emissions of a specific large point source of ammonia were reduced. Four of these sources are surface emissions and two sources have a high stack. Obviously, the reduction in the modelled deposition in the grid cell containing the source itself was considerably larger at the 2x2 km² resolution than at 7x7 km² resolution (a factor 4-5). Still, the differences are mainly present within the 7x7 km² cell as after 10 km the impact of the emission reductions was almost equal. These simulations also allowed to address the fraction of the ammonia emission deposited within a given distance to a source. To quantify the impact on the deposition independent of absolute reductions, depositions were calculated relative to the emission reduction. For the surface sources, about 18-22 % of the emitted mass is deposited within a radius of 20 km from the source. For the stack sources, the fraction of the emission deposited 20 km of the point source was calculated to be close to 5 %. Hence, for surface emissions a rule of thumb of 20 % within 20 km can be taken from these simulations, while for stack sources, this number is a factor four lower.

Figure 4: Distance dependent cumulative deposited fraction of NH_4 as a result of ammonia emission change for each of the point sources.

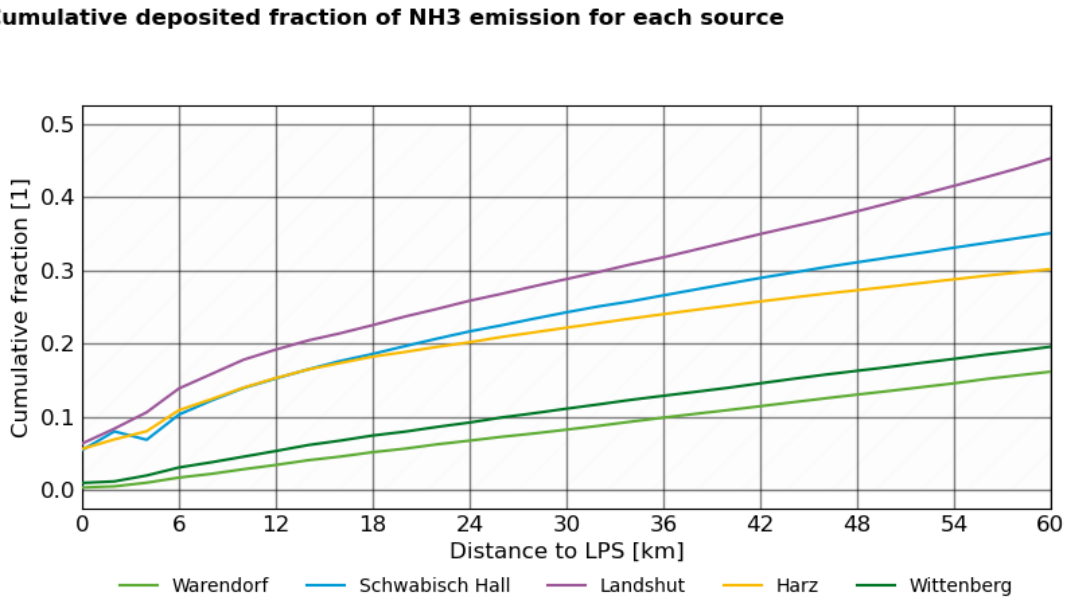

Source: This study

4. Outlook

This study describes the successful extension of the PINETI time series with a higher underlying resolution of the modelling efforts. As the modelling of nitrogen and sulphur deposition is complex and systematic differences to (variability in) observed concentrations and fluxes are observed, a constant effort is made to explore directions for improvement. It is anticipated that these ongoing development activities (when proven successful) lead to implementations to be consolidated into the operational model code of LOTOS-EUROS or the PINETI mapping procedure. Ongoing efforts aim at:

- Detailing the spatial and temporal emission variability for agriculture and other sectors;
- Application of novel satellite data on ammonia and nitrogen dioxide to evaluate emissions;
- International model evaluation and comparisons for deposition calculations;
- Expanding the number of land use categories and detailing their vegetation characteristics;
- Incorporation of improved input data on meteorology and boundary conditions

Zusammenfassung

1. Hintergrund und Ziele

Der Eintrag von Luftschadstoffen in Ökosysteme stellt eine Bedrohung für die biologische Vielfalt in Deutschland dar (Bobbink et al., 2022; Dise et al., 2011; Ströher et al., 2016). Die wichtigsten Wirkungspfade sind Eutrophierung und Versauerung. Beide Wirkungen werden durch reaktive Stickstoffeinträge verursacht, während früher hauptsächlich Schwefelverbindungen zu Versauerung führten.

Um zu beurteilen, inwieweit ein Ökosystem gefährdet ist, wurde das Konzept der ökosystemspezifischen Belastungsgrenzen entwickelt (Hettelingh et al., 1995). Eine kritische Belastungsgrenze ist definiert als "eine quantitative Schätzung der Exposition gegenüber einem oder mehreren Schadstoffen, unterhalb derer nach heutigem Kenntnisstand keine signifikanten schädlichen Auswirkungen auf ein bestimmtes Ökosystem auftreten" (Nilsson, 1988). In der vorangegangenen Bewertung der atmosphärischen Einträge in Ökosysteme in Deutschland (PINETI-3) wurde geschätzt, dass im Jahr 2015 etwa 68 % der terrestrischen Ökosysteme in Deutschland mehr Stickstoff erhielten als ihre jeweiligen Belastungsgrenzen für Eutrophierung zulassen (Schaap et al., 2018). Die Fläche, in der die Belastungsgrenzen für die Versauerung überschritten wurde, wurde auf deutlich weniger geschätzt (26 %). Kurz gesagt, ein großer Teil der natürlichen Ökosysteme in Deutschland ist durch die atmosphärische Deposition von stickstoff- und schwefelhaltigen Verbindungen bedroht.

Die Überschreitung der kritischen Belastung durch Stickstoff- und Säureeinträge wird als Indikator für Wirkungen von Luftverschmutzung und zur Bewertung von Strategien zur Verbesserung der Luftqualität sowohl auf nationaler als auch internationaler Ebene genutzt. Der Zero Pollution Action Plan der EU-KOM gibt als Ziel vor, die Anzahl der Ökosysteme mit Überschreitungen der kritischen Belastungsgrenzen bis 2030 auf 25 % zu reduzieren. Die dafür notwendigen Emissionsminderungen sollen u.a. durch die NEC-Richtlinie (EU 2016/2284) erreicht werden. In der deutschen Nachhaltigkeitsstrategie 2016 wurde festgelegt, die Stickstoffdeposition bis 2030 so weit zu reduzieren, dass die Fläche empfindlicher Ökosysteme mit Überschreitungen der Belastungsgrenzen um 35 % gegenüber 2005 verringert werden soll (Bundesregierung 2016).

Diese Ziele sind ehrgeizig und erfordern erhebliche Investitionen in Minderungsmaßnahmen. Das Umweltbundesamt (UBA) und der Sachverständigenrat für Umweltfragen (SRU, 2015) haben kürzlich die Entwicklung einer nationalen, ressortübergreifenden Stickstoffstrategie empfohlen. Um die Definition von (Emissions-)Zielen zu unterstützen, werden derzeit mehrere Ansätze zur Entwicklung eines integrierten Stickstoffindikators (Geupel et al., 2021) auf der Grundlage eines nationalen Stickstoffbudgets (NNB) für Deutschland (Häußermann et al., 2021) entwickelt.

Um die Einhaltung der gesetzten Umweltqualitätsziele zu überprüfen und das nationale Stickstoffbudget zu quantifizieren, werden aktuelle Daten über Schadstoffeinträge benötigt. Um Maßnahmen zur Verringerung der Deposition und der Überschreitung der kritischen Belastung besser planen zu können, ist es wichtig, die Ursachen der Überschreitungen besser zu erkennen. Um die Depositionsdaten und die daraus abgeleiteten Überschreitungen der Belastungsgrenzen in Deutschland für gesetzgeberische Anforderungen (z.B. Genehmigungspraxis nach TA Luft 4.8) oder für die Berichterstattung im Rahmen der NEC-Richtlinie nutzen zu können, sollten die Instrumente zur Berechnung der Schadstoffeinträge dem wissenschaftlichen Stand der Technik entsprechen.

In einer Reihe von PINETI-Projekten (Pollutant INput and EcosysTem Impact) wurden im Auftrag des Umweltbundesamtes nationale hochauflösende Karten zur atmosphärischen Deposition in Deutschland erstellt. Das letzte verfügbare Jahr, für das PINETI-3 Informationen lieferte, war 2015. Das Gesamtziel des Projekts PINETI-4 war es, die Zeitreihen der Stickstoff- und Schwefeldeposition in Deutschland für den Zeitraum 2015-2019 auf der Grundlage eines verbesserten Kartierungsverfahrens zu erweitern und quantitative Informationen über die Beiträge der Bundesländer und der lokalen Emissionen zur Stickstoffdeposition bereitzustellen.

Zur Erreichung dieser Ziele wurden die folgenden Schwerpunkte festgelegt:

1. Erhöhung der Auflösung des LOTOS-EUROS-Modells und Bewertung der Modellleistung bei Verwendung höher aufgelöster meteorologischer Daten des Deutschen Wetterdienstes;
2. Bewertung der Ergebnisse des LOTOS-EUROS-Modells im Vergleich zu Messungen und anderen Modellen;
3. Bewertung der Aussagekraft der hochaufgelösten Ergebnisse für die Genehmigungspraxis für eine kleine Anzahl von Fällen;
4. Quantifizierung des Anteils der Stickstoffdeposition, der durch Emissionen aus allen Bundesländern und Nachbarländern verursacht wird, für jedes Bundesland;
5. Ausweitung der Depositionszeitreihen für Stickstoff- und Schwefelverbindungen für die Jahre 2016 bis 2019 und Neubewertung der Stichjahre 2000, 2005, 2010 und 2015 mit der aktualisierten PINETI-4-Methodik.

2. Methodologischer Ansatz

Die Ablagerung von atmosphärischen Verbindungen in Ökosystemen erfolgt über drei Pfade: trockene, nasse und okkulte Deposition.

Abbildung 1: Schematische Darstellung der Depositionspfade von Stickstoffverbindungen

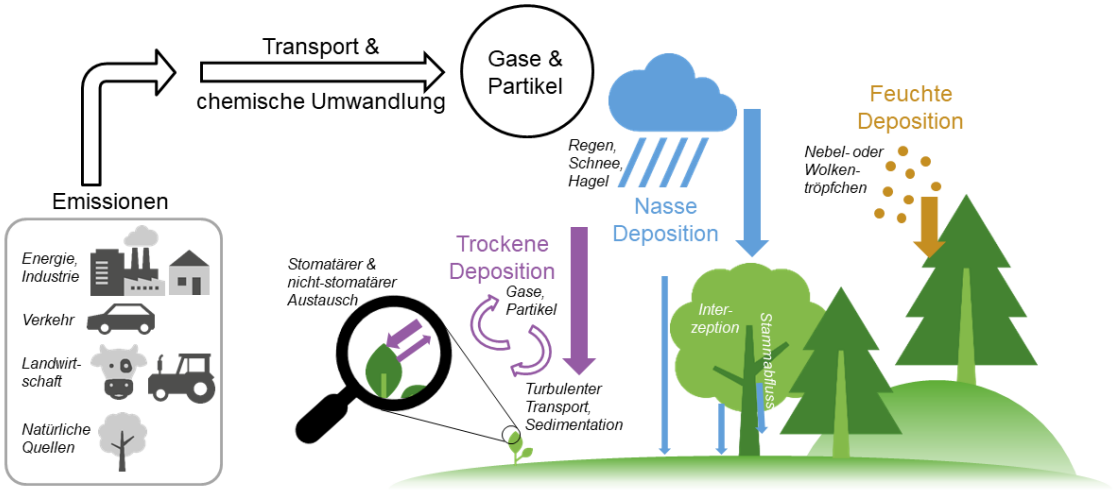

Source: German Environment Agency

Um die Gesamtdeposition zu bestimmen, werden die trockene, nasse und okkulte Deposition von NH_x, NO_y und SO_x berechnet und addiert. In dieser Studie werden zu diesem Zweck vier Berechnungsschritte durchgeführt:

a) Trockene Deposition

Berechnung von Depositions- und Konzentrationsfeldern auf der Grundlage von meteorologischen Daten und einer Emissionsdatenbank unter Verwendung eines chemischen Transportmodells (Ergebnis: trockene Deposition für NH_x, NO_y und SO_x).

Messungen der trockenen Depositionsflüsse werden derzeit nur im Rahmen von Forschungsprojekten durchgeführt; es gibt kein Beobachtungsnetz für trockene Deposition. Das bedeutet, dass die Quantifizierung der trockenen Deposition mit Hilfe eines Chemie-Transportmodells erfolgen kann. Die Güte der Modelle kann beurteilt werden indem man ihre Ergebnisse z.B. mit Beobachtungen von Schadstoffkonzentrationen in der Luft vergleicht oder indem man ihre Ergebnisse mit denen von anderen Modellen vergleicht.

In dieser Studie wird das Modell LOTOS-EUROS verwendet, das bei der Untersuchung der atmosphärischen Stickstoff- und Schwefelkreisläufe bereits bewährt hat. Viele wissenschaftliche Studien wurden mit dem LOTOS-EUROS-Modell durchgeführt, um sekundäre anorganische Aerosole (Erisman und Schaap, 2004; Schaap et al., 2004; Banzhaf et al., 2015; Schaap et al., 2011), Meeressalz (Manders et al, 2010), Feinstaub (Hendriks et al., 2013; Manders et al., 2009), Ozon (Beltman et al., 2013; Curier et al., 2012), Stickstoffdioxid (Curier et al., 2014; Schaap et al., 2013) und Ammoniak (Hendriks et al., 2016; Van Damme et al., 2014; Wichink Kruit et al., 2012) zu untersuchen.

Das Modell wird über Deutschland mit einer Auflösung von etwa 2x2 km^2 betrieben. Entscheidende Eingabedaten sind meteorologische Daten, Landnutzungsdaten und die offiziell gemeldeten Emissionsdaten. Die räumliche Verteilung der Emissionen wird aus dem UBA-Gridding Emission Tool for ArcGIS (GRETA) Version 1.2.0.1 in einer Auflösung von circa 1x1km^2 bereitgestellt. Meteorologische Daten wurden vom Europäischen Zentrum für mittelfristige Wettervorhersage (ECMWF) bezogen.

b) Nasse Deposition

Die Berechnung der Nassdepositionsfelder basiert auf Beobachtungen. Durch Interpolation von Ergebnisse gemessener Konzentrationen im Regen wird mit geostatistischen Methoden ein flächendeckendes Depositionsfeld für Deutschland erstellt, wobei die Informationen über die räumliche Verteilung aus dem Chemietransportmodell auch für NH_x, NO_y und SO_x verwendet werden. Mit hochauflösenden Daten für die Niederschlagsverteilung (1x1km^2) wird eine Karte für die nasse Deposition erzeugt.

c) Okkulte Deposition

Zur Schätzung der okkulten Deposition wird ein heuristischer Ansatz verwendet. Die Konzentration im Nebelwasser wird mit Hilfe empirischer Faktoren von der Konzentration im Regenwasser abgeleitet. Mit den berechneten Ablagerungsraten des Nebelwassers wird der Beitrag des Nebelwassers zur Gesamtablagerung berechnet.

d) Gesamtdeposition

Die Karten der trockenen und okkulten Deposition werden in das feine 1x1km^2-Gitter der nassen Deposition transformiert. Die Addition der nassen, trockenen und okkulten Depositionsflüsse führt zu der Gesamtdeposition mit einer räumlichen Auflösung von 1x1 km^2.

Abbildung 2: Zeitreihe der durchschnittlichen jährlichen Stickstoffdeposition über Deutschland

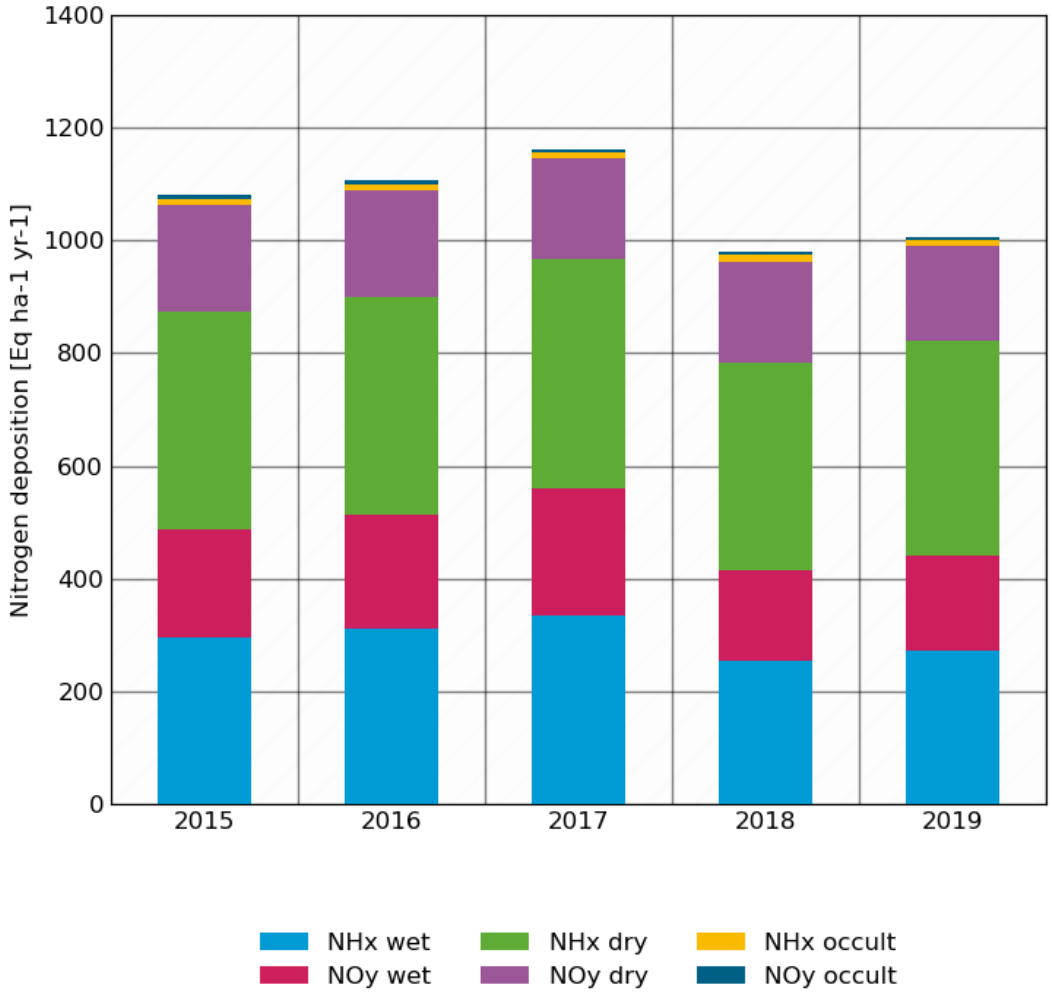

Source: This study

3. Hauptergebnisse

Die neuen Berechnungen ergeben nationale mittlere Gesamtstickstoffdepositionsflüsse zwischen 14,1 und 16,2 kg N ha^{-1} yr^{-1} (1000 und 1160 eq ha^{-1} yr^{-1}). Von 2015 bis 2017 steigt die gesamte N-Deposition von 15,1 auf 16,2 kg N ha- yr^{-1} (1080 auf 1160 eq ha^{-1} yr^{-1}), während die niedrigsten Werte um 14 kg N ha^{-1} yr^{-1} (1000 eq ha^{-1} yr^{-1}) für 2018 und 2019 berechnet wurden. Letzteres ist auf niedrigere (beobachtete) nasse Depositionsflüsse zurückzuführen, da 2018 und 2019 deutlich weniger Niederschlag fiel als in den Vorjahren und insbesondere 2017. Im Durchschnitt trägt NH_x etwa 60 % zur gesamten N-Deposition bei, während NO_y 40 % ausmacht. Betrachtet man die räumliche Verteilung, so werden die größten Stickstoffdepositionen in den landwirtschaftlich geprägten Regionen im Nordwesten des Landes sowie im südlichen Teil Bayerns kartiert. Bei Schwefel sind die größten Werte ebenfalls im Nordwesten Deutschlands zu finden, aber auch die an die Tschechische Republik angrenzenden Regionen weisen erhebliche Depositionen auf. Die Schwefeldepositionsschätzungen zeigen ein ähnliches Verhalten mit größeren nationalen Mittelwerten (200-225 eq ha^{-1} yr^{-1}) für 2015 bis 2017 und niedrigeren Werten (175 eq ha^{-1} yr^{-1}) für 2018 und 2019. Dies ist auch auf die geringere nasse Deposition zurückzuführen. Die resultierenden Karten ersetzen die PINETI-3-Karten im hochauflösenden (1x1 km^2) und Kartendienst zur Stickstoffhintergrundbelastung des UBA.

Das in PINETI-4 angewandte Kartierungsverfahren wurde im Vergleich zu dem in PINETI-3 verwendeten Verfahren durch Aktualisierungen der LOTOS-EUROS-Modellierung verbessert.

Die Simulationen wurden durch die Einbeziehung der neuesten verfügbaren Emissionsinformationen (d.h. nationale Gesamtmenge und deren räumliche Verteilungen; insbesondere für den landwirtschaftlichen Sektor), durch die Einbeziehung dynamischer Emissionszeitprofile und durch eine beträchtliche Erhöhung der horizontalen und vertikalen Modellauflösung des Modells verbessert. Aufgrund eines Mangels an (konsistenten) meteorologischen Daten in dieser Auflösung wurde die Implementierung von hochauflösenden meteorologischen Daten leider verschoben. Für 2015 konnte gezeigt werden, dass sich diese Aktualisierungen generell positiv auf die Modellleistung auswirken. Die zeitlichen und räumlichen Korrelationen für alle gasförmigen Komponenten nahmen zu oder blieben nahezu unverändert. So stieg beispielsweise die räumliche Korrelation für die jährlichen mittleren NO_2-Konzentrationen von 0,57 auf 0,64, während die durchschnittliche zeitliche Korrelation über alle Stationen von 0,50 auf 0,54 anstieg. Auch die systematischen Unterschiede zwischen Modell und Messung und der RMSE wurden für die Luftkonzentrationen verbessert. Die größte Auswirkung wurde für Ozon festgestellt, wobei die mittlere Überschätzung durch das Modell von 18 µg m^{-3} auf weniger als 5 µg m^{-3} reduziert wurde. Die systematische Unterschätzung der nassen Deposition wurde bei NO_y und SO_x leicht erhöht, während die räumliche Korrelation zunahmen. Insgesamt kommen wir zu dem Schluss, dass die Modellperformance im Vergleich zu PINETI-3 zugenommen hat.

Angesichts der durchgeführten Aktualisierung der Methodik wurden für die Stichjahre 2000, 2005, 2010 und 2015 unter Verwendung der PINETI-4-Methode und der Eingabedaten Neubewertungen durchgeführt. Im Durchschnitt sind die neuen Berechnungen für Gesamtstickstoff um 12 % und für Gesamtschwefel um 9 % höher als die Ergebnisse der vorherigen Studie (PINETI-3). Die Unterschiede sind hauptsächlich auf größere modellierte Flüsse für die trockene Deposition zurückzuführen, die sich aus den aktualisierten Emissionsdaten und der Detailierung der vertikalen Auflösung des Modells ergeben.

Die Berechnung der Critical Load Überschreitungen erfolgte für dieselben Jahre wie die Depositionsmodellierung, d.h. 2000, 2005, 2010 und die Jahre 2015 bis 2019. Für die Critical Loads wurden der gleiche Datensatz wie in PINETI-3 verwendet. Die Critical Load Überschreitungen für Eutrophierung wurden mit der modellierten Gesamtstickstoffdeposition und für Versauerung mit der Stickstoff- und Schwefeldeposition berechnet. Die Critical Load Überschreitungen für Versauerung haben in dem untersuchten Zeitraum deutlich abgenommen. So stieg die Anzahl der Flächen ohne Critical Load Überschreitung von 29,6 % (2000) auf 73,9 % (2019) an. Für den Critical Load für Eutrophierung ist auch eine Verbesserung zu verzeichnen, allerdings ist der Anteil der Ökosysteme mit Critical Load Überschreitungen noch hoch. Der Anteil der Ökosysteme ohne Überschreitungen stieg von rund 15,7 % (2000) auf rund 31,5 % (2019). Das bedeutet, dass im Jahr 2019 noch etwa 68,5 % der analysierten Ökosysteme von Eutrophierung bedroht waren.

Durch die Anwendung der Quellenzuordnungsfunktionalität von LOTOS-EUROS haben wir zum ersten Mal eine Quellenzuordnung auf Länderebene vorgenommen. Hamburg und Bremen weisen die höchsten durchschnittlichen Stickstoffdepositionen in Deutschland auf, gefolgt von Niedersachsen, Nordrhein-Westfalen und Schleswig-Holstein. Sowohl Hamburg als auch Bremen sind kleine Stadtstaaten mit relativ hohen NO_x-Emissionsdichten und sind von landwirtschaftlichen Regionen umgeben. Die lokalen Emissionen in diesen Bundesländern spielen aufgrund ihrer geringen Größe nur eine begrenzte Rolle bei der Deposition auf Landesebene (ca. 20 %). Niedersachsen und Schleswig-Holstein weisen aufgrund ihrer ausgeprägten Landwirtschaft, die große Mengen an Ammoniak emittiert, höhere Werte auf. Selbst in Nordrhein-Westfalen mit großen Stickoxidemittenten wird die Deposition durch NH_x dominiert. Im Allgemeinen wird für diese Bundesländer ein eigener Beitrag von 40 % ermittelt.

Für alle anderen Bundesländer liegen die modellierten eigenen Beiträge bei etwa 20 %. Es überrascht nicht, dass aufgrund der bevorzugten Westwinde ein erhöhter Beitrag der Nachbarstaaten in Ost-West-Richtung festzustellen ist. Darüber hinaus gibt es beträchtliche Beiträge aus den Nachbarländern, insbesondere aus den Ländern westlich von Deutschland. Die Niederlande tragen hauptsächlich in Bremen, Hamburg, Niedersachsen, Nordrhein-Westfalen und Schleswig-Holstein bei, während Frankreich im Saarland und in Baden-Württemberg einen signifikanten Beitrag leistet. Die Beiträge Polens und der Tschechischen Republik zur Deposition in den östlichen Bundesländern sind aufgrund der bevorzugten Westwinde relativ geringer. Die oben dargestellten Ergebnisse zeigen, dass nationale und internationale Anstrengungen erforderlich sind, um die Stickstoffdeposition in Deutschland zu verringern. Eine gezielte Minderung von Ammoniakemissionen ist der wirksamste Weg, um die Depositionsminderung in Deutschland zu gewährleisten.

Abbildung 3: Beitrag zur Stickstoffdeposition in jedem Bundesland in Deutschland. In Grün der Beitrag des eigenen Bundeslandes, in blau die Beiträge aller anderen Staaten und Länder.

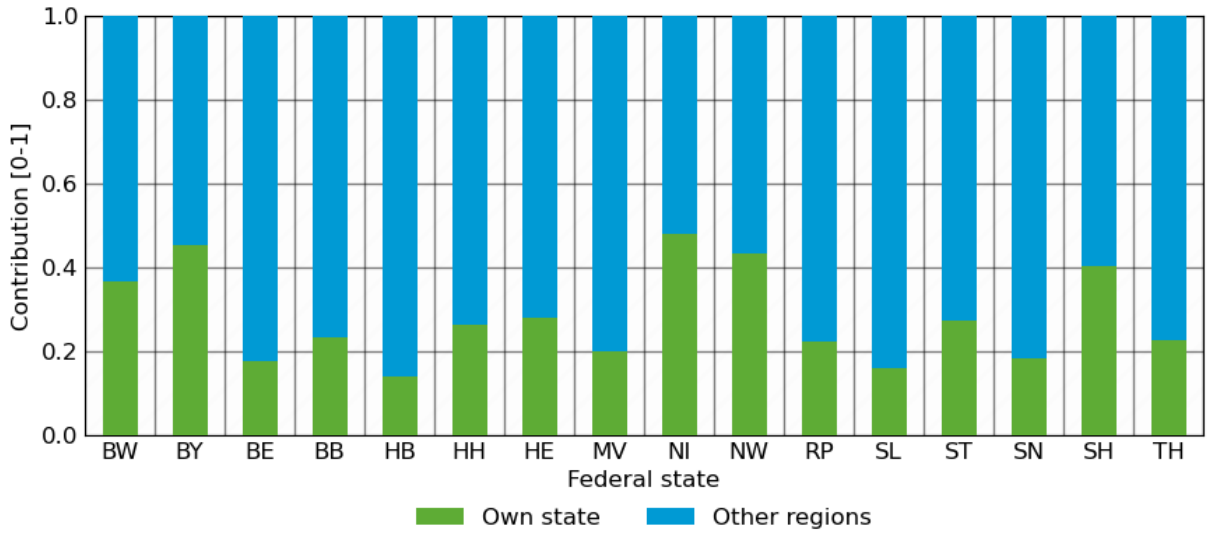

Source: This study

Um die Auswirkungen der Reduzierung bestimmter lokaler Emissionsquellen auf die modellierte Stickstoffdeposition zu bewerten, wurden zusätzliche Berechnungen durchgeführt. In sechs Kreise wurden die Emissionen einer bestimmten großen Punktquelle für Ammoniak reduziert. Bei vier dieser Quellen handelte es sich um Oberflächenemissionen und zwei Quellen haben einen hohen Schornstein. Offensichtlich war die Verringerung der modellierten Deposition in der Gitterzelle, in der sich die Quelle selbst befindet, bei einer Auflösung von 2x2 km² erheblich größer als bei einer Auflösung von 7x7 km² (Faktor 4-5). Dennoch sind die Unterschiede hauptsächlich innerhalb der 7x7 km²-Zelle vorhanden, da nach 10 km die Auswirkungen der Emissionsminderungen fast gleich waren. Diese Simulationen ermöglichten es auch, den Anteil der Ammoniakemissionen zu bestimmen, der sich in einer bestimmten Entfernung zu einer Quelle deponiert. Um die Auswirkungen auf die Deposition unabhängig von den absoluten Reduktionen zu quantifizieren, wurden die Depositionen relativ zur Emissionsreduktion berechnet. Bei den Oberflächenquellen werden etwa 18-22 % der emittierten Masse innerhalb einer Entfernung von 20 km deponiert. Für die Schornsteinquellen wurde berechnet, dass dieser Anteil nahe bei 5 % liegt. Daher kann für Emissionen nahe der

Oberfläche eine Deposition von 20 % bis 20 km Entfernung abgeleitet werden, während diese Zahl für Schornsteinquellen um den Faktor 4 niedriger ist.

Abbildung 4: Entfernungsabhängiger kumulativer deponierter Anteil von NH_4 als Folge der Änderung der Ammoniakemissionen für jede der Punktquellen.

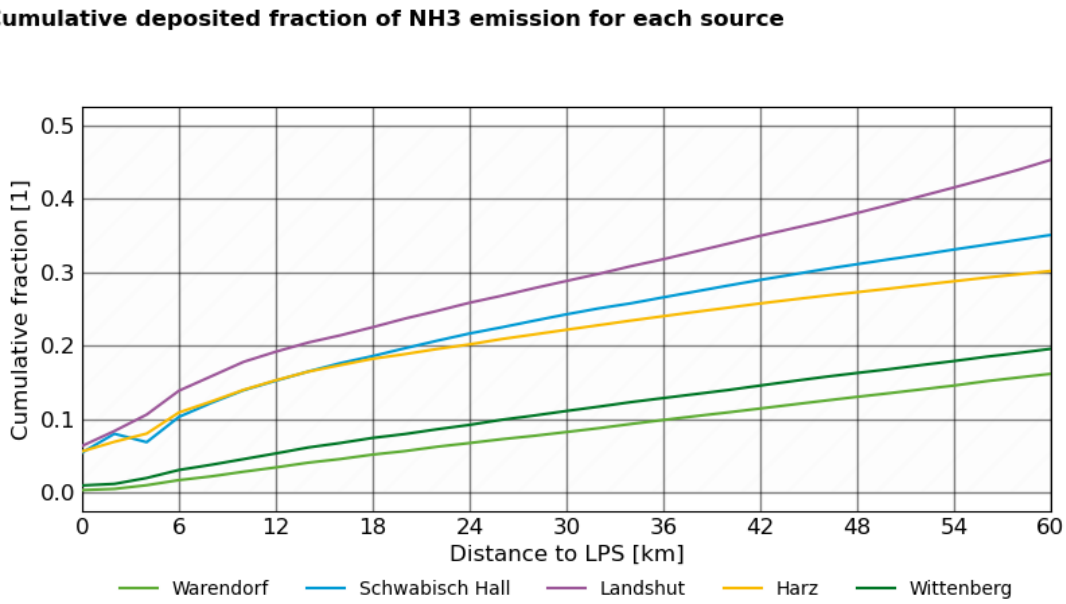

Source: This study

4. Ausblick

Diese Studie beschreibt die erfolgreiche Erweiterung der PINETI-Zeitreihen mit einer höheren zugrunde liegenden Auflösung der Chemietransportmodellierung. Da die Modellierung der Stickstoff- und Schwefeleinträge komplex ist und systematische Unterschiede zu den beobachteten Konzentrationen und Flüssen (bzw. deren Variabilität) zu beobachten sind, werden ständig Verbesserungsmöglichkeiten untersucht. Es wird erwartet, dass laufenden Entwicklungsaktivitäten (wenn sie sich als erfolgreich erweisen) zu Implementierungen führen, die in den operationellen Modellcode von LOTOS-EUROS oder das PINETI-Kartierungsverfahren integriert werden können. Die laufenden Entwicklungsaktivitäten zielen auf Folgendes ab:

- Detaillierung der räumlichen und zeitlichen Emissionsvariabilität für die Landwirtschaft und andere Sektoren;
- Anwendung neuer Satellitendaten von Ammoniak und Stickstoffdioxid zur Bewertung der Emissionen;
- Internationale Modellevaluierung und -vergleiche für Depositionsberechnungen;
- Erweiterung der Anzahl von Landnutzungskategorien und detaillierte Beschreibung ihrer Vegetationsparameter;
- Einbeziehung verbesserter Eingangsdaten für Meteorologie und für den Randbedingungen.

1 Introduction

1.1 Background

The input of air pollutants into ecosystems poses a threat to biodiversity in Germany (Bobbink et al., 2022; Dise et al., 2011; Ströher et al., 2016). The main impact pathways are through eutrophication and acidification. Both impact pathways currently relate to reactive nitrogen inputs while the latter used to be mainly controlled by sulphur compounds.

Production of reactive nitrogen (Nr) through anthropogenic activities is tenfold higher than in the late 19th century due to increased agricultural production and energy consumption (Galloway et al., 2003). A large part of the reactive nitrogen enters the atmosphere in the form of ammonia (NH_3) through animal husbandry and fertilizer use as well as in the form of nitrogen oxides (NO_x) through combustion of fossil fuels (Erisman et al., 2011). The remainder is released as nitrous oxide (N_2O) to the atmosphere or as nitrate (NO_3) to the soil-water compartment. Besides the loss of aquatic and terrestrial biodiversity, these emissions cause numerous problems including adverse health impacts through air pollution, both warming and cooling impacts on the climate system as well as increased nitrate levels in groundwater and drinking water. The negative impacts on biodiversity and ecosystem functioning are partly caused by deposition of reactive nitrogen (Sutton et al., 2011), especially in ecosystems adapted to nutrient poor conditions. In these ecosystems a long-term and sizeable input of reactive nitrogen may negatively affect plant communities (Bobbink et al., 2010) and species diversity (Damgaard et al., 2011). Nutrient-loving, fast-growing plants deprive others of light and space for growth and dispersal. Such changes are often not directly and immediately noticeable because of the time lag. In addition, the susceptibility of many plants to other stress factors (for example, frost, drought, or herbivory) is increased by increased nitrogen availability (Bobbink et al., 2010). Although the nitrogen issues have been identified decades ago, progress to solving them has been limited. Globally, nitrogen deposition is considered one of the top five drivers of biodiversity threats. Rockström et al. (2009) and Steffen et al. (2015) proposed a planetary boundary for anthropogenic nitrogen fixation and identified the alteration of the nitrogen cycle as one of the three most urgent fields of action. The urgent need for biodiversity protection and for a sustainable nitrogen management has recently led to the adoption of the Kunming-Montreal Global Biodiversity Framework (GBF) at the UN Biodiversity Conference: COP15 in Montréal. One of the actions as part of this framework is to reduce excess nutrients lost to the environment by at least half through more efficient nutrient cycling and use and is to be initiated immediately and completed by 2030.

The acid input due to atmospheric deposition of nitrogen and sulphur compounds to soils lowers the soils pH value. Due to the buffer capacity of soils, the reduction in pH does not happen initially. However, in case the buffering substance is depleted, the acidification of soils continues. This leads to a release of soil nutrients like calcium and magnesium ions and toxic metals like aluminium (Al) and iron (Fe) ions (Meng et al., 2019) and subsequently to a leaching into rivers and lakes. High Al and Fe concentrations in combination with a low pH are toxic for plants resulting in a dieback of roots and reduced microbial activity and thus affecting biodiversity.

Nitrogen oxides are also responsible for the development of ground-level ozone. In Germany and large parts of Europe, exposure of plants to ozone also causes damages, leading to decreased crop yields and potential impairment of biological diversity (Mills & Harmens, 2011). The deposition of ozone is not a focus of this study and we refer to Bender et al. (2015) for information for Germany.

To assess the extent to which an ecosystem is at risk, the critical load concept has been developed (Hettelingh et al., 1995). A critical load is defined as "a quantitative estimate of an exposure to one or more pollutants below which significant harmful effects on specified ecosystem do not occur according to present knowledge" (Nilsson, 1988). In the previous assessment on atmospheric inputs to ecosystems in Germany (PINETI-3) it was estimated that in 2015 about 68 % of the terrestrial ecosystems in Germany received more nitrogen than their respective critical loads for eutrophication (Schaap et al., 2018). The area of exceedance of the critical load for acidification was estimated to be much smaller (26 %). In short, a large proportion of the natural ecosystems in Germany is threatened by atmospheric deposition of nitrogen and sulphur containing compounds. Almost half of the plant species on the "Red List" are endangered by increased nutrient inputs (German Federal Agency for Nature Conservation (BfN), (Ströher et al., (2016)).

The critical load exceedance situation due to nitrogen and acid deposition is used as an indicator for sustainability of air pollution impacts and for assessing air pollution abatement strategies on national and international level. The European Commission's Zero Pollution Action Plan claims to reduce critical load exceedances by targeting to reduce the amount of EU ecosystems where air pollution threatens biodiversity by 25 % by 2030. For this, the emission reductions are to be achieved, among others, through the NEC Directive (EU 2016/2284). In the German Sustainable Development Strategy 2016, it was agreed to reduce nutrient deposition to such an extent by 2030 that the area of sensitive ecosystem with critical load exceedances is to be reduced by 35 % compared to 2005 (Federal Government 2016).

These targets are ambitious and require significant investment in mitigation measures. The German Environment Agency (UBA) and the German Advisory Council on the Environment (SRU, 2015) recently recommended the development of a national, interdepartmental nitrogen strategy, which has been adopted by the Federal Government (Salomon et al., 2016). To support the setting of (emission) targets, several approaches concerning the development of an integrated nitrogen indicator (Geupel et al., 2021) informed by a national nitrogen budget (NNB) for Germany (Häußermann et al., 2021) are under development. To verify compliance with the set environmental quality targets and to quantify the national nitrogen budget, current data on pollutant inputs are required. For the planning of measures to reduce the deposition and critical load exceedances more effectively, it is important to better identify the causes of exceedances. To be able to use deposition data and the critical load exceedances derived from them in Germany for legislative requirements (i.e. permitting practice according to TA Luft 4.8) or for reporting within the framework of the NEC Directive, the instruments for calculating pollutant inputs should correspond to the scientific state of the art.

To assess depositions over Germany, a series of projects has been setup by UBA in the past decades.

FKZ 200 85 212 (Schlutow & Huebener, 2004)

FKZ 204 63 252 (Gauger et al., 2008)

FKZ 3707 64 200 MAPESI (Builtjes et al., 2011)

FKZ 3710 63 246 PINETI-1 (Wichink Kruit et al., 2014)

FKZ 3712 63 240 1 PINETI-2 (Schaap et al., 2017)

FKZ 3714 64 201 0 PINETI-3 (Schaap et al., 2018)

In continuation, a new project PINETI-4 (Pollutant INput and EcosysTem Impact) is setup to determine depositions for 2015-2019 and additional information on source contributions and local emissions.

1.2 Mapping methodology

The deposition of atmospheric compounds into ecosystems occurs via three pathways: dry deposition, wet deposition, and occult deposition. A schematic overview is shown in Figure 5. To determine the total deposition, the dry, wet and occult deposition of NH_x, NO_y, and SO_x are calculated and summed. In the mapping procedure, four calculation steps are carried out to this end. The steps as performed as in the PINETI-3 project (Schaap et al., 2018) and outlined below, in section 2.1 a detailed description of the mapping procedure is given.

1. **Calculation of dry deposition and concentration fields based on meteorological data and an emission database using a chemistry transport model**. Dry deposition flux measurements are currently only performed in research projects; there is no observation network for dry deposition. This means that the quantification of the dry deposition across Germany can only be performed by using a chemistry transport model. These models can be evaluated by comparing their results to e.g. observations of pollutant concentrations in air or by comparing their results to those of other models. (Result: Dry deposition fluxes over Germany)
5. **Calculation of wet deposition fields based on observations.** The interpolation of observations of measured concentrations in rain to produce a deposition field covering the entire surface of Germany is performed using geostatistical methods, whereby the information about the spatial distribution from the chemistry transport model is also used for N and S. (Result: Wet deposition fluxes over Germany)
6. **Use of a simple approach to estimate occult deposition.** The concentration in fog water is derived from the concentration in rainwater (see point 2) using empirical factors. Using calculated cloud water deposition rates, the contribution of cloud water to the total deposition is calculated. (Result: Occult deposition fluxes over Germany)
7. **Addition of different pathways.** Results of dry and occult deposition are transformed onto the finely resolved 1x1 km^2 raster and added to the wet deposition fluxes to get the total deposition with a spatial resolution of 1x1 km^2. (Result: Total deposition fluxes over Germany)

Figure 5: Schematic overview of deposition pathways for nitrogen.

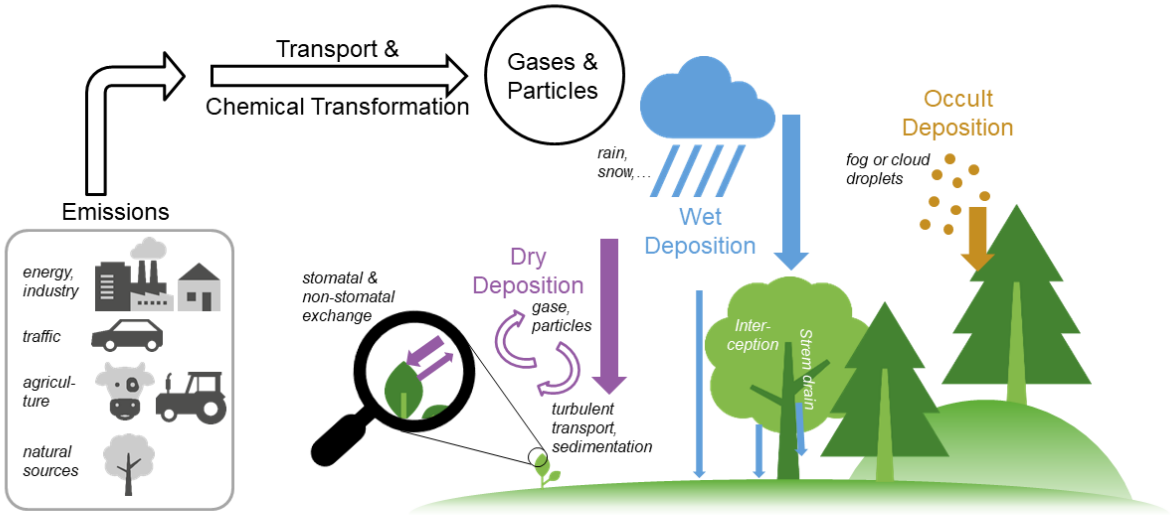

Source: German Environment Agency

1.3 Structure of the report

An overview of the mapping procedure is given in Chapter 1.4, illustrated by the update of the deposition maps for 2015, the last simulated year for the preceding PINETI-3 project. Further necessary model improvements and their impact on model performance are also discussed in this chapter. Model results are given in Chapter 3. Base simulations are evaluated with observations, and impact scenarios plus source contributions are described in the subsections of this chapter. In Chapter 4, observations for wet deposition are added to the model results to obtain the final timeseries of depositions over the required period of 2015-2019. Also, the continuation and comparison with the timeseries from previous PINETI-3 project are described. In Chapter 5, conclusion and outlook for possible model improvements are listed for different subjects of modelling nitrogen and sulphur deposition.

1.4 Objectives

The overall goal of the PINETI-4 project was to extend the time series of nitrogen and sulphur deposition in Germany for the period 2015-2019, based on an improved mapping procedure and to provide quantitative information on the contributions of federal states and local emissions to nitrogen deposition.

The following objectives were defined:

1. To increase the resolution of the LOTOS-EUROS model and assess the model performance of using higher resolved meteorological data from the German Weather Service;
2. To evaluate the results of the LOTOS-EUROS model against measurements;
3. To evaluate the informative value of the high-resolution results for the permitting practice for a small number of cases;
4. To quantify for each federal state the share of the nitrogen deposition caused by emissions from all federal states and neighbouring countries;
5. To extend the deposition time series for nitrogen and sulphur compounds for the years 2015 to 2019 and provide reassessments of the pillar years of 2000, 2005 and 2010 with the updated PINETI-4 methodology.

The resulting maps should replace the current ones in the high-resolution (1x1 km^2) and nation-wide UBA GIS service for determining the background deposition to ecosystems, which is used, for example, in the context of air quality control approval procedures (TA Luft No. 4.8) (http://gis.uba.de/website/depo1).

2 Methodology and PINETI-4 improvements

2.1 General mapping methodology

2.1.1 Chemistry Transport Modelling for dry deposition estimates and ambient concentrations

As there is no large dataset of dry deposition observations we rely on chemistry transport modelling to assess the land use specific dry deposition distributions across Germany. For this purpose, the 3-D regional chemistry transport model LOTOS-EUROS (Manders et al., 2017) is applied within PINETI. The model is of intermediate complexity in the sense that the relevant processes are parameterized in such a way that the computational demands are modest enabling hour-by-hour calculations over extended periods of several years within acceptable computational time. The model is a so-called Eulerian grid model, which means that the calculations for advection, vertical mixing, chemical transformations and removal by wet and dry deposition are performed on a three-dimensional grid. The LOTOS-EUROS model has a long history studying the atmospheric nitrogen and sulphur cycles. Many scientific studies have been carried out with the LOTOS-EUROS model studying secondary inorganic aerosol (SIA) (Banzhaf et al., 2015; Erisman & Schaap, 2004; Schaap et al., 2004, 2011), sea salt (Manders et al., 2010), particulate matter (Hendriks et al., 2013; Manders et al., 2009), ozone (Beltman et al., 2013; Curier et al., 2012), nitrogen dioxide (Curier et al., 2014; Schaap et al., 2013) and ammonia (Hendriks et al., 2016; Van Damme et al., 2014; Wichink Kruit et al., 2012). For additional details on the model we refer to these publications.

The LOTOS-EUROS modelling system describes the budget of air pollutants across a larger region. Understanding the budget requires a good representation of the emissions, dispersion, chemistry and removal of ammonia, nitrogen oxides, sulphur dioxide, their particulate reaction products and their interactions. All abovementioned processes take place at the same time and the concentrations and deposition of the nitrogen and sulphur compounds are resultants of these processes. The process descriptions are driven by meteorological data from e.g. ECMWF or ICON and used to perform hour-by-hour calculations across the study period. With the PINETI-3 methodology, the model was applied to Germany through a one-way nesting procedure on a resolution of 0.125° longitude by 0.0625° latitude, approximately 7x7 km². The high-resolution domain is nested in a European domain with a resolution of 0.5° longitude by 0.25° latitude, approximately 28 by 28 km². For PINETI-4 model resolution is increased significantly to 0.03125° longitude by 0.015625° latitude, which is approximately 2x2 km². Note, that for the production runs the resolution of the ECMWF meteorological input data was 0.1° longitude by 0.05° latitude (approximately 6x6 km²), which was interpolated to fit the 2x2 km² model resolution. The impacts of the increases model resolution are discussed in Section 2.2.1.

The emissions for the European domain are taken from the Copernicus Atmosphere Monitoring Service (CAMS) and the German emissions are replaced by deliveries from the UBA-GRETA dataset. For both datasets, the reporting year of the emissions is an important feature to be aware of as emission estimates may differ significantly between submission years due to methodological changes. The temporal variation of the emissions is represented by monthly, day-of-the-week and hourly time profiles that break down the annual totals for each source category. The retrieved hourly emission estimates are added to the concentration fields in the model and are subject to gas phase and multi-phase chemistry. LOTOS-EUROS incorporates parametrizations for the gas phase chemistry (CBM-IV;Gery et al., 1988), the partitioning between the gas and aerosol phase for ammonia/ammonium and nitric acid/nitrate (ISORROPIA2; Fountoukis and Nenes, 2007) as well as the heterogeneous loss reaction of nitric

acid with sea salt to form coarse sodium nitrate. Finally, the model also includes a pH dependent cloud chemistry scheme (Banzhaf et al., 2012).

The wet deposition estimates used for total deposition results are retrieved through a procedure including observational precipitation concentration data (see Section 2.1.2). Still, the modelled rain water concentration is used as an a-priori distribution for the interpolation of observational data for the wet deposition estimate (Section 2.1.2), but not directly to retrieve the wet deposition. However, the wet deposition needs to be represented within LOTOS-EUROS model as the scavenging process lowers the atmospheric concentration of gases and particles and thereby impacts the dry deposition estimates through the resistance approach explained further below.

The two main wet deposition processes are in-cloud and below-cloud scavenging. In-cloud scavenging, also called rain-out, is the process where condensation of humid air forms cloud droplets on aerosol particles. Subsequently, water soluble gases may dissolve in the cloud water. In case cloud droplets rain out, the material is lost to the surface. While falling through the air column below the clouds, further gases and particles may be incorporated into droplets due to impaction (particles) or dissolution (gases). This process is called below-cloud scavenging, or wash-out, (Banzhaf et al., 2012). The removal of particles depends mostly on their size, as impaction and diffusion are the main mechanisms for the particles to be “caught” by the falling droplets. Below-cloud scavenging is an effective way to remove water soluble gases from the atmosphere, as the removal efficiency is governed by their water solubility (Henry constant). Hence, the efficiency with which the highly soluble ammonia and nitric acid are removed is much larger than those of medium solubility. Low soluble gases like NO and NO_2 are much less efficiently removed by wet deposition. Note that the solubility of gases like ammonia and sulphur dioxide depends on the pH of the solution. Hence, the effectivity of removal between these compounds is connected and some models include pH dependent wet removal as well as saturation effects in their process descriptions. The scheme for in- and below-cloud scavenging of gases and particles in LOTOS-EUROS accounts for these droplet saturation (Banzhaf et al., 2012). A third type of wet deposition is the removal of gases or particles via early morning dew or fog. Direct deposition of wind-driven cloud water on mountain ridges known as occult deposition is also included in this process. The description of this process is neglected in LOTOS-EUROS as there is no good process description and no information is available for the direct water deposition from meteorological models.

Dry deposition is the direct removal of atmospheric gases and particles by vegetation, soils, or surface waters (Fowler et al., 2013). The dry deposition flux of trace gases depends on the surface concentrations and the dry deposition velocity. A common way to parameterize the dry deposition velocity is the use of a resistance analogy. In a resistance model, the most important pathways along which trace gases are taken up by the surface are parameterized. The dry deposition velocity in the DEPAC module used in LOTOS-EUROS is represented as the reciprocal sum of the aerodynamic resistance, the quasi-laminar resistance and the canopy resistance (Van Zanten et al., 2010). Here, the aerodynamic resistance describes the resistance for the turbulent transport from a given height to the surface. This resistance is lower for an instable atmosphere than for a stable one and it is lower for rough surfaces than for smooth surfaces. Hence, the aerodynamic resistances induce diurnal cycles and seasonal cycles in the dry deposition effectivity, as well as a strong dependence on surface type. This term in the deposition process affects all compounds equally. The quasi-laminar resistance accounts for transport by molecular diffusion through the laminar layer close to the surface. Although it depends on the molecular weight of the gases and particle size, this term is mostly a small part of the total resistance. Lastly, the canopy resistance accounts for the uptake at the surface itself. The surface can be a

soil or a water surface, but in case of vegetation the leaves and their stomata play a key role. In principle, the efficiency of removal is determined by the reactivity and solubility of the pollutants combined with the phenology and behaviour of the stomata. Stomata opening is controlled by sunlight and temperature conditions. In darkness and at extreme temperatures stomata close and this deposition pathway is shut. The same happens when plants are in drought stress. Hence, the pathway is mostly effective during daytime during the growing season (as the presence of leaves is a prerequisite). Given an air flux into the stomata, the solubility in the leaves' apoplastic fluid determines how efficiently a gas is taken up by the plant through the stomata. The pollutants may also stick to external surface area of a plant or tree, which is especially effective for reactive compounds like nitric acid. In case the canopy is wet, the droplets in the plants may take up gases like ammonia (NH_3) and SO_2 effectively, although they may be (partially) released into the atmosphere again.

For ammonia, the surface-atmosphere exchange is bi-directional, i.e. NH_3 can be re-emitted from surfaces into the atmosphere. The reason is that NH_3 has a non-zero vapor pressure over its solution. Plants, for instance, can act as a source of NH_3 when the NH_3 concentrations in their stomata exceed the ambient atmospheric NH_3 concentrations. The direction of the NH_3 flux depends on the so-called compensation point. The compensation point is defined as the NH_3 concentration at which no net NH_3 exchange takes place between the surface and the atmosphere (Nemitz et al., 2000). For plants, the compensation point is determined by the temperature, pH, and the ammonium concentration in-side the stomata (Massad et al., 2008). The LOTOS-EUROS model is one of the few chemistry transport models that uses a description of the bi-directional surface-atmosphere exchange of NH_3 (Wichink Kruit et al., 2012). The module in LOTOS-EUROS was expanded to include the co-deposition effect of sulphur dioxide and ammonia as the dry deposition velocities of NH_3 and SO_2 are connected (Fowler et al., 2001). As the pH of the fluids in the system determines the rate in which either gas is dissolved, NH_3 has an increased deposition velocity in conditions with higher sulphur dioxide ambient concentrations.

The output of the model system consists of hourly distributions of concentrations, wet deposition and land use specific dry deposition fluxes. The wet deposition and concentration results are used for validation purposes and averaged to the observation time spans (e.g. daily). The dry deposition fluxes represent an end product. The modelled wet deposition results are provided to the mapping procedure as explained in the next section.

2.1.2 Wet deposition estimation

Traditionally, the assessment of wet deposition fluxes to ecosystems in Germany is performed with an empirical approach making use of observed wet deposition fluxes at a large number of stations (Builtjes et al., 2011; Gauger et al., 2008). In this second step of the procedure we derive rain water concentrations at the measurement locations and interpolate these data across Germany to arrive at a nationwide distribution. The distribution of the concentration in rain water is then multiplied with a high-resolution precipitation map to arrive at the wet deposition estimates:

$$F_{wet} = C_{rainwater} * Precipitation\ amount \qquad (Equation\ 1)$$

Datasets on precipitation chemistry from various national and regional monitoring programs in Germany are compiled by UBA and provide data for about 230 sites. The national UBA network (n=6 in 2019) samples on a weekly rhythm, whereas the regional networks may operate at a weekly, two-weekly, four-weekly or monthly basis. Unfortunately, the sampling strategies of the regional networks are not synchronized, only allowing an assessment on annual average basis. The majority of the wet deposition data is obtained with bulk samplers as only about 40 stations

are equipped with wet-only samplers. Hence, the data from the bulk samplers that pass our quality control procedures were corrected for the dry deposition into the funnels using species dependent correction factors (Gauger et al., 2008). As the wet deposition data are obtained from many different sources, a common quality assessment and quality control (QAQC) protocol and data selection procedure was applied to the whole database. Following EMEP protocols (EMEP, 1996), the ion balance is calculated for all samples. In case the net ion-charge exceeds ±20 %, the measurement is rejected. To remove further outliers a statistical outlier test is performed for the time series of each station using the Grubbs test (Grubbs, 1969). The procedure is iterative in the sense that the procedure is repeated after identifying and removing an outlier until no outliers are found anymore, or too many entries from the series are removed. As we log-transform the data in the interpolation scheme (see below), the procedure is applied to the time series of log-concentrations. All in all, most data flagged invalid are largely due to the ion balance check.

During the PINETI-4 project it is noticed that a few stations pass this QAQC procedure with very different rain water concentrations as compared to those measured at nearby stations. As this is assumed to be unrealistic, an extra quality criterion was incorporated in the process. For each monitoring station, the annual deposition is compared with all stations within 200 km distance. If the annual value for a station falls outside the range of the mean value for the neighbouring stations plus or minus three times the standard deviation, the station is flagged as outlier with respect to neighbours and not taken in the interpolation process.

A minimum valid data coverage of 40 % for a given year is required to be included in further analyses. This criterion is a compromise between including as many stations as possible and maintaining high data quality. The 40 % criterion was established based on a pragmatic approach in which we averaged the concentration in precipitation measured at UBA stations for 1000 random subsets of the available 52 weekly measurements for different data availabilities, i.e. 100 %, 80 %, 60 %, 40 % and 20 %. As expected, the variability around the annual mean increases when data availability becomes smaller. At 40 % availability the standard deviation is around 15 % of the mean concentration values for sulphate, nitrate and ammonium, which is in line with uncertainties in precipitation amounts and other concentration data.

A residual kriging methodology is used to interpolate the concentrations in rain water to generate a distribution of concentrations in rain water across Germany on a 1x1km^2 resolution (Wichink Kruit et al., 2014). Within this procedure the difference or residual between the observations and an a-priori distribution is interpolated. The a-priori distribution is the modelled average rain water concentration from the LOTOS-EUROS model. The advantage of using LOTOS-EUROS distributions as a-priori is that process knowledge is included in the interpolation, which results in better validation statistics (Wichink Kruit et al., 2014). As there can be considerable variability between observed concentrations at stations at distances rather close to each other, there remains a residual between the observed and optimized distribution. Evaluations of the interpolated fields with the measured data shows that for ammonium the differences can be as large as 25 %, whereas the differences for nitrate and sulphate are much smaller (~10 %). This can be explained by the much smaller gradients across Germany observed in the rain water concentrations for nitrate and sulphate compared to those for ammonium.

Finally, the rain water concentration is multiplied by a high-resolution precipitation map for Germany (see Figure 6). This map is derived from precipitation measurements by the German Weather Service (DWD) using a geostatistical approach (Rauthe et al., 2013). A mean error of less than 6 % was estimated for the annual precipitation amounts by Rauthe et al. (2013). We previously validated this distribution against the independent information on precipitation amounts from the stations with precipitation chemistry. Overall, the comparison is very good

with most annual totals within 15 % of each other (Schaap et al., 2018). The higher inaccuracy reported here could well be associated to the host of different samplers and the long sampling periods (up to one month) used within the wet deposition networks. Field inter-comparisons of different bulk and wet-only samplers has found it difficult to estimate precipitation volumes accurately. For instance, an accuracy better than 10 % was only reached for 10–20 % of the individual samples during a comparison held in the Netherlands with samplers from 20 different (Erisman et al., 2003).

Figure 6: **Modelled concentration of NO_3 in rain water (upper left), result of kriging approach (upper right). Rain amount on high resolution (lower left), combined result for wet deposition flux on high resolution (lower left). Shown are result for 2015 using the PINETI-3 methodology with an increased number of wet deposition measurements.**

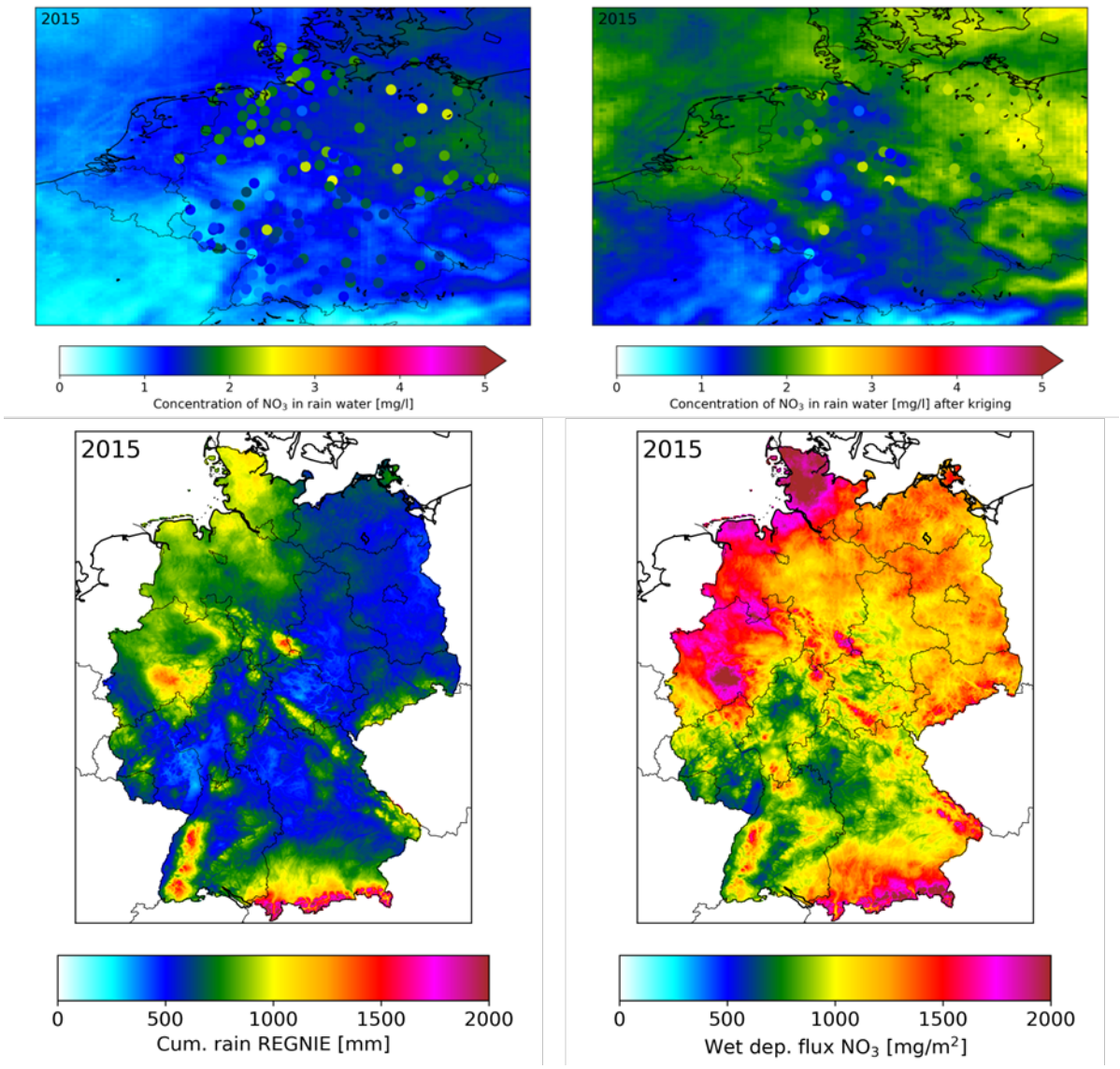

Source: TNO

An example of the wet deposition mapping procedure is provided in Figure 6. This example for nitrate in rain shows that the systematic underestimation of the modelled field (shown in the upper left panel) is corrected for by the kriging. After multiplication of the rain water concentrations with the annual precipitation map the annual wet depiction flux maps are

obtained. The obtained rain water concentration distribution is provided to the occult deposition mapping procedure as explained in the next section.

2.1.3 Occult deposition estimation

Currently, none of the European Eulerian chemistry transport models incorporates a parameterization of the occult deposition. For countries with only a small fraction of elevated areas, this will not lead to significant underestimates in total deposition. However, for elevated locations occult deposition may be a substantial contribution to total deposition. In this study the occult deposition flux is derived by estimating the deposition flux of cloud and fog water which is combined with the pollutant concentration in the cloud water.

The occult deposition computed within the PINETI context refers to nitrogen input by orographic clouds, which is the result of condensation processes in moist air lifted by mountains. Generally, the occult flux (F_{occult}) is derived by the multiplication of the deposition flux of fog water (F_{fog}) and the pollutant concentration in the fog water (C_{fog}):

$$F_{occult} = F_{fog} * C_{fog} \qquad (Equation\ 2)$$

The calculation of fog water deposition (F_{fog}) follows the approach by Katata et al., (2008, 2011). In Katata et al. (2008), a simple linear equation for the fog deposition velocity based only on horizontal wind speed has been derived from numerical experiments using a detailed multilayer land surface model that includes fog deposition onto vegetation (SOLVEG):

$$v_d = A * U \qquad (Equation\ 3)$$

Where A is a factor that depends on vegetation characteristics (nondimensional), and U the horizontal wind speed [m s^{-1}] above the canopy. A is calculated by:

$$A = 0.0164 * \left(\frac{LAI}{h}\right)^{-0.5} \qquad (Equation\ 4)$$

where LAI is the Leaf Area Index and h the canopy height [m]. The calculations of A using Equation 4 agreed with observations in various cloud forests with $LAI/h > 0.2$ (Katata et al., 2008) and it was stated that Equation 4 can be widely used to predict cloud water deposition on forests with $LAI/h > 0.2$. Using V_d the flux of fog water deposition F_{fog} [kg m^{-2} s^{-1}] is calculated using:

$$F_{fog} = v_d * \rho * q_c = A * u * \rho * q_c \qquad (Equation\ 5)$$

where ρ is the air density [kg m^{-3}], u and q_c are the horizontal wind speed [m s^{-1}] and the liquid water content [kg-water kg-air^{-1}] near the surface, respectively. The accuracy of Equation 5 in the amount of fog deposition has been validated with data on turbulent fog flux over a coniferous forest in Germany (Klemm & Wrzesinsky, 2007) with a prediction error of 13 % (Katata et al., 2011).

The meteorological input to calculate the occult deposition flux was taken from the COSMO-EU model which is the operational numerical weather prediction model of the DWD. COSMO-EU was chosen as it provides the meteorological fields over Germany on a rather high grid resolution of ca. 7x7 km^2. Hourly data of the meteorological fields were used to calculate the annual fog water deposition flux based on Equation 5 with:

$$F_{fog(annual)} = \sum_t v_d(t) * \rho(t) * q_c(t) = A * \sum_t u(t) * \rho(t) * q_c(t) \qquad (Equation\ 6)$$

where ρ is the air density [kg m^{-3}], q_c the liquid water content [kg-water-kg air^{-1}] at the lowest atmospheric model layer and u the horizontal wind speed at 10 m [m s^{-1}]. The elevation of u may be different from that of U in Equation 3 in some cases, but this does not cause a significant error in representative wind speed according to the logarithmic wind profile in the surface boundary layer (Katata et al., 2011).

A specific challenge in the assessment of the PINETI-3 time series was that the COSMO-EU model has only been in use since September 2005. Therefore, model data for the calculation of the fog water deposition flow was not available for the entire period from 2000 to 2015. For this reason, and because of the high degree of uncertainty in the "liquid water content" data, which has a significant influence on the calculated quantity and distribution of the fog water deposition flux, it was decided to assume a 5-year averaged fog water deposition flux for the entire period. The years 2007, 2008, 2009, 2010 and 2012 were chosen as meteorological years for the derivation of an average fog water deposition flux. The fog water deposition on coniferous forest calculated for these five years is shown in Figure 7. The year 2011 was omitted because it was exceptionally low in precipitation and would have significantly affected the fog water deposition flux. Because those five years still represent average fog water depositions, these years are also used in the calculations for PINETI-4. Figure 7 shows that the fog water deposition is enhanced especially over the mountainous regions in Germany, such as the Erzgebirge, the Harz or the Bavarian Forest, with values reaching up to 125 kg-water m^{-2} yr^{-1}. In addition, secondary maxima of up to 60 kg-water m^{-2} yr^{-1} occur - in most years - over the Black Forest, along the Swabian and Franconian Alps and in the Eifel. While the spatial distribution of the calculated fog water deposition flow is similar for the individual years, the amount of deposited water varies from year to year. This is partly due to meteorological variability. In addition, the description and parameterization of the COSMO-EU model experienced a number of changes between 2007 and 2012. These changes also had an impact on the microphysical properties of the model and thus influenced, among other things, the "liquid water content" model parameter. Compared to previous years, these changes in the model calculation process have, for example, led to a systematic decrease in the calculated fog water deposition flow from mid-2009. Using the average value around the year 2009 basically means choosing the midpoint of the time series. In PINETI-4 we have kept this fog water deposition map for all years.

Figure 7: Five year mean (2007,2008,2009,2010,2012) distribution of fog water deposition to coniferous forest.

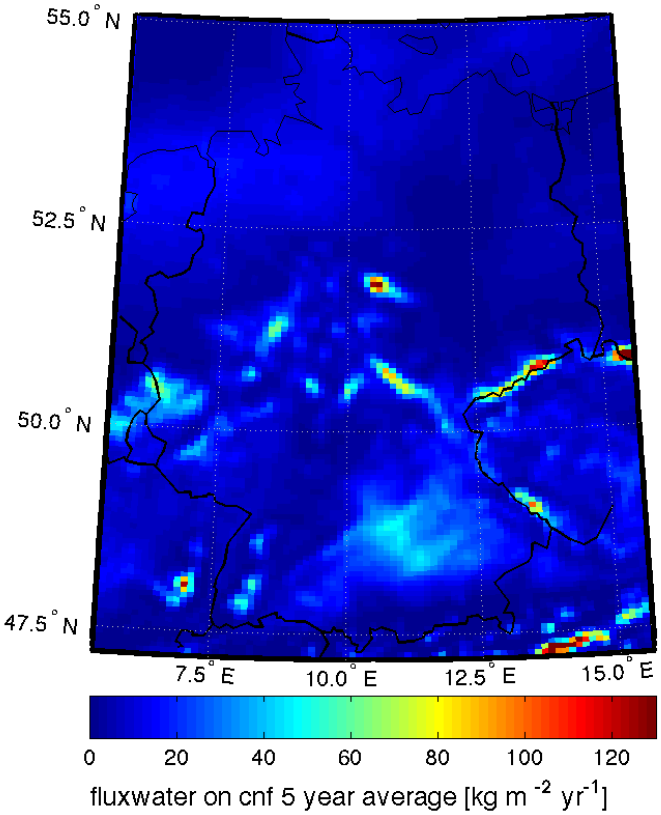

Source: Schaap et al., 2018

The approach following Katata et al. (2008, 2011) as described above is based on experimental data in forests and hence, provides an estimation of fog water deposition on forests only. Furthermore, the input on vegetation by fog is much more relevant for forests than for other land use categories as e.g. for grassland as the area of incidence is largest for forests when they filter the air mass passing through including fog or clouds. Hence, available studies on the occult input on vegetation are limited on forests and therefore fog water deposition on land use categories other than forest categories are neglected.

The mean pollutant concentration in fog water (C_{fog}) was estimated from the annual mean concentration in rainwater using so called enrichment factors (*EF*):

$$C_{cloud} = C_{rain} * EF \qquad (Equation\ 7)$$

Hereby, the annual mean concentrations in rainwater per species stem from the interpolated concentration fields derived for the calculation of the wet deposition flux. The enrichment factors for the different species were derived from a compilation of field data from studies that provide simultaneous observations of fog and rain water chemistry (Schaap et al., 2018). Enrichment factors are greater than unity for all species as within all available studies and for all species the concentration in fog water was higher than in rain water. This can be explained by a lower dilution in fog/cloud droplets as these are smaller than rain droplets and contain less water. The variability between the individual studies is large indicating the enrichment factors may be a large source of uncertainty.

The output of this procedure is an annual occult deposition flux map for forests in Germany. Note that the resolution of the meteorological data is not able to capture the variability on very

local scales which depend on altitude, slopes and local meteorology. Hence, the obtained occult deposition maps reflect background values for larger regions and do not reflect the deposition at very exposed sites.

2.1.4 Addition of the fluxes

Maps of the total deposition of NH_x, NO_y and SO_x over Germany were created by adding dry, wet and occult deposition. These maps are made available in ASCII-format covering Germany at 1x1 km². In Figure 8, an overview is shown of the complete mapping methodology used for Germany.

Figure 8: Overview of the mapping methodology used in PINETI. The scheme introduces important input data (dark blue boxes), key intermediate results (light blue boxes), calculation steps (dashed boxes) and final results (green boxes). The arrows indicate the data flow and dependencies.

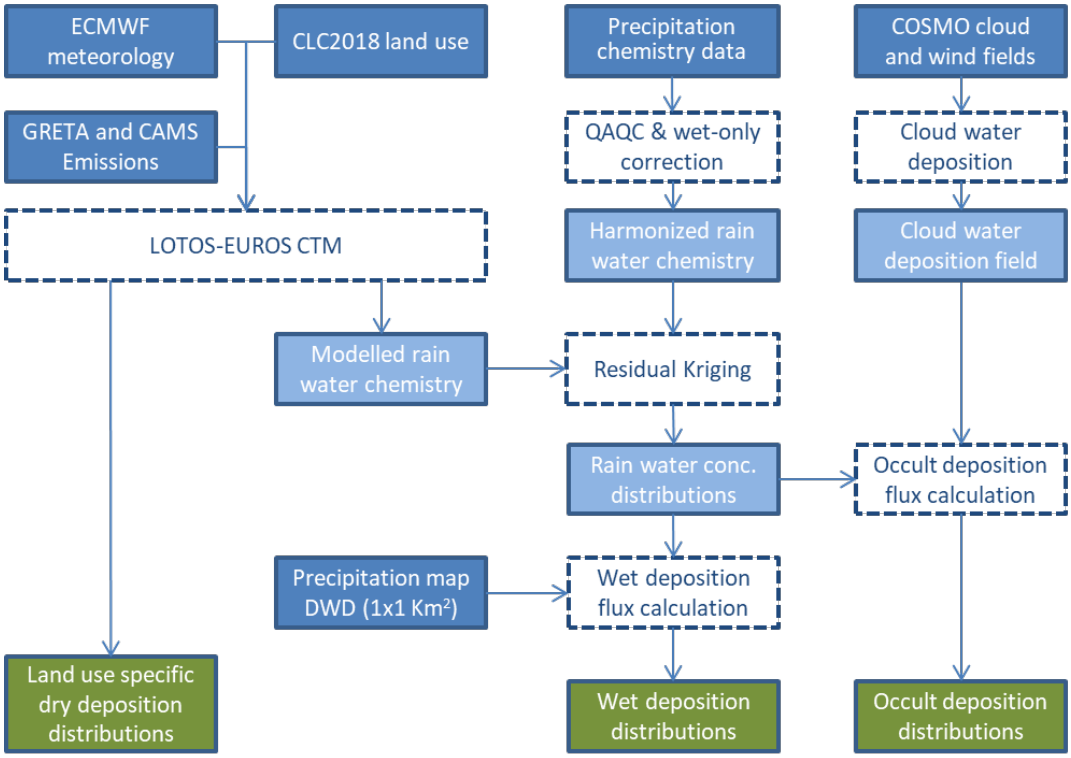

Source: TNO

2.1.5 Uncertainties due to model resolution

The largest source of uncertainty for the derived total deposition maps is related to the dry deposition modelling. This is explained by the complex nature of the nitrogen and sulphur cycles and their interdependencies, the small experimental basis underlying the dry deposition parametrizations and the quality of the model input data on e.g. emissions.

Increasing the model resolution can have a positive impact on the model performance of primary pollutants, such as nitrogen oxides and ammonia. Until now, however, this was not pursued in the PINETI mapping procedures as the information on agricultural NH_3 emissions was only available at district (German: "Kreis") level without information where the emissions are actually located within these rather large regions. In addition, the meteorology used in the model simulation (from ECMWF) was representative for approximately 10x10 km² km resolution. A recent comparison against dry deposition flux measurements (Wintjen et al., 2022) showed that the largest part of the difference between observed and modelled fluxes was due to

the overestimation of the concentrations in ambient air of NH_3. Hence, improved model resolution could provide benefits, especially in combination with improved representation of emissions. As also non-hydrostatic high-resolution meteorological data is becoming available to support higher resolution simulations, the aim of the development work in PINETI-4 was to improve the model resolution to 2x2 km^2.

2.2 Methodological improvements in PINETI-4

In order to assess the impacts of model improvements, PINETI-4 results were evaluated against PINETI-3. For this, the year 2015 was chosen, where simulations for both methodologies were available. Below, the development steps are described as follows:

1. Update 2015 mapping results based on latest information of wet deposition observations
2. Increase model resolution
    a) Model version with domain decomposition
    b) Vertical and horizontal resolution
3. Improved emission information
    a) Annual totals
    b) Spatial distribution
    c) Emission heights
    d) Temporal variability

Since the wet deposition observation database for 2015 was not complete during the finalization phase of the PINETI-3 project in 2017, a lower quality of the kriging method was observed. This turned out to be important for Niedersachsen. The steps and their impact on the estimated average deposition in Germany is presented below and summarized in Table 1.

In the newly available wet deposition data set for 2015, data from 80 additional stations were used. The data set included additional observations for Berlin, Hamburg, Bremen, Saarland, Hessen and Niedersachsen. Including the observations of Niedersachsen and the other states into the residual kriging leads to smaller average fluxes for both wet-NH_x and wet-NO_y. Overall, due to a complete observation set, the annual nitrogen deposition for 2015 is estimated to be 980 eq ha^{-1} yr^{-1}, which is lower than the original result (1039 eq ha^{-1} yr^{-1}) of PINETI-3.

Within PINETI-3, the chemistry transport modelling for 2000-2015 was performed with the European emission data from the MACC project, which was provided following the SNAP categorization. The newer European emission data from CAMS, which were used in PINETI-4, have adopted the GNFR sector definitions and are based on 2015 emissions reported by the member states in 2018. Hence, the emission processing module of LOTOS-EUROS was adopted to cope with this new data structure. Moreover, the slightly different sector categorization required to adapt the prescribed time and height profiles used to produce the hourly emission information from the annual inventory. The most important update was for the agricultural sector. In GNFR, agricultural emissions are split in animal housing and other agriculture (dominated by manure application), while the SNAP system has only one generic agricultural sector. Following the GNFR sector classification, two different temporal profiles are used for housing and other emissions. Compared to the application of a single profile in the SNAP classification, relatively larger emissions are allocated to the summer season using the profiles following GNFR definition. Besides a different sector classification, also the CAMS data are available on a slightly higher resolution and a different submission year is used (2017-PINETI-3,

2018-PINETI-4). Due to methodological differences between submission years, the total German emission of NO_x are larger by ~5 % whereas those of NH_3 are lower by ~12 % compared to the emission set used in the original PINETI-3 simulation. Impacts on annual depositions are listed in Table 1. The modelled dry and wet depositions are changing in line with changes in the emission submission for both NH_3 and NO_x. Hence, they partly compensate each other in terms of total modelled N deposition, which is lowered by about 20 eq ha^{-1} yr^{-1} for both average dry and wet deposition. Note that impact on the mapped wet deposition is considerably smaller as the residual kriging pulls the distribution to the observed fluxes. Overall, the initial update for 2015 resulted at an average N deposition of 954 eq ha^{-1} yr^{-1}, compared to 1038 eq ha^{-1} yr^{-1} with original version. The largest part (59 eq ha^{-1} yr^{-1}) of the difference can be attributed to the completion of the wet deposition data set and a smaller part to changes in the emission submission. For sulphur deposition, the only significant effect is due to the renewed wet deposition mapping.

Table 1: Comparison of the average modelled dry and wet, kriged wet and occult deposition fluxes (eq ha^{-1} yr^{-1}) for 2015 for PINETI-3 (original) and for the updates using all wet deposition data (Obs) and the emissions of the 2018 reporting (Obs+Emis (GNFR)).

Component	Model configuration	Dry modelled	Wet modelled	Wet kriging	Occult	Total
NH_x	Original	354	342	342	9	706
”	Obs	354	342	299	9	663
”	Obs+Emis (GNFR)	320	311	296	9	625
NO_y	Original	118	134	208	7	332
”	Obs	118	134	193	7	318
”	Obs+Emis (GNFR)	132	143	190	7	329
N	Original	473	476	550	16	1039
”	Obs	473	476	492	16	980
”	Obs+Emis (GNFR)	452	454	486	16	954
SO_x	Original	65	67	148	3	215
”	Obs	65	67	133	2	200
”	Obs+Emis (GNFR)	63	61	131	2	197

To evaluate the LOTOS-EUROS model performance, modelled concentrations and wet deposition fluxes are compared with observations across Germany. Observations are performed by different state authorities and gathered by UBA to a consistent data set. For NO_2, O_3 and SO_2, observed data are available on hourly basis. With these data, annual concentrations over the country are analyzed, and biases, RMSE and spatial correlations are calculated. Also, temporal behavior is calculated for all stations. In Table 2, an overview of statistical parameters is given to quantify model performance with respect to observations available on hourly resolution. Further model simulations are compared with sample data which are available on irregular temporal resolutions varying from daily to monthly. Therefore, it is not possible to give a relevant value for temporal correlations for gaseous NH_3 concentrations and wet deposition observations, but annual averages and spatially dependent statistics were calculated,

see Table 3.

In general, concentration and deposition levels for reduced nitrogen (NH_3 and NH_4) are well modelled by LOTOS-EUROS. However, spatial and temporal distributions can be improved. Oxidized nitrogen compounds (NO, NO_2 and NO_y) are generally underestimated by about 30 % for both concentrations in air and wet depositions. For sulphur components, gaseous SO_2 is slightly overestimated, while wet deposition of SO_x is underestimated by a factor 2. The statistical results from Table 2 and Table 3, serve a as basis to evaluate model improvements performed in PINETI-4.

Table 2: Statistical parameters for the updated (Obs+Emis (GNFR)) model simulations, compared with observations on hourly basis for NO, NO_2, O_3 and SO_2.

Component	Bias	Spatial correlation	Spatial RMSE	Average temporal correlation	Average temporal RMSE
NO	-16.3	0.22	7.6	0.39	29.0
NO_2	-13.0	0.57	8.4	0.50	19.2
O_3	17.5	0.33	18.9	0.79	26.8
SO_2	0.3	0.33	1.7	0.30	3.5

Table 3: Statistical parameters for the updated (Obs+Emis (GNFR)) model simulations, compared with irregular observations of NH_3 and wet depositions of NH_x, NO_y and SO_x.

Component	Bias	Spatial correlation	Spatial RMSE	Average temporal correlation	Average temporal RMSE
NH_3	0.2	0.64	1.60	-	-
NH_x wflux	4.0	0.59	100.0	-	-
NO_y wflux	-59.3	0.26	77.8	-	-
SO_x wflux	-90.4	0.34	115.8	-	-

2.2.1 Increasing the model resolution

Increasing the resolution of a modelling system is not a straightforward process. Although many input variables are actually read in at a higher resolution than the model requires them and thus require no attention, the higher spatial resolution causes and much larger computational burden. Normally, an increase of a spatial resolution by a factor 2 causes a computational effort that is related to the number of grid cells (2x2) and the implicit doubling of the time step (x 2), which results in a factor 8 more computation time. The latter is without increasing the number of vertical levels. In PINETI-4 we are more than doubling the resolution which would have increased the computational burden by a factor 25-30. Hence, a technical development involving domain decomposition to speed up the model system was required to cope with the additional computational demand. This development was largely funded through parallel activities for which we also acknowledge funding from the federal state of Baden-Wurttemberg (StickstoffBW). The domain decomposition splits the model domain in small sub-domains and

runs these in parallel. The parallel computations allow to reach a large speedup of the system. Due to small adaptions and numerical impacts the total deposition of nitrogen increased on average by ~1 %, with slightly higher impact on dry deposition of NO_y.

As a next step, the model resolution was increased to approximately 2x2km². As a result, the gradients in modelled concentrations and deposition fluxes are sharper, whereas the annual means or totals averaged across a larger region hardly change. In Table 4, the latter is illustrated for the Germany averaged deposition fluxes. Only small increases of modelled wet deposition fluxes are observed, as well as a small decrease in NO_y dry deposition.

Table 4: Comparison of the average modelled dry and wet, kriged wet and occult deposition fluxes (eq ha^{-1} yr^{-1}) for 2015 for the increase in resolution

Component	Model configuration	Dry modelled	Wet modelled	Wet kriging	Occult	Total
NH_x	Domain decomp.	320	291	298	9	627
”	Higher horiz. res.	320	300	297	9	627
”	Higher vert. res.	425	256	295	9	729
NO_y	Domain decomp.	140	143	190	7	336
”	Higher horiz. res.	132	145	190	7	328
”	Higher vert. res.	176	131	189	7	371
N	Domain decomp.	460	434	487	16	963
”	Higher horiz. res.	452	445	488	16	956
”	Higher vert. res.	601	387	484	16	1100
SO_x	Domain decomp.	63	59	131	2	197
”	Higher horiz. res.	63	60	131	2	197
”	Higher vert. res.	91	66	133	2	226

While the increase in horizontal resolution showed only little impact on the national total depositions, the increase in the vertical resolution has a much larger impact. In the LOTOS-EUROS version applied in PINETI-3, the model runs on five vertical layers applying the dynamic boundary layer concept. The first two layers consisted of a surface layer of 25 m depth and the remaining depth of the meteorological boundary layer as layer 2. This boundary layer was

assumed to be completely mixed and could reach depths of over 1000 m in the afternoon of summer days. The remaining three layers were used as reservoir layers up to an altitude of 5000 m above sea level. As the mixing layer was variable, the depth of the first two reservoir layers varied as well. With increasing spatial resolution, the assumption that the mixing layer is well mixed may not be valid anymore in source regions. For example, it takes about 15 minutes to vertically mix a pollutant through the mixing layer. At a wind speed of 10-20 km hr^{-1} the same air mass would have travelled 2.5 to 5 km. Hence, in source regions the mixed boundary layer assumption is less valid at 2x2 km than at 7x7 km resolution. Furthermore, recent sensitivity simulations with respect to particulate matter using LOTOS-EUROS indicated a fast mixing of pollutants from the boundary layer to higher layers, leading to an underestimation of the PM mass concentration in the Berlin agglomeration (Thürkow et al., 2021). Due to deep reservoir layers overestimated mixing, particular during stable weather conditions with low boundary layers, occurs. Therefore, recent model developments apply a much larger number of vertical layers to provide a better understanding of the vertical distribution of pollutants (Escudero et al., 2019). The multi-level version moves away from the assumption of a well-mixed PBL and better accounts for the residual layer dynamics (Thürkow et al., 2021). Here, we move to an implementation with 12 vertical layers with more detail in the boundary layer combined with a model top at 8000 m above sea level. The vertical structure basically follows the hybrid-sigma pressure layers of the ECMWF combining several layers into one further away from the surface. The mixing between the layers (within the boundary layer) is performed using Kz-theory.

Here we observe that the combination of increasing the number of layers in the vertical and moving away from the mixed boundary layer concept leads to less upward dilution of the modelled pollutants. As a consequence, the modelled concentrations of primary pollutants (NO, NO_2, NH_3, SO_2) all increase, especially in (agricultural (NH_3) and densely populated (NO_x)) source areas. By retaining more mass near the surface, the dry deposition estimates of all pollutants increase systematically by about 30 %, while the modelled wet deposition flux simultaneously goes down. The modelled average dry+wet deposition flux across the country increases, meaning that the modelled export of pollutants and thus the average transport distance is lower in the new setup. After application of kriging of wet deposition observation and adding the occult deposition, this results in an increase of 14 % in total N deposition with respect to the updated PINETI-3 result (obs+emis (GNFR)).

In Table 5 and Table 6, the results of the model evaluation against observations are presented. In general, increasing the horizontal resolution improves the spatial correlation between annual mean concentrations slightly. At the same time, we observe that the average temporal correlation and RMSE of the time series evaluations almost all become poorer. This is most visible for NO. Hence, the representation of average gradients for primary species becomes better at the cost of the representation of the temporal variability. Such behavior was observed before in a study in which several models only adapted their spatial resolution (Schaap et al., 2015). Looking at results for the higher vertical resolution shows that the increased concentrations lowers the biases and RMSE in the annual mean concentrations and, for all compounds, improves the temporal correlation. The latter comes with the lowest RMSE in the time series analyses. All in all, the improved resolution shows the best validation scores for the oxidized nitrogen compounds. For SO_2, the picture is more mixed. For the irregular observations, the evaluation on annual means is less informative than for the hourly timeseries. In general, the spread in the scatterplots become smaller, which is expressed in a larger spatial correlation coefficient. The slight changes in biases affects error calculation and shows a mixed picture. All in all, we conclude that the increased resolution has a generally positive impact on the LOTOS-EUROS model performance.

Table 5: Model evaluation statistics for the model updates towards higher spatial resolution for hourly time series of NO, NO_2, O_3 and SO_2.

Component	Model configuration	Bias	Spatial correlation	Spatial RMSE	Average temporal correlation	Average temporal RMSE
NO	Obs+emis (GNFR)	-16.3	0.22	7.6	0.39	29.0
"	Higher horiz. res.	-16.3	0.36	7.5	0.30	29.3
"	Higher vert. res.	-12.9	0.33	5.6	0.41	28.6
NO_2	Obs+emis (GNFR)	-13.0	0.57	8.4	0.50	19.2
"	Higher horiz. res.	-13.7	0.59	8.7	0.49	19.8
"	Higher vert. res.	-10.3	0.55	6.2	0.51	18.2
O_3	Obs+emis (GNFR)	17.9	0.33	18.9	0.79	26.8
"	Higher horiz. res.	17.8	0.34	19.2	0.79	26.9
"	Higher vert. res.	5.9	0.36	8.5	0.81	22.0
SO_2	Obs+emis (GNFR)	0.3	0.33	1.7	0.30	3.5
"	Higher horiz. res.	0.8	0.36	1.8	0.29	4.4
"	Higher vert. res.	1.2	0.32	2.5	0.32	4.0

Table 6: Model evaluation statistics for the model updates towards higher spatial resolution for irregular observations of NH_3 and wet depositions of NH_x, NO_y and SO_x.

Component	Model configuration	Bias	Spatial correlation	Spatial RMSE
NH_3	Obs+emis (GNFR)	0.2	0.64	1.6
"	Higher horiz. res.	0.05	0.59	1.4
"	Higher vert. res.	0.5	0.65	2.0
NH_x wflux	Obs+emis (GNFR)	4.0	0.59	100.0
"	Higher horiz. res.	14.6	0.60	99.6
"	Higher vert. res.	-29.8	0.62	97.5
NO_y wflux	Obs+emis (GNFR)	-59.3	0.26	77.8
"	Higher horiz. res.	-57.3	0.27	76.1
"	Higher vert. res.	-69.0	0.32	84.3
SO_x wflux	Obs+emis (GNFR)	-90.4	0.34	115.8
"	Higher horiz. res.	-88.9	0.35	114.5
"	Higher vert. res.	-83.9	0.38	109.2

2.2.2 Update of emission input data

2.2.2.1 Annual totals

The emission information for Germany was updated to the reporting of 2022. Emission inventories are reported every year for the complete timeseries of all past years. This is done to provide consistent time series and to ensure comparability by applying the newest methodology to all years. Hence, the whole timeseries includes a consistent set of emission factors, activity information and techniques to spatially allocate the emissions. As a consequence, for years in the past, emission totals have been reported several times. Due to changing methodologies and new insights in emission factors, reported emission totals may differ considerably between several submissions. In Figure 9, the reported emissions by Germany are shown for NH_3 and NO_x. A decreasing trend of emissions is found for total NH_3 and NO_x emissions in Germany from 2015 to 2019.

Focusing on the emissions reported for 2015, one can see the impact of methodological changes. The first reporting for this year in 2017 shows the largest emissions (759 kton), whereas the 2018 reports 670 kton. The submissions from 2021 and 2022 show again a significant downward revision (639 kton) with respect to submission of 2020 and before. Therefore, the incorporation of the 2022 emission information leads to lower NH_3 emissions in the model calculations in comparison to Chapter 3 and the PINETI-3 results. For NO_x, on the other hand, the national emissions reported in the submission in 2022 are larger than in the submissions of 2019 and before. This increase is mainly caused by emissions from road transport, due to better knowledge about emission factors for this sector. Hence, using emissions from submission 2020 or later instead of earlier years will put about 10 % more NO_x emissions in the model simulations. For SO_2 emissions, the differences between different reporting years are much smaller and not discussed here.

Figure 9: German reported emission totals of NH_3 (left) and NO_x (right) for 2010-2020, for reporting years 2017-2022.

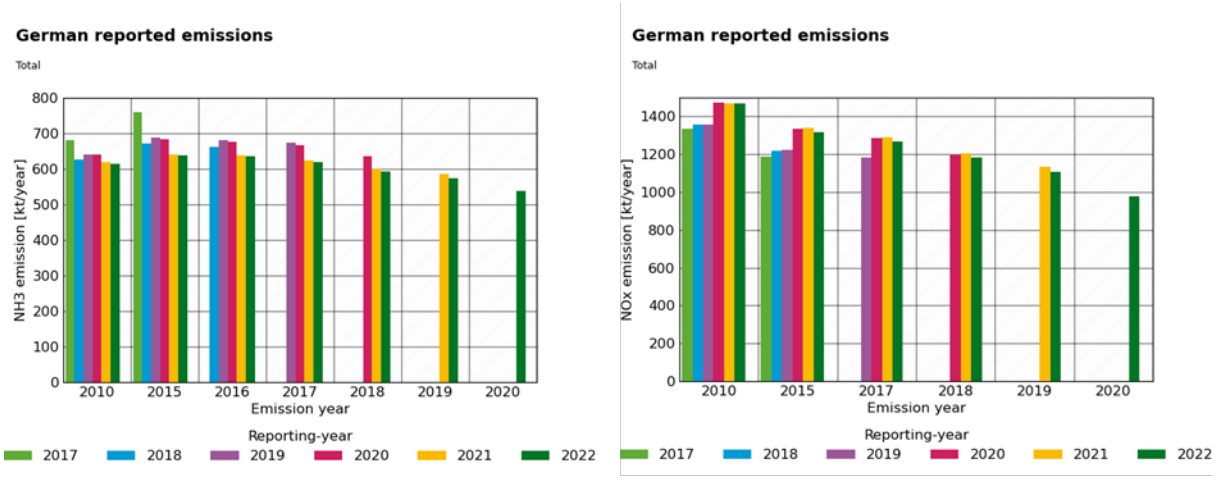

Source: CAMS 5.1

2.2.2.2 Spatial distribution for animal housing in Germany

For animal housing, an updated emission distribution is created by UBA with a better representation of locations for animal housing. With this update, a new emission distribution is generated with the GRETA tool for Germany. The country total of emissions remains the same for both distributions, equal to the reported values. Previous and updated annual emission maps are shown in Figure 10. In the updated distribution, the first part of the emission distribution is

not changed and takes place on a district-by-district basis using data from Thünen Institute. On district level, the GRETA tool distinguishes for the distribution of agricultural emissions between emissions from animal housing (NFR[1]: 3B1a-3B4gii) and emissions applied to soils (NFR: 3Da1-3I). For the emissions applied to soils data from CORINE land cover and additional filters for agricultural areas are used to create a distribution per district. For emissions of animal housing a new stable dataset was derived from the Digital land cover model for Germany (LBM-DE). In combination with available point sources from the Pollutant Release and Transfer Register (E-PRTR) these emissions are distributed like local point sources in the new GRETA version. As a result, higher local emissions are found around housing locations and general agricultural areas have slightly lower emissions. In Figure 11, absolute (left) and relative (right) differences are shown between both distributions.

Figure 10: Total emissions of ammonia (NH_3) for Germany. Left panel: old distribution for animal housing in Germany, right panel: new distribution for animal housing in Germany.

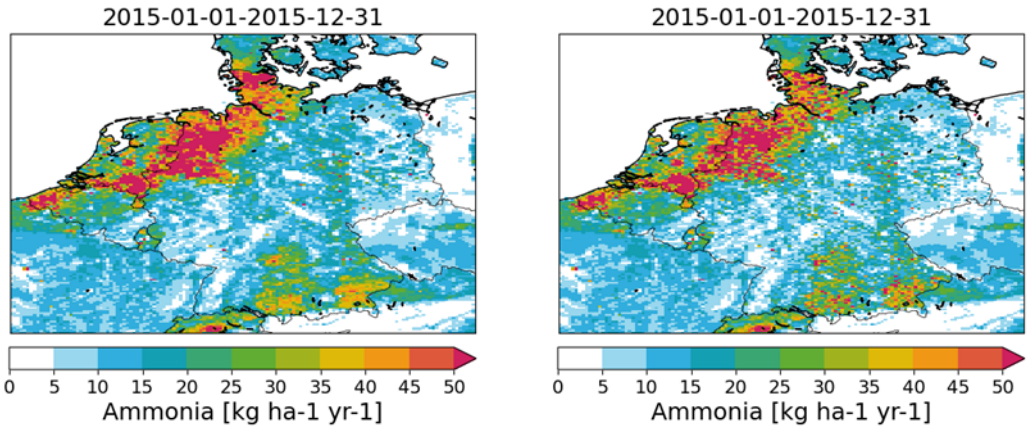

Source: this study

Figure 11: Differences between new and old emission distribution for animal housing. Left panel: Absolute difference(new-old), Right panel: Ratio (new/old).

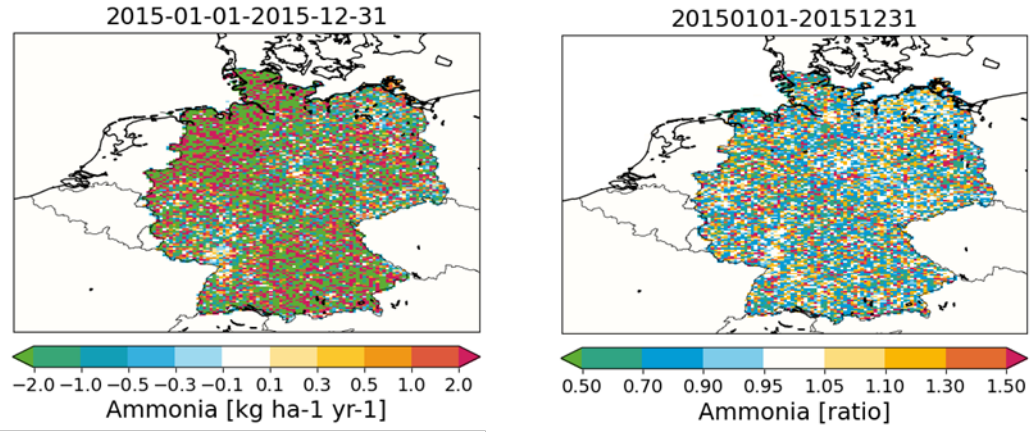

Source: this study

[1] NFR: Nomenclature for Reporting

2.2.2.3 Prescribed emission heights

In the default settings of LOTOS-EUROS, a general height distribution is used for all emissions within one emission sector. For stacked point sources, this distribution is based on average stack heights for each sector combined with generic estimates of plume rise. Thus, pollutants are emitted over a height interval dependent on the emission sector. In total, three different height distributions were used for sector A (Energy production), B (Industry) and J (Waste treatment). Combined with the current use of more vertical layers, it is expected that using more representative emission heights for large stack sources will increase model performance.

In this part, prescribed (static) height distributions by UBA for German sources were incorporated in the model simulations. For sources outside Germany, default distributions were kept in the simulations. Heights are described for German point sources reported in European E-PRTR. For each emission source a height value is assigned, however, all sources within the same (sub)sector of emissions are given the same height. Nine different height levels are given now, replacing only three distributions used before. Note that emissions are now emitted at one fixed height, instead of a (sector specific) height distribution. In general, heights provided by UBA are lower with respect to default height distributions used in LOTOS-EUROS before. As a result, it is expected that concentrations at surface level will be increased with respect to the default distributions.

Impact of using static profiles is shown with an example for coal-fired-powerplants. In the default distribution 51 % of the emissions is emitted between 184-324m and 43 % between 324-522m. With the prescribed heights, all emissions for coal-fired powerplants are emitting at 309m, overall a slightly lower emission height. In Figure 12, the impact is shown for NO_2 concentrations. Annual average concentrations from German coal-fired power plants increase up to 5 µg m^{-3} close to sources, which is an increase of a factor 2 of this source to a distance of 50 km around those large powerplants.

Figure 12: Difference in NO_2 concentrations due to German coal fired powerplants using prescribed static source heights.

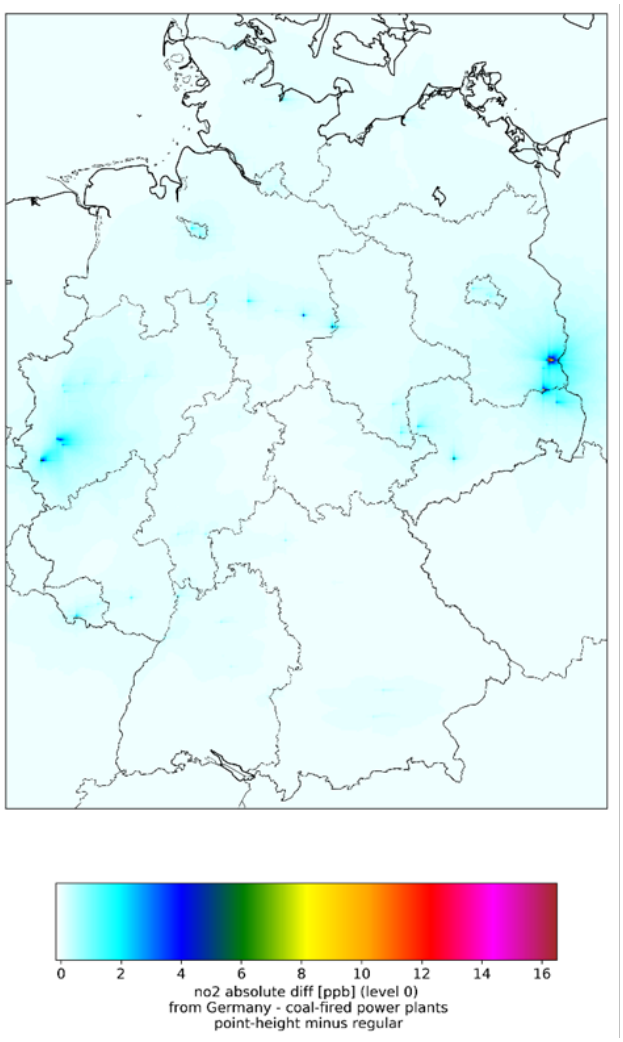

Source: TNO

2.2.2.4 Time profiles

The temporal variability of the emissions is important to prescribe, because they are a key driver to make it possible to model levels of air pollution on hourly resolution. For each emission sector, time profiles are applied to the emissions, which depend on the month, the day of the week and the time of day. Examples are shown in Figure 13 for energy production, agriculture and road transport. In the top panels, monthly profiles are shown with weekly profiles in the lower panels. Combining these profiles, an hourly profile over the year is generated with an average value of 1. In this section, meteorological dependent updates of these profiles are discussed for traffic (2.2.2.4.1) and manure application (2.2.2.4.2).

Figure 13: Default temporal profiles for Energy production and Agriculture (left) and Road- and Off-road Transport (right). Top panel: monthly profiles, lower panel: weekly profiles.

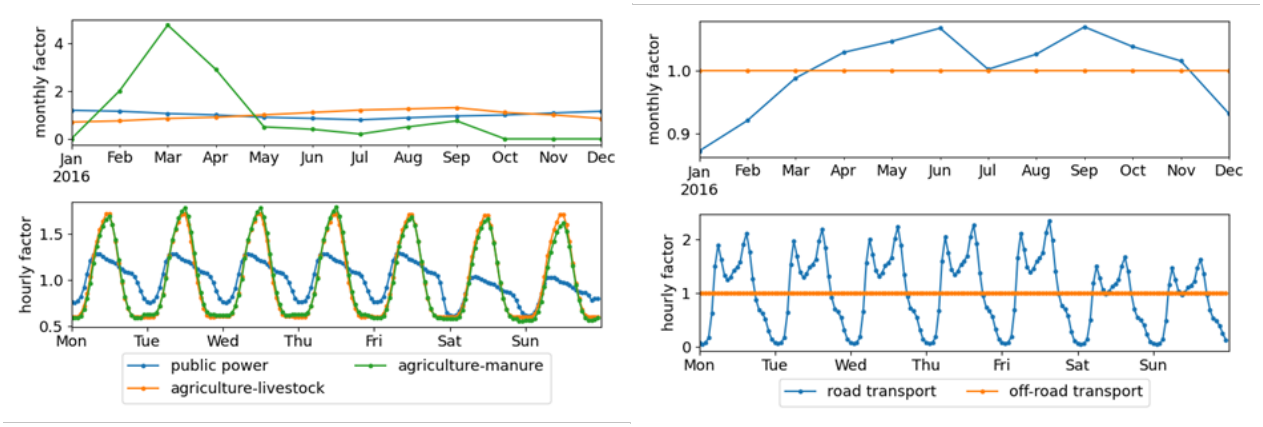

Source: TNO

2.2.2.4.1 Traffic

For traffic emissions, two updates are incorporated in the model calculations. First, generally used temporal profiles are replaced by traffic intensity counts as derived by Mues et al. (2014). These time profiles discriminate different vehicle types (passenger cars, light-duty vehicles and heavy-duty vehicles) and thus incorporate the different behavior during the week and seasons. Second, these profiles do not account for variability in the emission factors with different ambient conditions. This may be especially important for cars running with a cold engine, during which the emissions of several pollutants differ with respect to emissions from a hot engine and after treatment system. This is especially relevant for passenger cars, because they drive over relative short distances and thus a larger share of cold start emissions than long hauls of heavy-duty vehicles. Emissions during cold conditions are calculated via the 'tier 3' method described in the emission handbook of the European environmental agency (EEA)(Dore et al., 2019) . Incorporating an annual temperature pattern, these numbers are used as a temporal profile. In Figure 14, an example of the hourly time profile of NO_x is shown for Berlin for the first week in February 2015 (winter period). The main driver in this temporal pattern is the traffic intensity with high values at weekdays during the rush hours and lower values in the weekend. Temperature effects make significant differences, especially during cold periods. In this week, NO_x emissions are 8 % larger with the temperature dependent profile, with larger differences for some days.

Figure 14: Temporal profile of NO_x emissions in the first week of 2015. Default profiles based on traffic intensity in red. Impact of temperature shown in green.

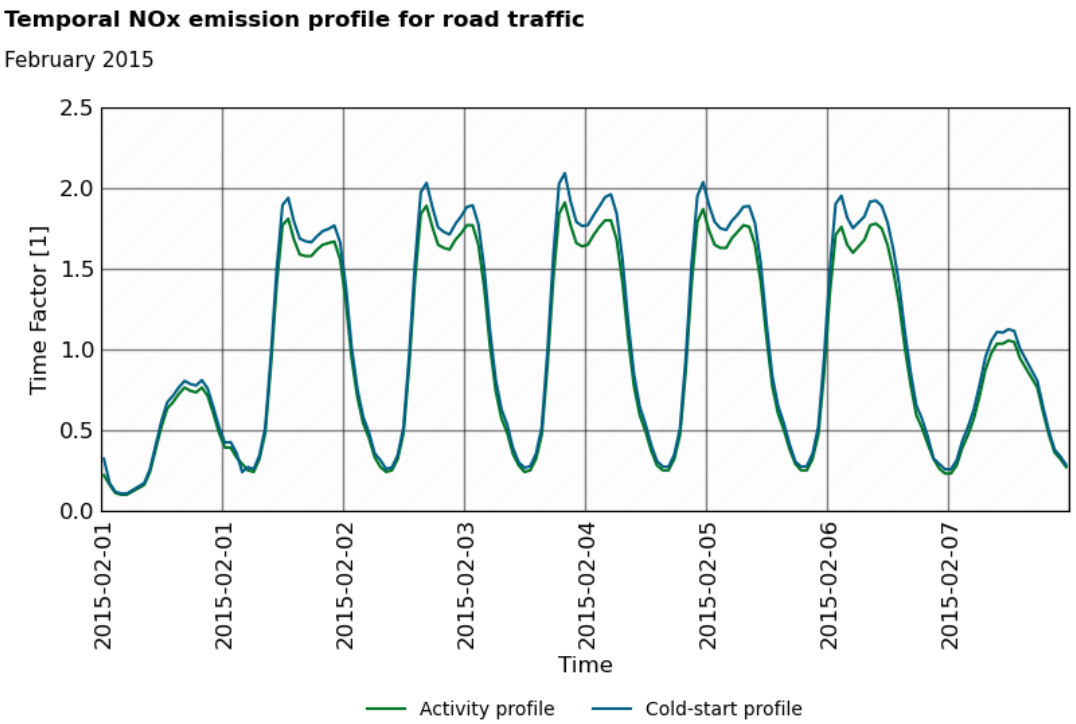

Source: TNO

2.2.2.4.2 Manure application

For ammonia emissions from manure applications, default profiles show high values in spring and slightly elevated levels in September, and low values in the rest of the year. These profiles do not account for different kind of crops, which has different application periods. Further, meteorological circumstances are not directly used in the profile.

To overcome issues discussed above, the method from Skjøth et al. (2011) is applied. This method predicts temporal emission profiles based on crop dependent temperature sums. In Hendriks et al. (2016) is shown that during periods with excessive rainfall or frozen soils, no manure application takes place in in the region of Flanders. This phenomenon is also applied in this update and used on the whole model domain. An example of the updated profile is shown in Figure 15 at the location of Altes Land in Niedersachsen, as this location is in the area with highest ammonia emissions in Germany. At this location, the annual pattern is comparable to the default distribution with emission maxima in spring. However, meteorological dependences show a day-to-day pattern. During the spring period, some days have no emission due to excessive rain fall.

Figure 15: Default and meteorological dependent emission profile for NH_3 at location of station Altes Land in Niedersachsen.

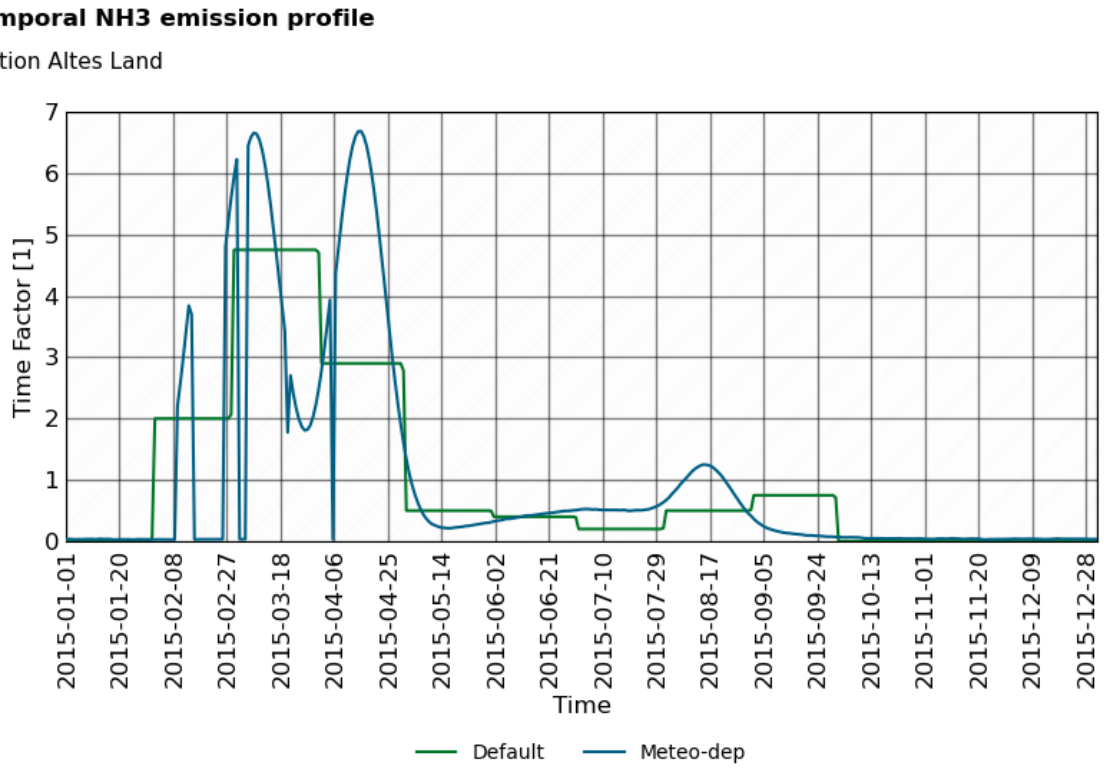

Source: TNO

2.2.2.5 Modelling domains

To setup the final production runs in this study, a three-way nested approach is used. First a simulation is performed covering Europe on ~20x20 km². After that, a simulation covering a large part of north-west Europe on ~6x6 km² is done, and finally the simulation over Germany on ~2x2 km² is nested in this run. Note that for the second domain, this is a small change in resolution from ~7x7 km² to ~6x6 km², with respect to PINETI-3. This is done to match with the resolution of the European CAMS emissions, which had the same change in resolution.

Figure 16: Total modelled depositions of NH_x(left) and NO_y(right) for all three model domains after incorporating all model updates. Top: European domain (~25x25 km), middle: North-west Europe (~6x6km), bottom: German domain (~2x2km).

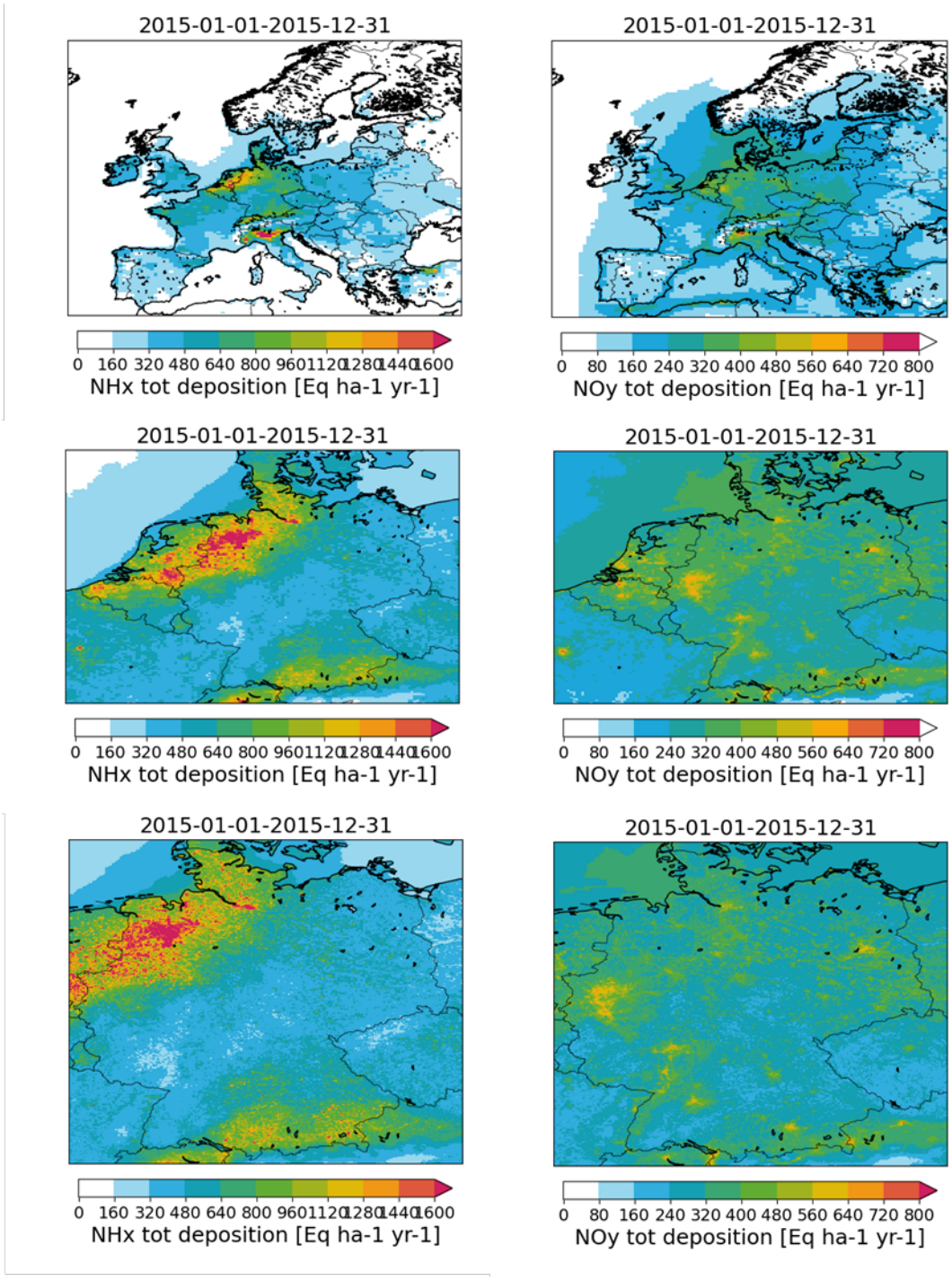

Source: TNO

2.2.2.6 Combined results of emission input updates

In Figure 16, modelled total depositions for NH_3 and NO_x are shown, combining all emission updates as described in Sections 2.2.2.1 to 2.2.2.4 together with updates for increased model resolution. In addition, simulations are provided for all three model domains (Section 2.2.1),

showing that the general patterns are similar across all domains, the higher spatial resolution is clearly visible.

The statistical analysis of all these updates are given in Table 7 and Table 8. Impacts on annual depositions over Germany are shown in Table 9. All results are compared with previous simulations, and updates discussed in this report, where "Production" denotes the simulations that include all updates in the final PINETI-4 model version.

In general, deposition values are increased (12 % for N, 9 % for SO_x) by these updates, mainly driven by increasing the vertical resolution.

Temporal and spatial correlations for all gaseous tracers are increased (or almost unchanged) by all the updates. For example, NO_2 spatial correlation is increased from 0.57 to 0.64 and temporal correlation from 0.50 to 0.54. Other gaseous tracers show comparable impacts. Biases and RMSE are also improved for air pollutants, largest impact is found for O_3, with an overestimation from 18 µg m^{-3} decreased to less than 5 µg m^{-3}. Also, other biases are improved.

For wet deposition fluxes, impacts do vary. For NH_x, biases are increased, ranging from a small overestimation at the beginning to a significant underestimation after implementing all updates. For NO_y and SO_x, impacts are much smaller, while the spatial correlations are increased for NO_y from 0.26 to 0.33.

In general, all improvements are based on methods which should represent reality in a better way. Sometimes this is only visible at specific locations or periods in the year. Overall, one can conclude that model performance is increased by implementing all these updates.

In Section 3, a detailed model evaluation of the production runs is shown to further justify the implemented updates.

Table 7: Model evaluation statistics for the model updates towards production run for hourly time series of NO, NO_2, O_3 and SO_2. In 'Obs+emis (GNFR)', emission updates to GNFR (section 2.2) are implemented. In 'Production', all emission inputs (Section 2.2.2.6) are included.

Component	Model configuration	Bias [µg m^{-3}]	Spatial correlation	Spatial RMSE	Average temporal correlation	Average temporal RMSE
NO	Obs+emis (GNFR)	-16.3	0.22	7.6	0.39	29.0
"	Higher horiz. res.	-16.3	0.36	7.5	0.30	29.3
"	Higher vert. res.	-12.9	0.33	5.6	0.41	28.6
"	Production	-11.8	0.40	5.0	0.43	28.6
NO_2	Obs+emis (GNFR)	-13.0	0.57	8.4	0.50	19.2
"	Higher horiz. res.	-13.7	0.59	8.7	0.49	19.8
"	Higher vert. res.	-10.3	0.55	6.2	0.51	18.2

Component	Model configuration	Bias [µg m^{-3}]	Spatial correlation	Spatial RMSE	Average temporal correlation	Average temporal RMSE
"	Production	-8.7	0.64	5.1	0.54	17.4
O_3	Obs+emis (GNFR)	17.9	0.33	18.9	0.79	26.8
"	Higher horiz. res.	17.8	0.34	19.2	0.79	26.9
"	Higher vert. res.	5.9	0.36	8.5	0.81	22.0
"	Production	4.8	0.42	7.1	0.82	20.8
SO_2	Obs+emis (GNFR)	0.3	0.33	1.7	0.30	3.5
"	Higher horiz. res.	0.8	0.36	1.8	0.29	4.4
"	Higher vert. res.	1.2	0.32	2.5	0.32	4.0
"	Production	0.7	0.31	1.3	0.30	4.2

Table 8: Model evaluation statistics for the model updates towards production run (current model version) for irregular observations of NH_3 and wet depositions of NH_x, NO_y and SO_x. In 'Obs+emis (GNFR)', emission updates to GNFR (section 2.2) are implemented. In 'Production', all emission inputs (Section 2.2.2.6) are included.

Component	Model configuration	Bias	Spatial correlation	Spatial RMSE
NH_3	Obs+emis (GNFR)	0.2	0.64	1.6
"	Higher horiz. res.	0.05	0.59	1.4
"	Higher vert. res.	0.5	0.65	2.0
"	Production	0.9	0.60	2.5
NH_x wflux	Obs+emis (GNFR)	4.0	0.59	100.0
"	Higher horiz. res.	14.6	0.60	99.6
"	Higher vert. res.	-29.8	0.62	97.5
"	Production	-38.3	0.55	110.4
NO_y wflux	Obs+emis (GNFR)	-59.3	0.26	77.8
"	Higher horiz. res.	-57.3	0.27	76.1
"	Higher vert. res.	-69.0	0.32	84.3
"	Production	-77.0	0.33	91.1
SO_x wflux	Obs+emis (GNFR)	-90.4	0.34	115.8
"	Higher horiz. res.	-88.9	0.35	114.5

Component	Model configuration	Bias	Spatial correlation	Spatial RMSE
"	Higher vert. res.	-83.9	0.38	109.2
"	Production	-95.4	0.40	118.3

Table 9: Comparison of the average modelled dry and wet, kriged wet and occult deposition fluxes (eq ha^{-1} yr^{-1}) for 2015 for production runs compared with previous updates. In 'Obs+emis (GNFR)', emission updates to GNFR (Section 2.2) are implemented. In 'Production', all emission inputs (Section 2.2.2.6) are included.

Component	Model configuration	Dry modelled	Wet modelled	Wet kriging	Occult	Total
NH_x	Obs+emis (GNFR)	320	291	298	9	627
"	Higher horiz. res.	320	300	297	9	627
"	Higher vert. res.	425	256	295	9	729
"	Production	388	259	296	10	694
NO_y	Obs+emis (GNFR)	140	143	190	7	336
"	Higher horiz. res.	132	145	190	7	328
"	Higher vert. res.	176	131	189	7	371
"	Production	189	128	190	7	386
N	Obs+emis (GNFR)	460	434	487	16	963
"	Higher horiz. res.	452	445	488	16	956
"	Higher vert. res.	601	387	484	16	1100
"	Production	577	388	486	16	1080
SO_x	Obs+emis (GNFR)	63	59	131	2	197
"	Higher horiz. res.	63	60	131	2	197
"	Higher vert. res.	91	66	133	2	226
"	Production	81	5	131	3	214

2.2.3 High-resolution meteorology

In the operational configuration LOTOS-EUROS is driven by meteorological input data from ECMWF. The meteorological forecast product provided by ECMWF has a horizontal resolution of about 9x9 km^2. The original aim of the project was to acquire meteorological data at a 2x2 km^2 resolution from the DWD to test the performance of the system using the higher resolved input data. The idea was to process the assimilation analyses of the DWD and to make them available as input data to the LOTOS-EUROS CTM. In Table 10, the availability is shown for the COSMO and ICON products from DWD. Contrary to expectations, not all meteorological input variables were available for the period from 2015-2019. For the time before June 2018, no data were available at all. Also, after June 2018 no consistent set of meteorological input became available because updates in the model versions are used in the operational production. This includes major updates from COSMO-DE, to COSMO-D2 and a subsequent change to the new model ICON-D2.

Table 10: Availability of DWD meteorological input

Source	Period available	particularities
COSMO (processed by IVU)	2018-2020	Cloud information not complete until 2018-06-01
COSMO (direct via DWD – Pamore)	2019-06-01 – 2021-02-10	Retrieved by automated download process, only last 18 months are stored. From 2021-02-10 changed to ICON-D2
ICON-D2 (direct via DWD – Pamore)	2021-02-10 --	ICON-D2

To overcome this issue, we have performed an activity to construct a consistent meteorological dataset for 2019 ourselves by setting up regional climate model simulations with ICON at the Institute for Meteorology (IfM) of the Freie Universität Berlin (FUB) and made available to TNO for the chemical transport modelling. The year 2019 was chosen as it is the only year in the production for which we could make a comparison with other products directly derived from DWD as well as with ECMWF. Unfortunately, the calculations are so extensive that the effort to produce a single year of meteorological data in hindsight was practically not possible. Based on the available data the interface with LOTOS-EUROS was developed and tested, meaning that the CTM is ready to use (future) data streams of ICON-DE. Evaluation of LOTOS-EUROS using the coarser ICON-EU data showed that the model performance using ECMWF outperforms the performance with ICON-EU. This fact and the unavailability of high-resolution information motivated to stick to the ECMWF meteorology (interpolated to match the 2x2 km grid) within PINETI-4.

Based on this work we recommend to closely follow the developments with respect the availability of ICON-DE data and to push for a reanalysis providing high-resolution meteorological data by the DWD, enabling a reanalysis of the PINETI timeseries.

3 Results of PINETI-4 model simulations

3.1 Model evaluation for concentrations and depositions

3.1.1 Concentrations

3.1.1.1 Gaseous tracers

Modelled annual average concentration distributions for gaseous tracers (NH_3, HNO_3, NO, NO_2, SO_2 and O_3) are shown in Figure 17. Direct emitted gases show largest concentrations in their source areas. For NH_3, agricultural source regions in Niedersachsen, Bavaria and the Netherlands shows the largest values, while modelled background NO and NO_2 concentrations show the largest values in urbanized and industrial areas. SO_2 concentrations are more confined to the industrial regions in the Ruhr area and the border regions with the Czech Republic. Secondary formed gases like O_3 and nitric acid (HNO_3) show a smoother pattern with less peak regions and a systematic background concentration over the country. The nitric acid concentrations show a minimum annual mean value in the source regions of ammonia, which illustrates the impact of the formation to ammonium nitrate. To verify these model results, all concentrations (except those of HNO_3) were compared with observations across Germany.

In Figure 18, the annual mean modelled concentrations are compared to the observed concentrations in the form of scatter plots. For NH_3, the observed and modelled patterns show a large degree of similarity, although the model shows a tendency to overestimate the concentrations in source regions. The measurement points with the highest observed concentrations are situated in intense agricultural regions in Niedersachsen. Many of the concentration values that are underestimated by the model originate from Mecklenburg-Vorpommern. The spread in the range of observed annual concentrations between 2-5 µg m^{-3} can still be improved. As local emissions have the large impact on the measured concentrations, a more precise localisation of emission sources would be necessary. Nitrogen oxides (NO and NO_2) show an average underestimation by the model, which tend to increase slightly towards higher range observations. NO_2 is systematically underestimated with approximately 10 %, but shows a relatively large correlation between model and observations.

For SO_2, the model overestimates the observed concentrations on an average basis. However, the spread is very large and the correlation is low. Inspection of the time series shows many issues with observational data, detection limits, etc. Hence, it is hard to draw firm conclusions on the poor performance.

In Figure 19, NH_3 concentrations are shown for two stations relatively close to each other in Niedersachsen. The stations at Weserbergland (top) and Altes land (bottom) are shown. Both stations are outside the largest agricultural area, but as they are near, they still have a clear pattern with higher concentrations in March and April during the main fertilisation periods. Also, simulations show higher values in March and April with a good agreement for Altes land, while Wesenbergland shows a clear overestimation by the model. In other regions in Germany similar performance is found, with sometimes large differences between stations closely located to each other. Overall, this indicates that on country scale concentrations are well captured by the model.

Figure 17: Modelled annual average concentrations for 2015. NH_3 (upper left), HNO_3 (upper right), NO (middle left), NO_2 (middle right), SO_2 (lower left), O_3 (lower right).

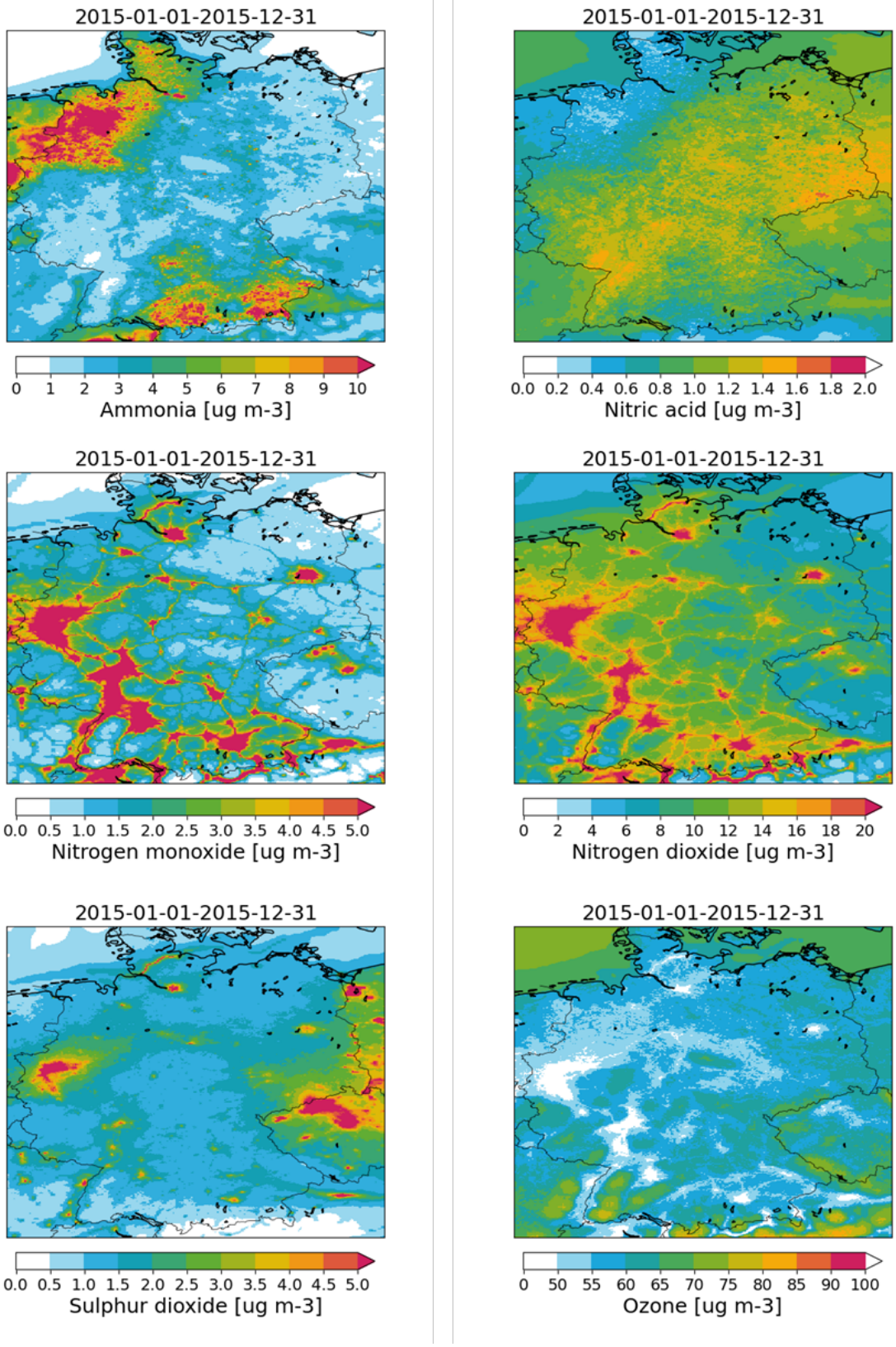

Source: TNO

Figure 18: Annual modelled vs observed concentrations. NH_3 (upper left), NO (middle left), NO_2 (middle right), SO_2 (lower left), O_3 (lower right).

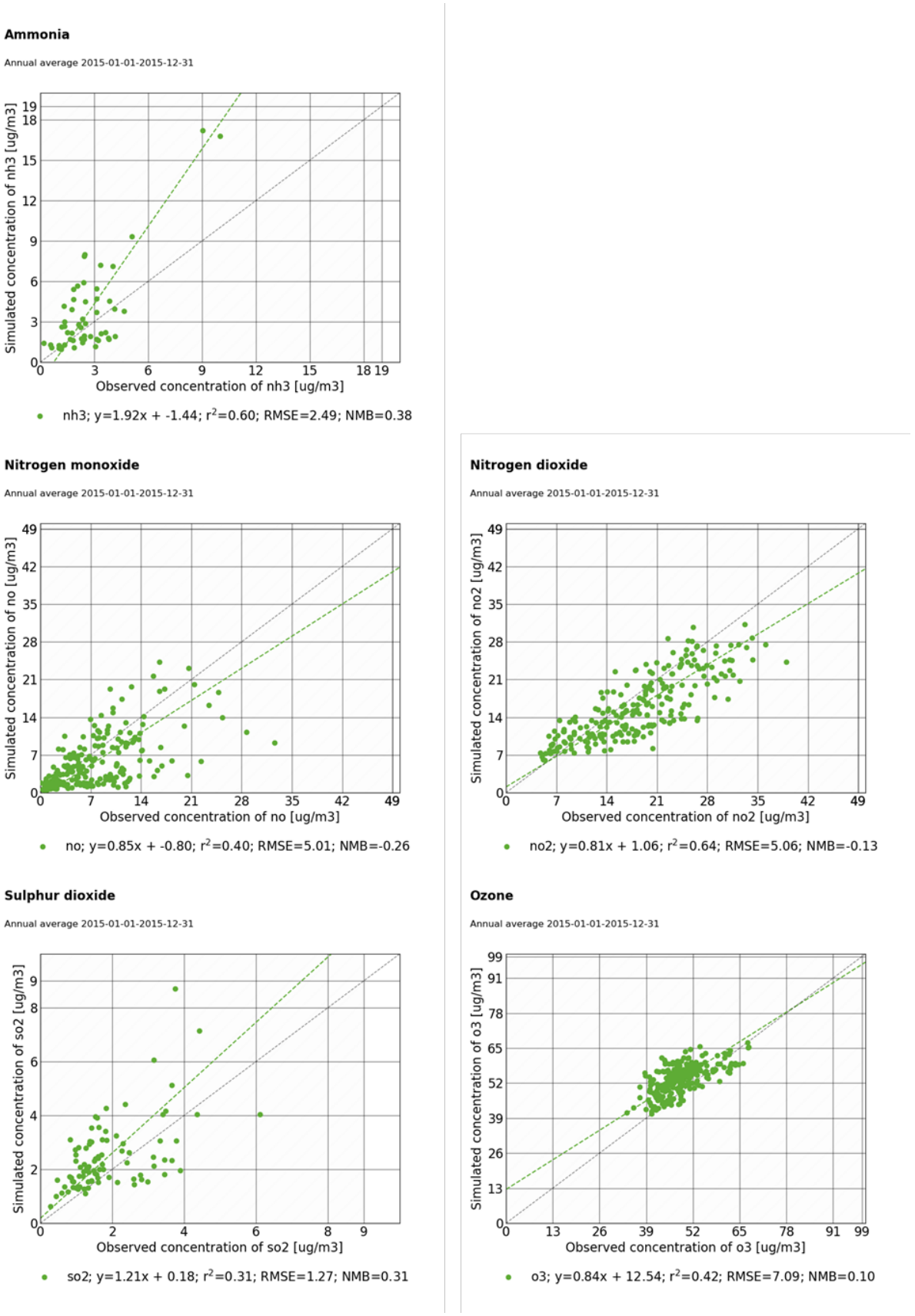

Source: TNO

Figure 19: Timeseries of ammonia simulations and observations for two stations in Niedersachsen; Wesenbergland (top) and Altes Land (bottom).

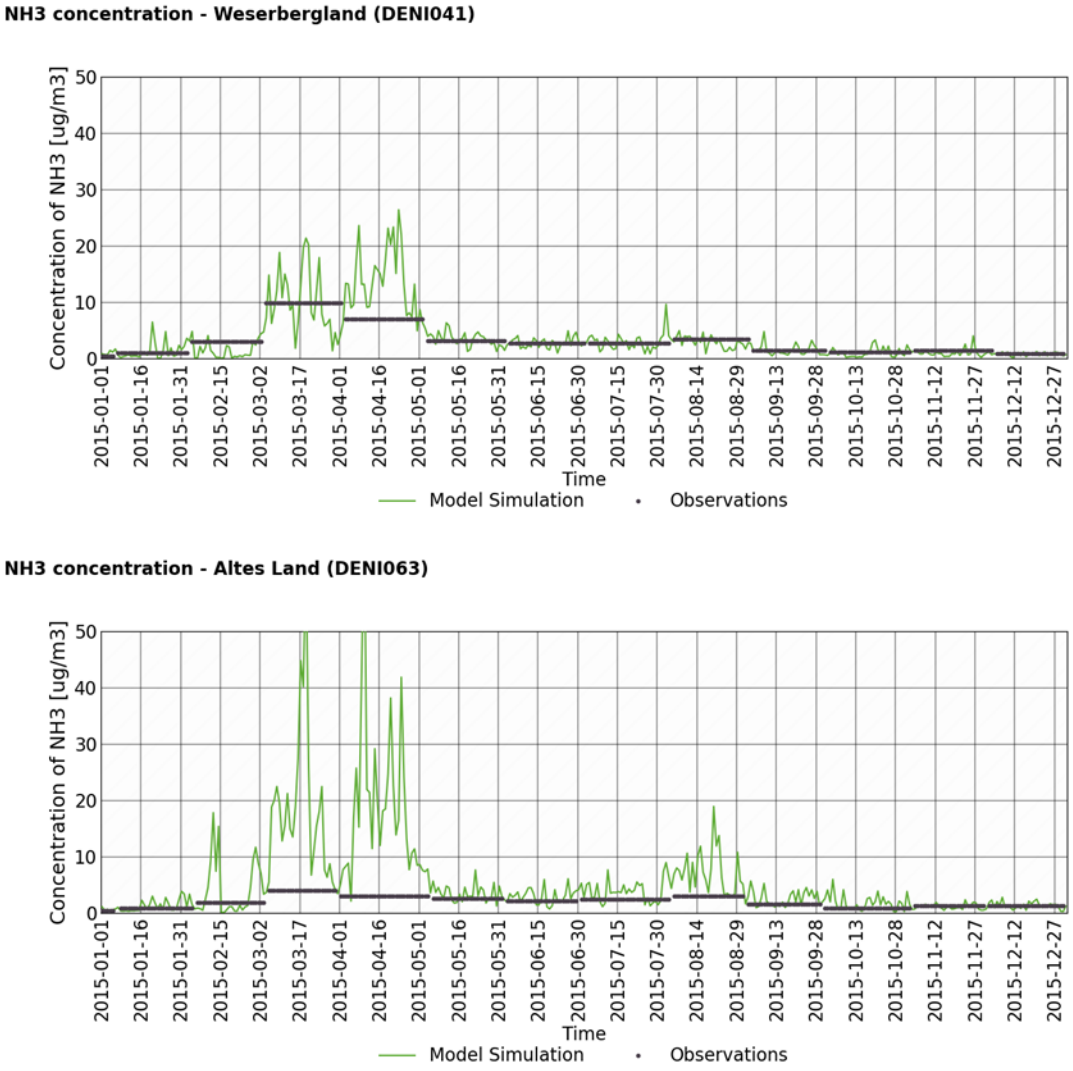

Source: TNO

Figure 20: Timeseries for NO_2 for Schauinsland (top) and Waldhof (bottom).

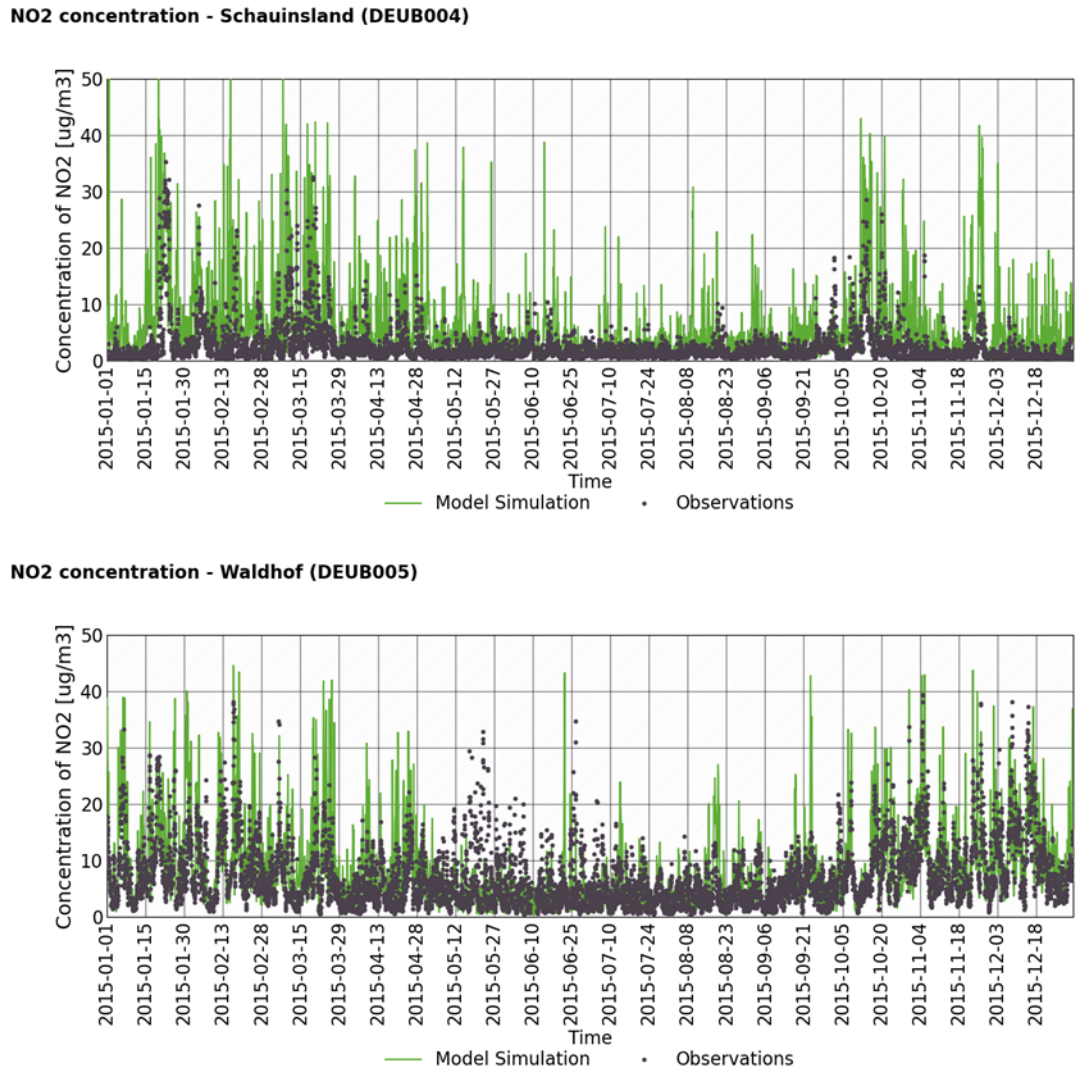

Source: TNO

Figure 21: Timeseries for O_3 for Schauinsland (top) and Waldhof (bottom).

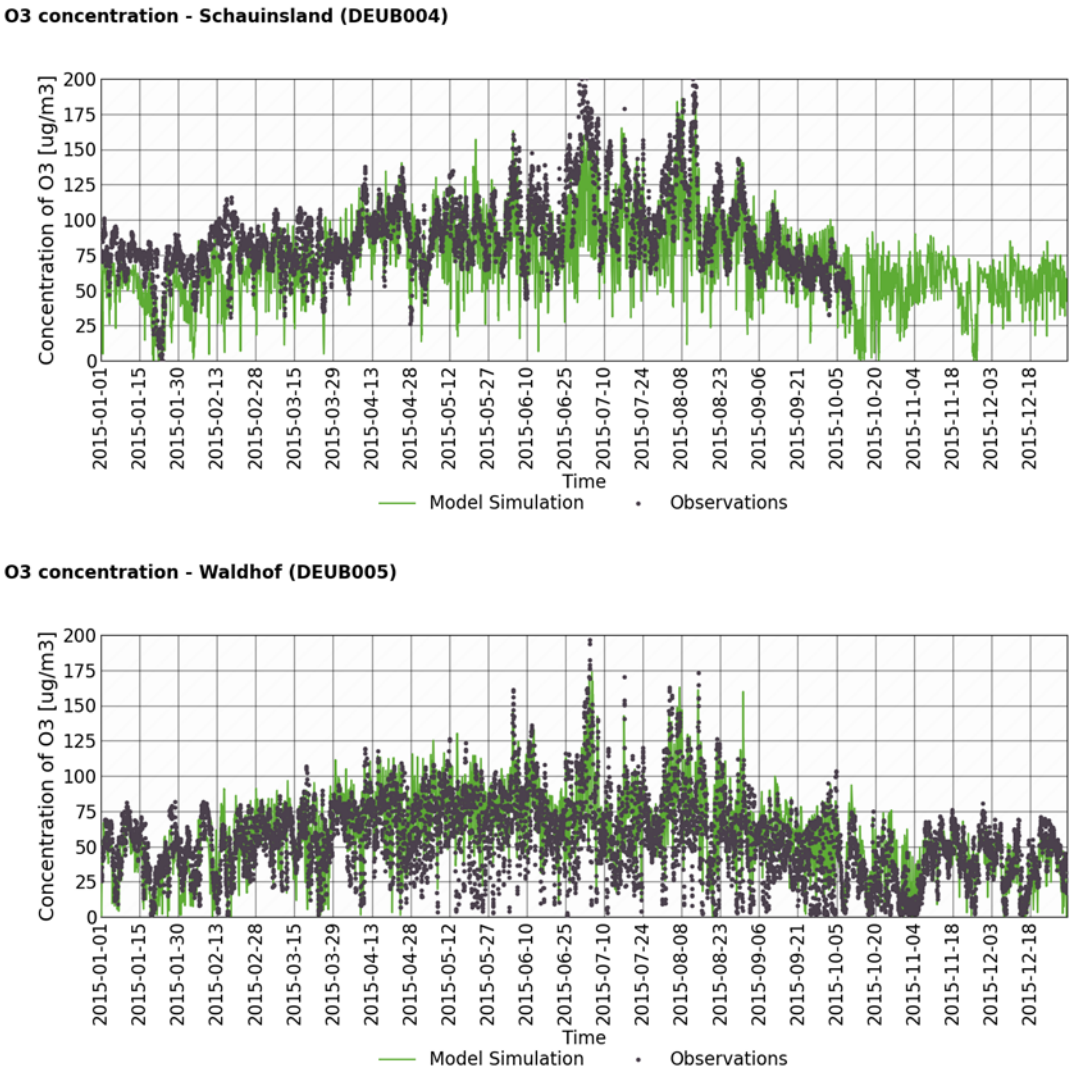

Source: TNO

For NO_2 and O_3, timeseries and diurnal cycles are shown in Figure 20 and Figure 21 for two UBA stations (Schauinsland and Waldhof). At Schauinsland, general values for NO_2 are overestimated by the model, mainly driven by several peaks during summer, which are not seen in the observations. Also, the diurnal cycle (Figure 22) shows two peaks during rush hour, which is not clearly found in the observations. This indicates that the influence by local emissions from road transport is overestimated in the model. For O_3, general values are underestimated, but the diurnal variability is captured well. At Waldhof, both NO_2 and O_3 concentrations are well represented by the model, with only a small overestimation. The diurnal cycle is also nicely captured by the model, with only a small overestimation during night.

Overall, the model shows a good spatial and temporal representation with respect to the observations. At some locations, model performance can be improved. For example, further improvements of emissions and dedicated location dependent temporal emission profiles are expected to increase model performance at specific locations.

Figure 22: Diurnal cycle for NO_2 and O_3 at Schauinsland (this page) and Waldhof (next page).

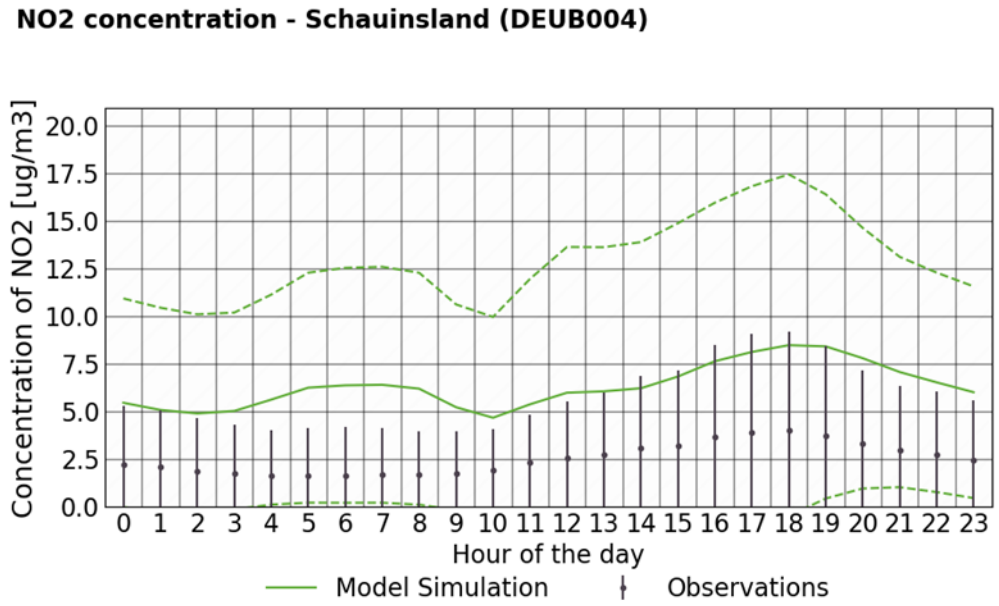

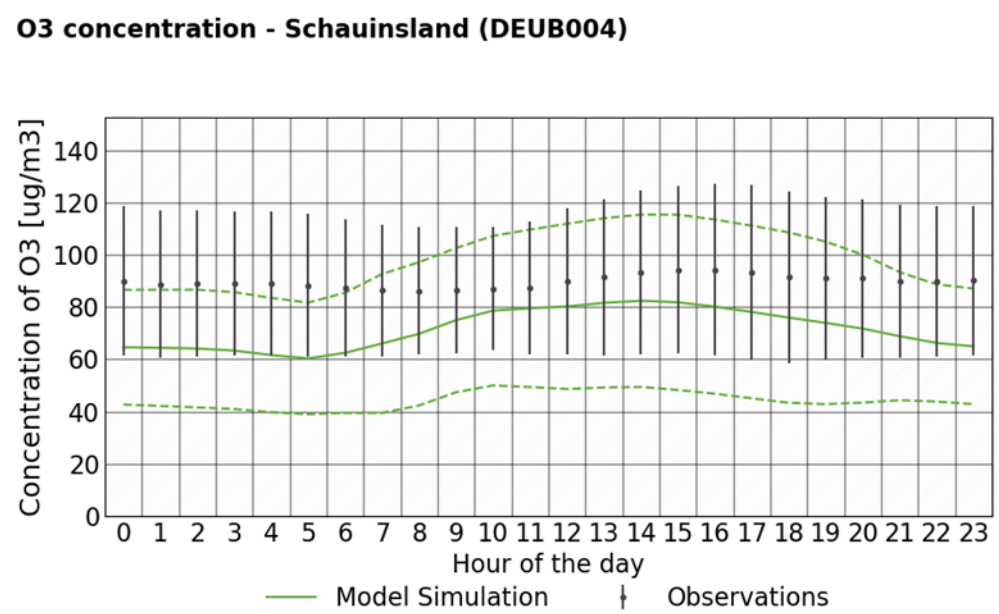

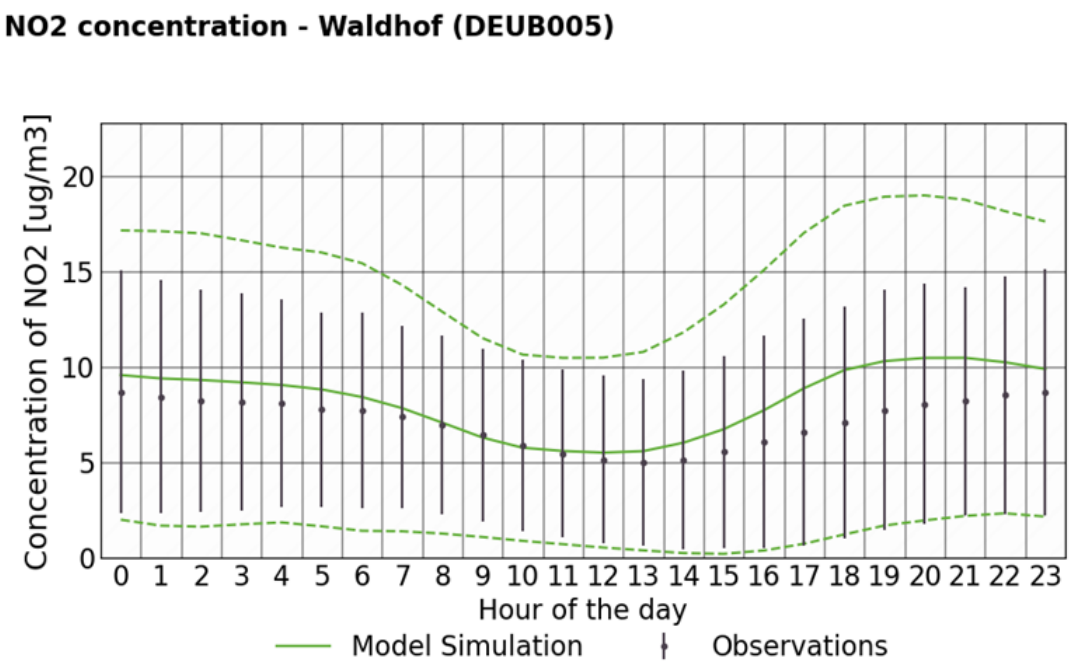

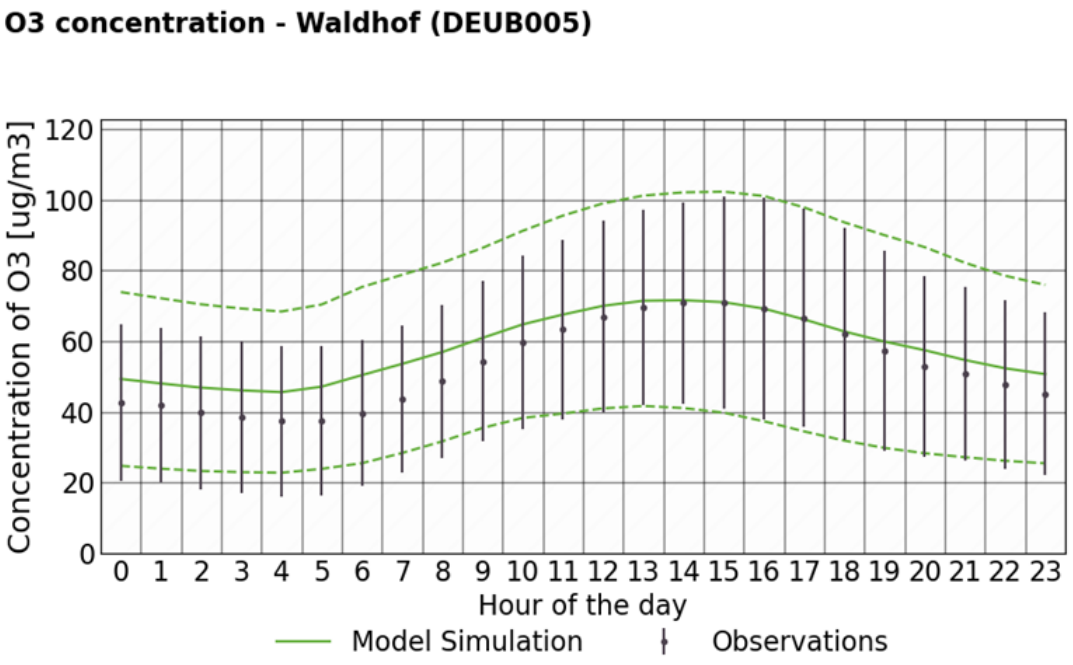

Source: TNO

3.1.1.2 Aerosol components

Unfortunately, much less observations are available for the range of aerosol components. In Figure 23, spatial distributions are shown for SIA components, ammonium, nitrate and sulphate. Because these components are not directly emitted, but formed in the atmosphere, they generate a much smoother spatial patterns gases or aerosols from primary emissions. However, local elevations of SIA are still found close to source areas.

It is difficult to determine a country-wide conclusion of the model performance for all aerosol components, because spatial coverage of observations is limited. In Figure 24 and Figure 25 (ammonium) and Figure 26 and Figure 27 (nitrate), timeseries are shown for UBA stations

Schauinsland and Zingst, together with data for Berlin and Stuttgart retrieved from local authorities. Both ammonium and nitrate are well captured at both UBA stations. Also, in city regions Berlin and Stuttgart, higher values in winter are well modelled, with almost zero concentrations in summer. Overall, SIA components are well captured by the model, so are temporal patterns, and elevated concentrations in cities.

Figure 23: Modelled annual average aerosol concentrations. NH_4 (top left), NO_3 (top right), SO_4 (bottom left).

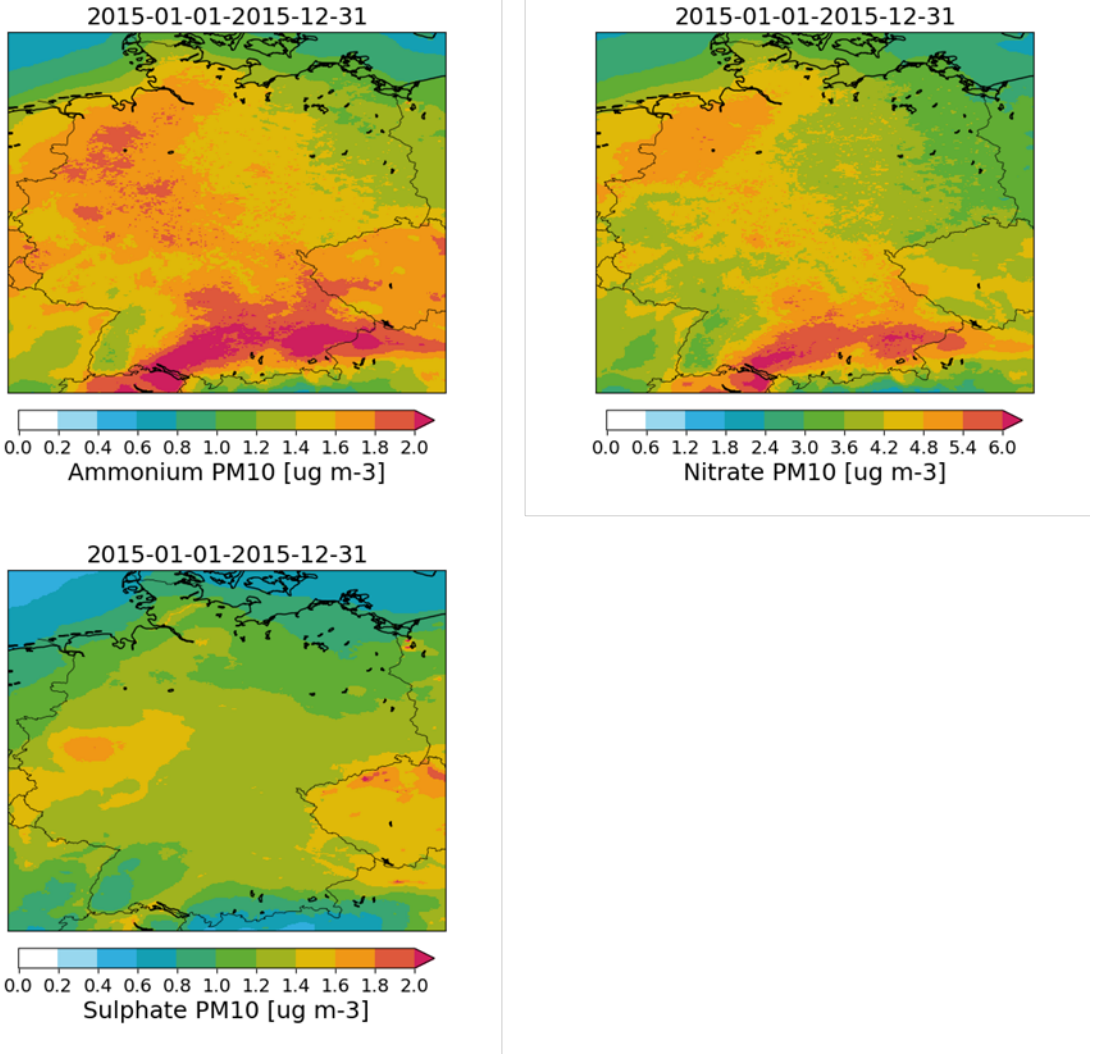

Source: TNO

Figure 24: Timeseries with simulated and observed ammonium concentrations in PM2.5. Observation locations: Schauinsland (top) and Zingst (bottom).

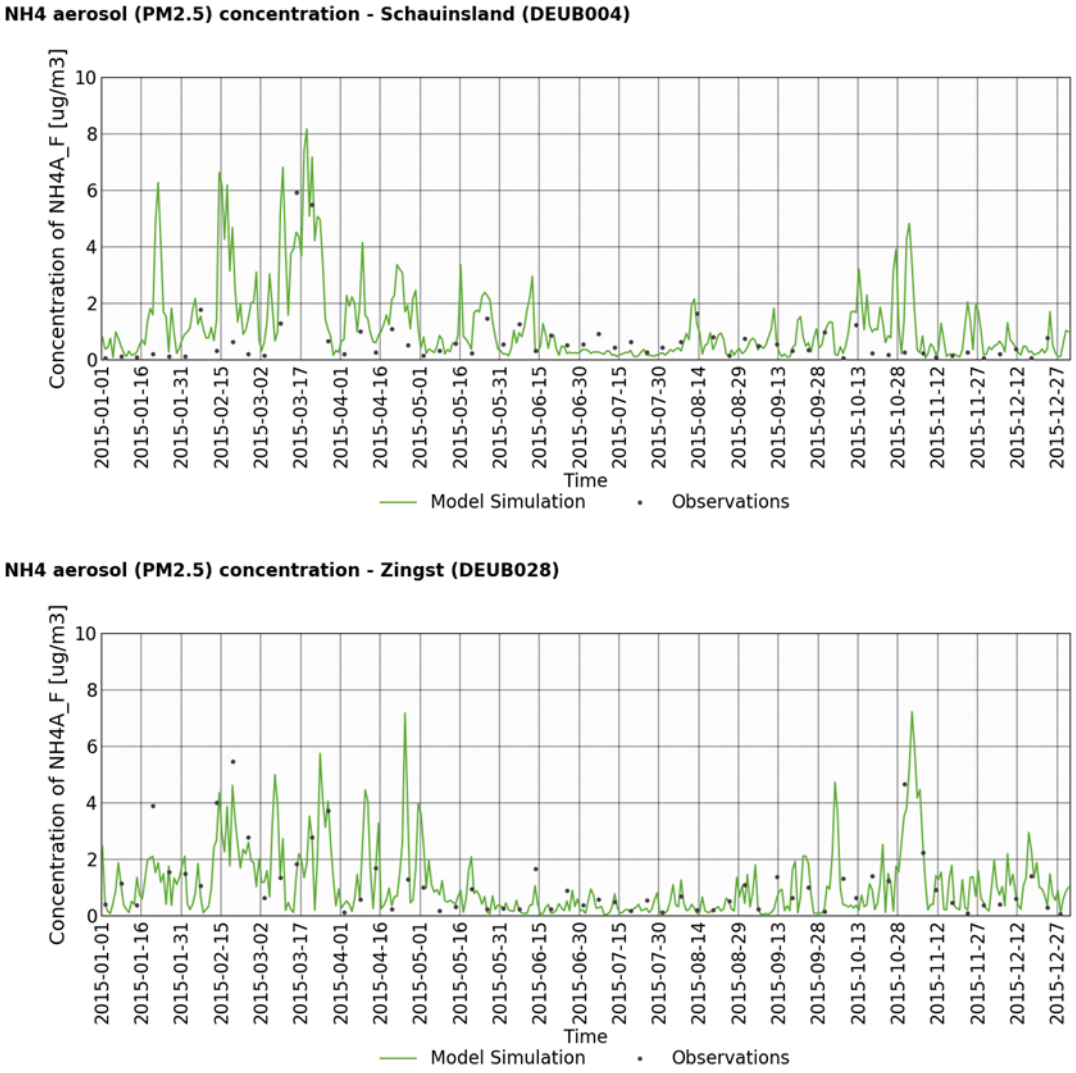

Source: TNO

Figure 25: Timeseries with simulated and observed ammonium concentrations in PM10. Observation locations: Berlin (top) and Stuttgart (bottom).

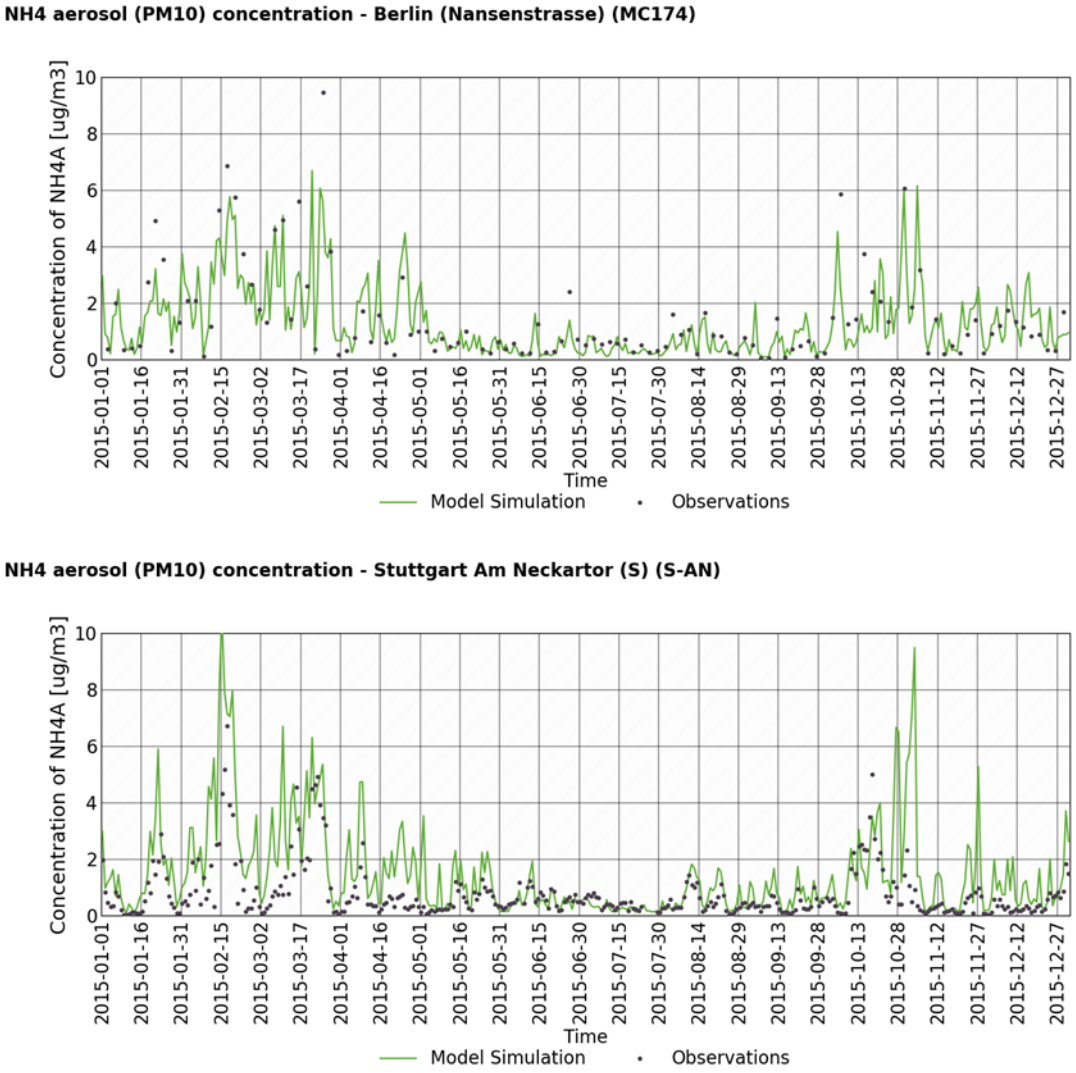

Source: TNO

Figure 26: Timeseries with simulated and observed nitrate concentrations in PM2.5. Observation locations: Schauinsland (top) and Zingst (bottom).

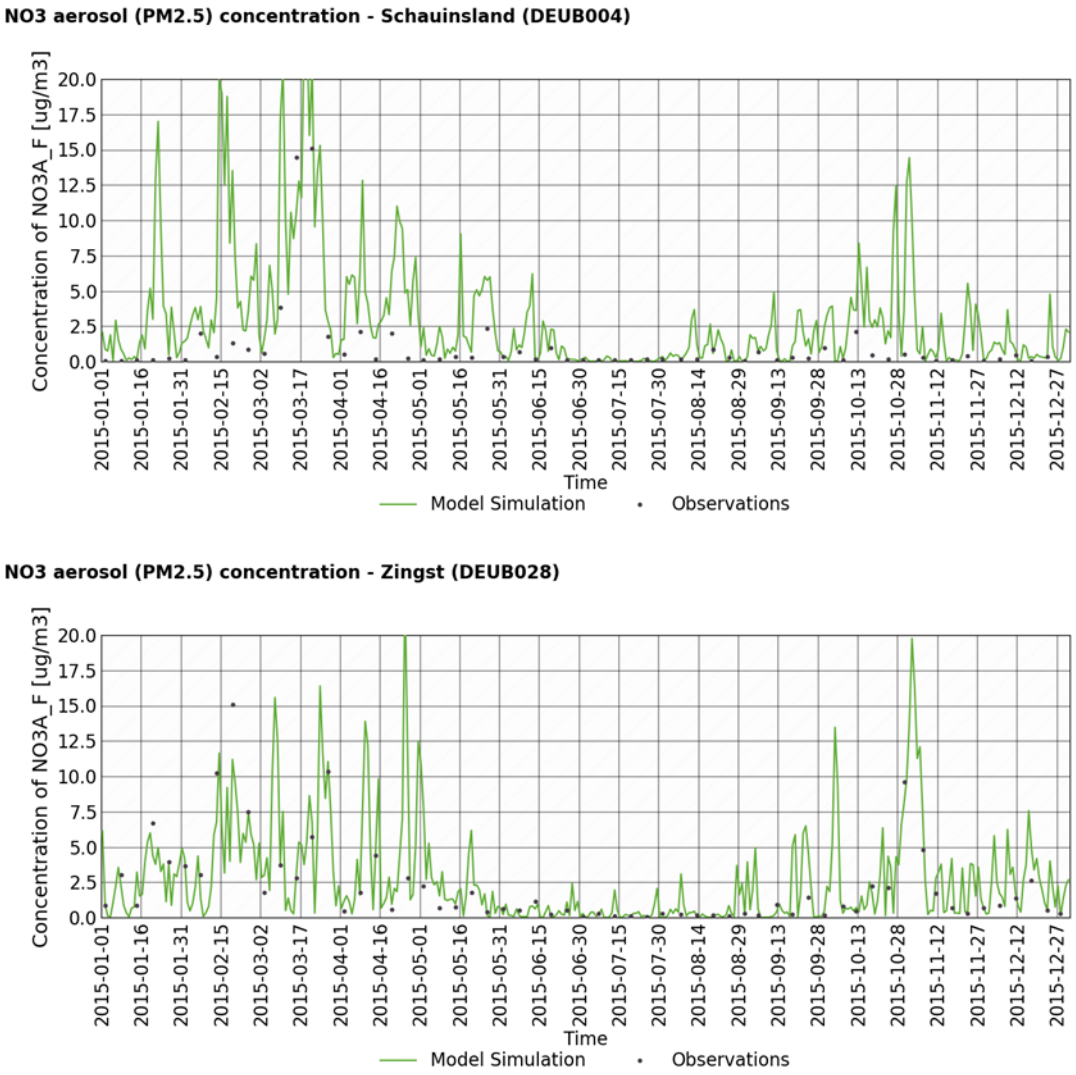

Source: TNO

Figure 27: Timeseries with simulated and observed nitrate concentrations in PM10. Observation locations: Berlin (top) and Stuttgart (bottom).

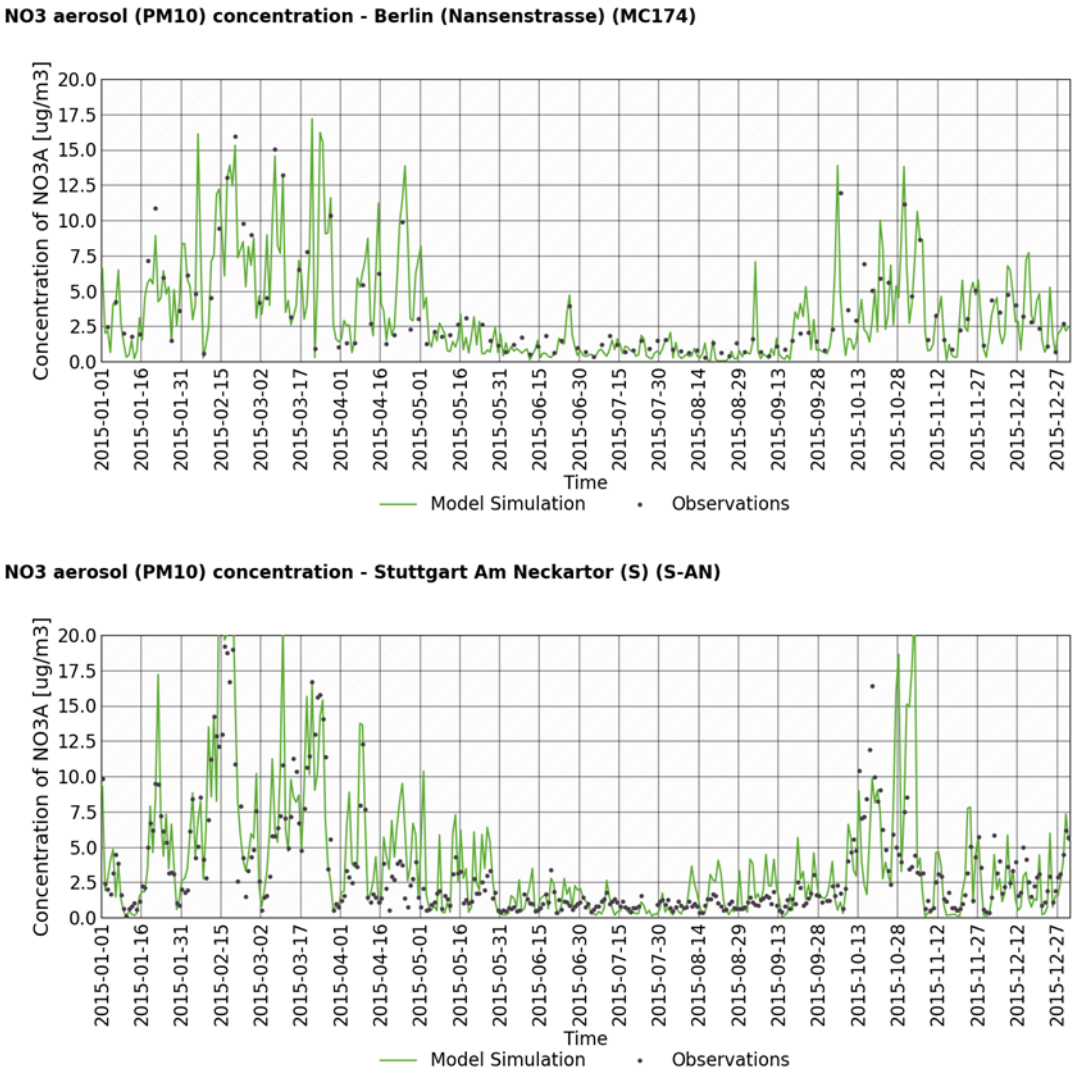

Source: TNO

3.1.2 Depositions

Next to concentrations of air pollutants in air, a large dataset of wet deposition measurements is available for Germany. For dry deposition, only a very limited amount of observations are available. On top of this, uncertainties are very large for these observations. Therefore, only a comparison with wet deposition observations is done. In this comparison both observations from precipitation samplers and bulk measurements are taken as one dataset. The modelled annual dry and wet deposition fields for reduced and oxidized nitrogen, sulphate and precipitation are shown in Figure 28 (dry deposition), Figure 29 (wet deposition of NH_x and NO_y) and Figure 30 (wet deposition of SO_x and precipitation). Values are shown in 'eq ha^{-1} yr^{-1}', which refers to the charges of the respective ions. Since these (NO_3^-, NH_4^+ and SO_4^-) are single charged, the unit 'eq ha^{-1} yr^{-1}' corresponds to mole N for nitrogen compounds and acidity (moles H^+) for sulphate per hectare per year. Dry deposition fields have a higher spatial detail, mostly close to source areas, matching NH_3 sources for NH_x deposition, NO_x sources for NO_y deposition and SO_2 sources for SO_x deposition. Wet deposition fields show identical regions with higher deposition values, but with a smoother pattern. This can be explained by precipitation fields,

which cover usually large spread areas. Annual average deposition for NH_x deposition values are well captured by the model, however local variabilities can be improved. Identical behavior was seen for NH_3 air concentrations in Section 3.1.1.1, which is another indication that reduced nitrogen is well modelled, but spatial (and temporal) detail can be improved. NO_y deposition is systematically underestimated by the model, again in line with NO_2 air concentrations in Section 3.1.1.1. Largest underestimations are found in the north-west part of the country, also mountain areas Harz and the border with Czech Republic show clear underestimations. Some of the large underestimations in southern Germany and the Harz coincide with large underestimations of total precipitation amounts. This indicates that for those regions, improved meteorological input can lead to a better model performance. Finally, for SO_x, also a systematic underestimation is found, while observations of SO_2 in air were generally overestimated (see Section 3.1.1.1). This is an indication that formation of sulphate from SO_2 as well as long range transport of SO_4 needs to be improved in the model.

Figure 28: Modelled annual average dry deposition fluxes. NH_x (upper left), NO_y (upper right), SO_x (lower).

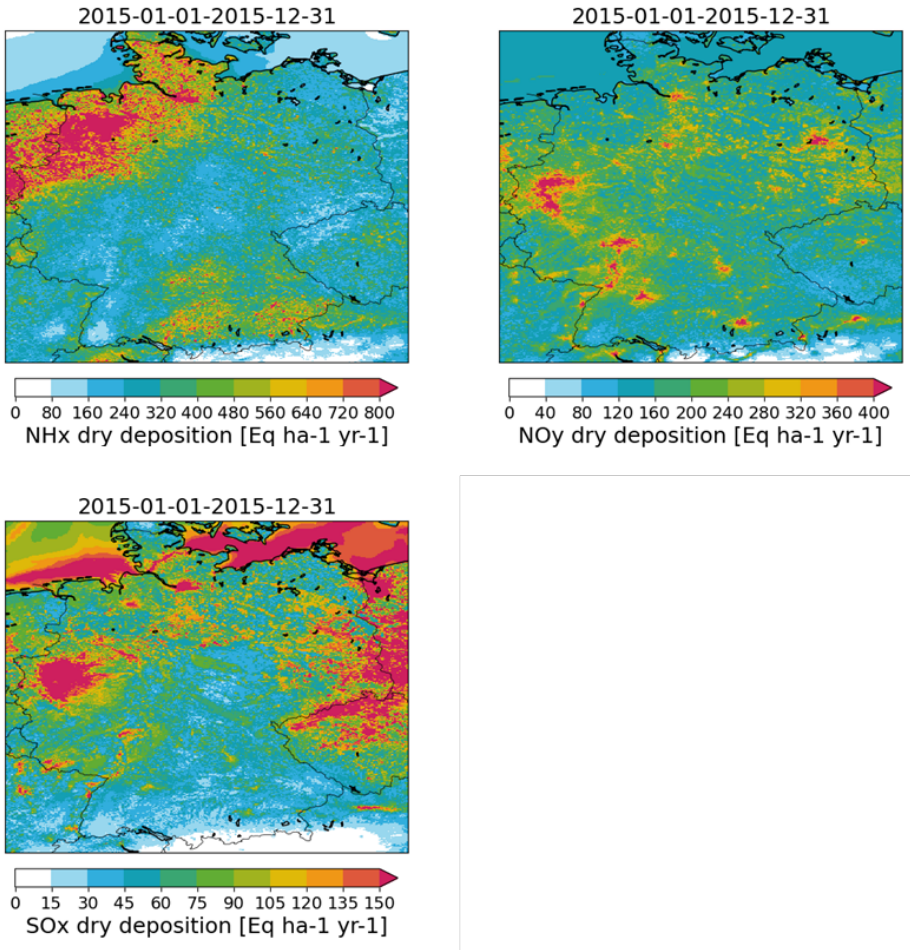

Source: TNO

Figure 29: Modelled and observed annual average wet deposition fluxes. NH_x (top), NO_y (bottom).

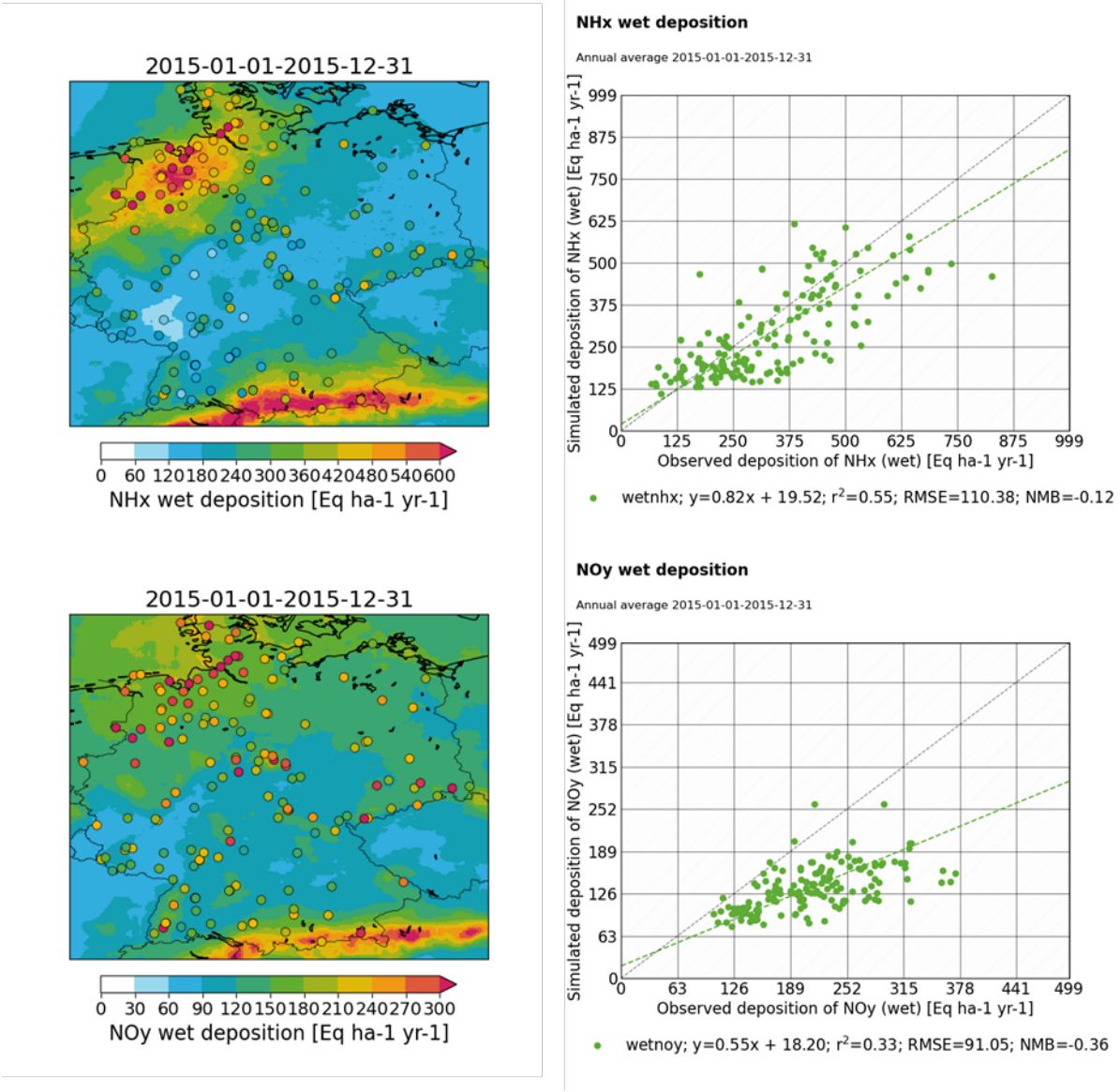

Source: TNO

Figure 30: Modelled and observed annual average wet deposition flux of SO_x (top) and annual precipitation amounts (bottom).

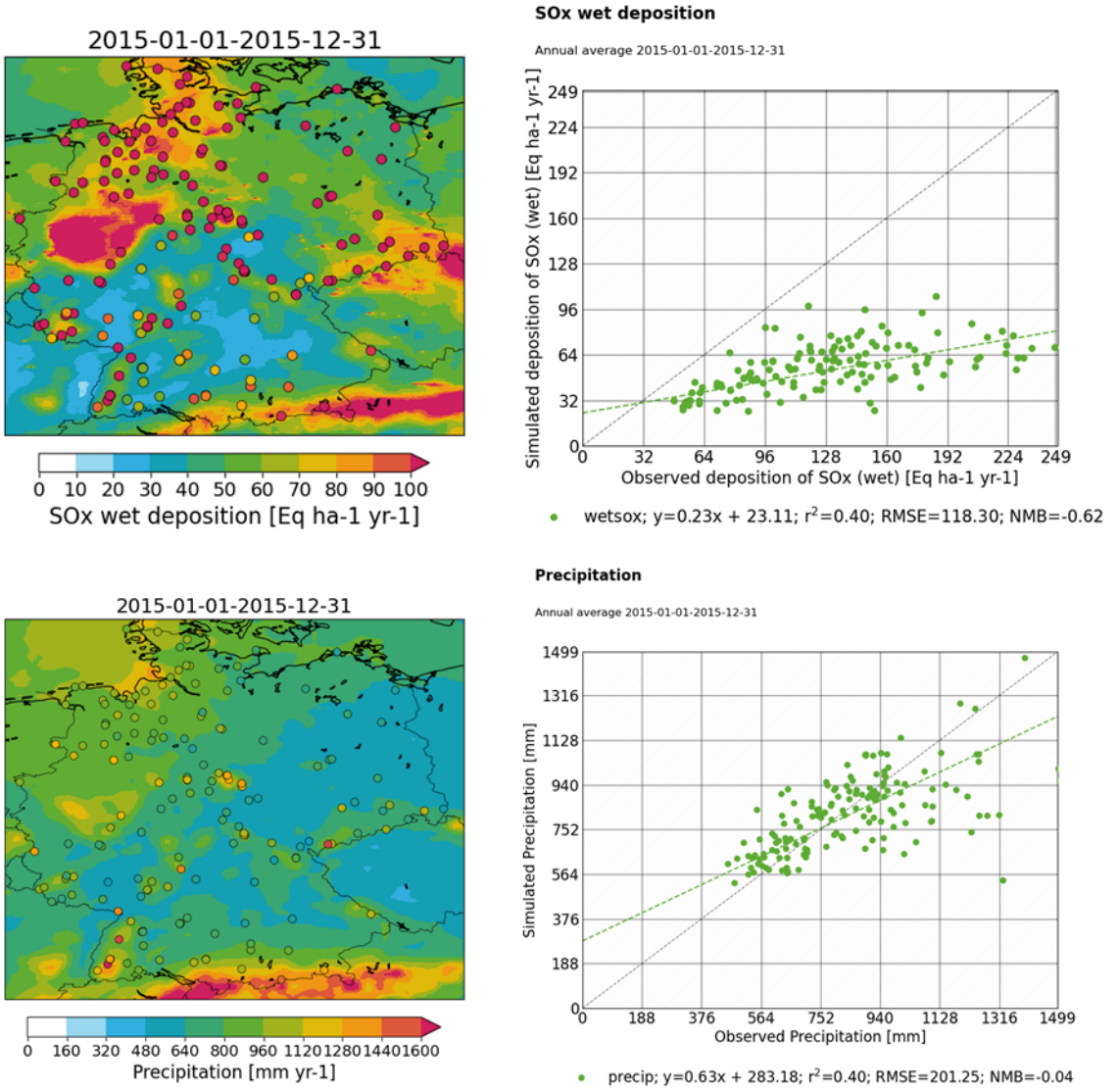

Source: TNO

3.1.3 Conclusions on the model evaluation

Model improvements shown in Section 2.2.1 and 2.2.2, shows a better model performance with respect to observations across Germany compared with the reference in that section. Looking at the statistics tables, biases are lower with about 30 % for NO and NO_2. Overestimation of O_3 is decreased from 17 µg m^{-3} to 5 µg m^{-3}. Both temporal and spatial correlations are also increased for these species. On the other hand, the underestimation of wet deposition is slightly increased for NO_y and SO_x, but spatial correlations are increased for both. Also, the extended model evaluation in Section 3.1 shows that model performance is good. However, improvements are needed for NO_y components and SO_x deposition. Overall, increasing the horizontal resolution and with that the vertical resolution is needed to provide the most detailed deposition maps over the country. Therefore, the current model version including updates from Sections 2.2.1 and 2.2.2 will be used in case studies (Section 3.2) and the production of the final PINETI-4

deposition dataset (Chapter 4). In Chapter 5, possible future improvements for the model and its input are discussed.

3.2 Impact scenarios and source apportionment

3.2.1 Contributions of federal states and neighbouring countries

To support the development of the national nitrogen strategy and devise regional emission targets an effort was made to provide insight into the geographic region of origin of the nitrogen deposited within the federal states.

Within the FP7 project EnerGEO, TNO has developed a system to track the impact of emission categories within a LOTOS-EUROS simulation based on a labelling technique (Kranenburg et al., 2013). In addition to species concentrations and deposition fluxes, the contributions of predefined source categories are calculated and tracked for each process description in the model. The labelling routine is designed for chemically active tracers with a C, N (reduced and oxidized), or S atom, since these are conserved and traceable. The source attribution module for LOTOS-EUROS provides source attribution valid for current atmospheric conditions, since all chemical transformations occur at the same concentrations of oxidants. For details and validation of this source attribution module, we refer to Kranenburg et al. (2013). The source attribution technique has previously been used with a focus on Germany to study the origin of particulate matter (Timmermans et al., 2022), nitrogen dioxide (Thürkow et al., 2023) as well as nitrogen deposition (Schaap et al., 2018).

To quantify the origin of N-deposition in each of the federal states, the model simulation for 2019 is repeated with the application of the labelling method described as above. The labels applied in this simulation encompass all emissions from the 16 individual states, all 9 neighbouring countries of Germany and countries further away (split in west, south, east and north-European countries). Additionally, labels are attached to international shipping emissions, natural emissions, and boundary conditions to cover intercontinental transport. In Table 11, the list of 32 labels can be found. Table 12 further details the countries grouped together in the combined labels. Due to the high computational demand for the labelling method, the model simulation was performed on a resolution of about 6x6 km^2. As shown in Section 2.2.1, increasing the spatial resolution has a limited impact on country-wide deposition values. Hence, it is expected that using the coarser resolution will not have a significant influence on average calculated depositions and contributions for each of the states. Note that results shown below are modelled results without any implementation of the kriging procedure for wet deposition.

Table 11: Predefined labels for source apportionment study, used to quantify origin of deposition in Germany.

German labels	Other labels
Baden-Württemberg (DE-BW)	Netherlands (NLD)
Bayern (DE-BY)	Belgium (BEL)
Berlin (DE-BE)	Luxemburg (LUX)
Brandenburg (DE-BB)	France (FRA)
Bremen (DE-HB)	Switzerland (CHE)

German labels	Other labels
Hamburg (DE-HH)	Austria (AUT)
Hessen (DE-HE)	Czech Republic (CZE)
Mecklenburg-Vorpommern (DE-MV)	Poland (POL)
Niedersachsen (DE-NI)	Denmark (DNK)
Nordrhein-Westfalen (DE-NW)	West-Europe (W-EUR)
Rheinland-Pfalz (DE-RP)	South-Europe (S-EUR)
Saarland (DE-SL)	East-Europe (E-EUR)
Sachsen-Anhalt (DE-ST)	North-Europe (N-EUR)
Sachsen (DE-SN)	International Shipping (Int-Ship)
Schleswig-Holstein (DE-SH)	Natural emissions (Nat)
Thüringen (DE-TH)	Boundary conditions (BC)

Table 12: Specification of combined labels.

Combined labels	Specification
West-Europe	Great Britain, Ireland
South-Europe	Italy, Malta, Portugal, Spain + African countries within European model simulation
East-Europe	Albania, Armenia, Azerbaijan, Belarus, Bosnia, Bulgaria, Croatia, Cyprus, Estonia, Georgia, Greece, Hungary, Kosovo, Latvia, Lithuania, Moldova, Montenegro, North-Macedonia, Romania, Russia, Serbia, Slovakia, Slovenia, Turkey, Ukraine + middle-east countries within European model simulation
North-Europe	Norway, Sweden, Finland

Figure 31: **Contribution to nitrogen deposition on each state in Germany. In green and blue, contribution from own state for NH_x and NO_y, In purple and red contribution from all other states and countries for NH_x and NO_y. Absolute values in the top panel, relative contributions in lower panel.**

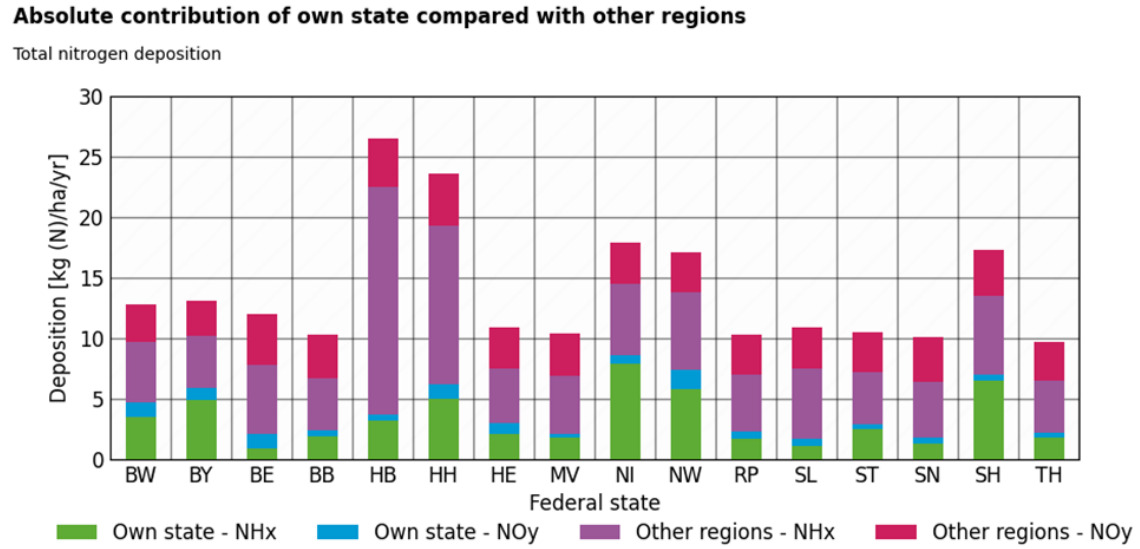

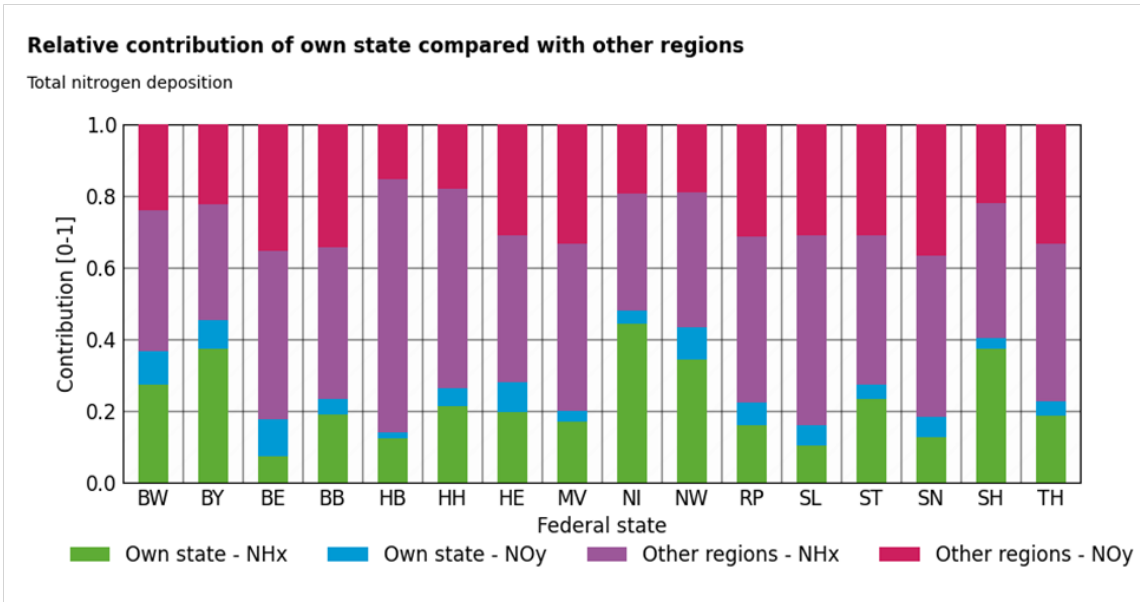

Source: TNO

The contribution of each state's own emissions on the total nitrogen deposition in that state is plotted in Figure 31, together with the contributions of from other regions. In the top panel, absolute depositions are shown for each of the states, with relative contributions in the lower panel. From the figure, it is clear that Hamburg and Bremen have the largest average depositions in Germany, followed by Niedersachsen, Nordrhein-Westfalen and Schleswig-Holstein. Both Hamburg and Bremen are small city states with relatively high NO_x emission densities. However, the local emissions in these states only play a limited role in the local deposition (approx. 20 %), due to their small size. Hence, the main contributions to nitrogen deposition in these city states originate from neighbouring areas, in particular Niedersachsen and Schleswig-Holstein due to their prominent agricultural sector that emits large amounts of ammonia.

The average total nitrogen deposition in Nordrhein-Westfalen is comparable to that of Niedersachsen and Schleswig-Holstein. Despite the abundance of large emitters of nitrogen oxides in the large industrial areas of Nordrhein-Westfalen, nitrogen depositions are also dominated by NH_x, similar to Niedersachsen and Schleswig-Holstein. This can be explained by the height at which these emissions take place: the agricultural (ammonia) emissions take place on ground level, while the industrial (nitrogen oxides) emissions take place at significant heights, causing the emissions to be diluted more by turbulence in the atmosphere and transported over longer distances.

Focussing on the relative contributions of local versus remote contributions to nitrogen deposition (Figure 31, lower graph), a general trend can be spotted that states with dominant NH_x emissions also have the highest local deposition. This holds for Baden-Württemberg, Bayern, Niedersachsen, Nordrhein-Westfalen and Schleswig-Holstein, where on average 40 % of the nitrogen deposition originates from the sources within each state.

In Table 13 and Table 14, the full source receptor matrix is given. The larger absolute average contributions above 1 kg N ha^{-1} yr^{-1} are marked in bold. Focussing on these contributions alone, a couple of conclusions can be drawn. For all states, the contributions from within the state are above 1.0 kg N ha^{-1} yr^{-1}. In addition, there are a few significant features for remote contributions are observed: The highest total nitrogen deposition in the table is the contribution of Niedersachsen on Bremen, which is explained from the fact that Bremen is embedded in Niedersachsen and quite small in size. Similarly, but to a lesser extent, this is the case for Berlin being embedded in Brandenburg and for Hamburg that is wedged between its two largest contributors Niedersachsen and Schleswig-Holstein. The final column represents the deposition on the modelled domain outside Germany, so from each state the deposition outside Germany can be calculated. Note that the total modelled area outside Germany is much larger with respect to German states, therefore depositions are given in different unit. In Appendix A, tables with the source receptor matric are split in (modelled) wet and dry depositions for both NH_x and NO_y. Dry depositions of NH_x have the largest domestic contribution, while wet depositions and especially that of NO_y does not have a large local influence at all.

In general, a trend can be seen of elevated contributions by neighbouring states, especially in the east-west direction. For many states, there is also a considerable contribution of countries surrounding Germany. Emissions from The Netherlands contribute mainly in Bremen, Hamburg, Niedersachsen, Nordrhein-Westfalen and Schleswig-Holstein. This can be attributed to frequent westerly winds that transport nitrogen containing species to countries to the East of The Netherlands. In fact, in all these cases, the foreign contribution to the mentioned states is largest for emissions from The Netherlands. In Nordrhein-Westfalen the Dutch contribution even exceeds the contribution from all other German states together. The other main contributor is France, affecting the southern states most. In particular, the deposition in Saarland is dominated by the French contribution, which even exceeds the sum of all German contributions. Again, this is an effect of Saarland's limited size in combination with the proximity to France.

Regarding the proportion of NO_y in the total nitrogen deposition, it can be concluded that this is larger for larger distances between emission source and the states where deposition takes place. There are two important explanations for this. As already mentioned, a significant proportion of the nitrogen oxide emissions take place at considerable heights in the atmosphere. The second phenomenon that plays a role is atmospheric chemistry. Nitrogen oxides first have to be transformed to HNO_3 before efficient removal takes place. Moreover, during cooler conditions the formation of fine particulate matter is favoured, which is carried over longer distances than its precursors.

The result outlined above indicate that national and international efforts are required to lower the nitrogen deposition across Germany. Targeting NH_3 is the most effective route to ensure local or regional deposition reductions.

Table 13: Contributions to total nitrogen deposition [kg N ha^{-1} yr^{-1}] for each state, (source areas in rows, receiving states in columns). The larger absolute average contributions above 1 kg N ha^{-1} yr^{-1} are marked in bold, contributions from the state on itself are marked in red. Final column Abroad* has different unit (g N ha^{-1} yr^{-1}], because total area is much larger.

	BB	BE	BW	BY	HB	HE	HH	MV
DE-BB	**2.4**	2.1	0.0	0.0	0.1	0.0	0.1	0.4
DE-BE	0.1	**2.1**	0.0	0.0	0.0	0.0	0.0	0.0
DE-BW	0.1	0.1	**4.7**	**1.1**	0.1	0.4	0.1	0.1
DE-BY	0.2	0.2	1.2	**6.0**	0.2	0.5	0.2	0.1
DE-HB	0.0	0.0	0.0	0.0	**3.7**	0.0	0.1	0.0
DE-HE	0.1	0.1	0.1	0.2	0.1	**3.0**	0.1	0.1
DE-HH	0.1	0.1	0.0	0.0	0.1	0.0	**6.2**	0.1
DE-MV	0.2	0.1	0.0	0.0	0.1	0.0	0.2	**2.1**
DE-NI	0.9	0.9	0.1	0.1	**14.1**	0.3	**7.4**	1.2
DE-NW	0.5	0.5	0.2	0.3	**1.3**	0.9	0.9	0.5
DE-RP	0.1	0.1	0.2	0.2	0.1	0.6	0.1	0.1
DE-SL	0.0	0.0	0.0	0.0	0.0	0.1	0.0	0.0
DE-SH	0.2	0.2	0.0	0.0	0.2	0.0	**2.1**	0.8
DE-SN	0.3	0.2	0.0	0.1	0.0	0.1	0.1	0.1
DE-ST	0.7	0.6	0.0	0.0	0.1	0.1	0.1	0.2
DE-TH	0.1	0.1	0.0	0.1	0.0	0.1	0.0	0.1
NLD	0.4	0.4	0.2	0.2	**1.8**	0.4	1.2	0.5
BEL	0.2	0.2	0.2	0.2	0.5	0.3	0.4	0.2
LUX	0.0	0.0	0.0	0.0	0.0	0.1	0.0	0.0
FRA	0.5	0.5	**2.0**	**1.1**	**1.0**	**1.4**	0.8	0.5
CHE	0.1	0.1	0.7	0.5	0.0	0.1	0.0	0.0
AUT	0.1	0.1	0.2	0.5	0.1	0.1	0.1	0.1
CZE	0.3	0.2	0.2	0.3	0.1	0.1	0.1	0.1
POL	0.7	0.7	0.3	0.2	0.2	0.2	0.3	0.5
DNK	0.1	0.1	0.0	0.0	0.1	0.0	0.1	0.2
W-EUR	0.4	0.4	0.3	0.2	0.9	0.4	0.9	0.5
S-EUR	0.1	0.1	0.6	0.5	0.2	0.3	0.2	0.1
E-EUR	0.3	0.3	0.2	0.2	0.2	0.2	0.3	0.3
N-EUR	0.0	0.1	0.0	0.0	0.0	0.0	0.1	0.1

	BB	BE	BW	BY	HB	HE	HH	MV
Int-Ship	0.4	0.4	0.2	0.2	0.7	0.3	0.8	0.6
Nat	0.3	0.3	0.3	0.3	0.2	0.3	0.3	0.3
BC	0.3	0.4	0.6	0.5	0.4	0.4	0.4	0.3
Total	**10.3**	**12.0**	**12.8**	**13.2**	**26.5**	**10.9**	**23.6**	**10.4**
Area	**29349**	**904**	**35862**	**70718**	**334**	**20881**	**735**	**23151**

Table 14: Continuation of Table 13

	NI	NW	RP	SL	SH	SN	ST	TH	Abr.*
DE-BB	0.1	0.0	0.0	0.0	0.1	0.2	0.2	0.1	21
DE-BE	0.0	0.0	0.0	0.0	0.0	0.0	0.0	0.0	1
DE-BW	0.1	0.1	0.3	0.3	0.1	0.2	0.1	0.3	22
DE-BY	0.2	0.2	0.4	0.4	0.1	0.6	0.3	0.8	49
DE-HB	0.1	0.0	0.0	0.0	0.1	0.0	0.0	0.0	1
DE-HE	0.2	0.2	0.3	0.2	0.1	0.2	0.2	0.6	13
DE-HH	0.1	0.0	0.0	0.0	0.4	0.0	0.0	0.0	1
DE-MV	0.1	0.0	0.0	0.0	0.2	0.0	0.1	0.0	15
DE-NI	**8.6**	0.9	0.1	0.1	**2.4**	0.6	**1.3**	0.5	54
DE-NW	**1.7**	**7.4**	0.6	0.3	0.6	0.5	0.7	0.6	50
DE-RP	0.1	0.3	**2.3**	0.5	0.1	0.1	0.1	0.2	11
DE-SL	0.0	0.0	0.2	**1.8**	0.0	0.0	0.0	0.0	2
DE-SH	0.2	0.0	0.0	0.0	**7.0**	0.1	0.1	0.0	21
DE-SN	0.0	0.0	0.0	0.0	0.0	**1.8**	0.2	0.2	16
DE-ST	0.2	0.1	0.0	0.0	0.1	0.5	**2.9**	0.3	16
DE-TH	0.1	0.1	0.0	0.0	0.0	0.5	0.4	**2.2**	11
NLD	**1.7**	**2.1**	0.4	0.2	**1.1**	0.3	0.4	0.4	93
BEL	0.5	**1.0**	0.5	0.3	0.3	0.2	0.2	0.2	59
LUX	0.0	0.1	0.3	0.2	0.0	0.0	0.0	0.0	4
FRA	0.9	**1.5**	**2.4**	**4.3**	0.7	0.6	0.6	0.9	435
CHE	0.1	0.1	0.2	0.2	0.0	0.1	0.1	0.1	34
AUT	0.1	0.1	0.1	0.1	0.1	0.2	0.1	0.1	52
CZE	0.1	0.1	0.1	0.1	0.1	0.6	0.2	0.2	59
POL	0.2	0.1	0.1	0.1	0.3	0.5	0.3	0.2	271
DNK	0.1	0.0	0.0	0.0	0.3	0.1	0.0	0.0	55
W-EUR	0.8	0.9	0.4	0.4	0.9	0.3	0.4	0.3	360
S-EUR	0.2	0.2	0.3	0.4	0.2	0.2	0.2	0.3	650
E-EUR	0.2	0.1	0.1	0.1	0.2	0.4	0.2	0.2	851

	NI	NW	RP	SL	SH	SN	ST	TH	Abr.*
N-EUR	0.0	0.0	0.0	0.0	0.1	0.0	0.0	0.0	104
Int-Ship	0.6	0.5	0.3	0.3	**1.1**	0.3	0.3	0.3	437
Nat	0.3	0.3	0.2	0.3	0.3	0.3	0.3	0.3	160
BC	0.4	0.4	0.4	0.5	0.4	0.4	0.3	0.4	481
Total	**17.9**	**17.1**	**10.3**	**10.9**	**17.4**	**10.1**	**10.5**	**9.7**	**4407**
Area	**4741**	**34244**	**19912**	**2416**	**15492**	**18626**	**20442**	**16068**	**126116**

3.2.2 Impact of emission reduction scenario's

To assess the contribution of different source sectors in a district ("Landkreis" in German terminology) to the deposition in the surrounding regions scenario simulations were performed. These simulations focus on large point sources (Section 3.2.2.1) and area sources from fertilizer application and grazing (Section 3.2.2.2). Also, in Section 3.2.2.2, the impact of county-related emissions of the animal housing and the road transport sectors were assessed. UBA supplied emission reduction scenarios in the form of GRETA gridded inventories with emission reductions in six counties spread across Germany. These six counties were chosen such that areas are covered with different background concentrations of NH_3 and different types of emissions sources (see Table 15, Table 16 and Table 17). With this setup, the behaviour can be quantified within different background levels.

Table 15: Regions and point sources within those regions used for emission reduction scenarios. (*Area of Landshut includes the independent city of Landshut)

Region	NH_3 background	Emission height	Type of facility	NH_3 emissions [ton N]	NO_x emissions [ton N]	Area [km^2]
Warendorf	High	Stack (148 m)	Cement production	162.2	95.8	1319
Schwäbisch Hall	Medium/high	Surface (1 m)	Animal husbandry (poultry)	27.4	0.0	1484
Landshut*	Medium/high	Surface (1 m)	Animal husbandry (swine)	10.2	0.0	1413
Ludwigslust-Parchim	Low	Surface (1 m)	Animal husbandry (swine)	9.3	0.0	4767
Harz	Low	Surface (1 m)	Animal husbandry (swine)	233.9	0.0	2104
Wittenberg	Medium	Stack (136 m)	Fertilizer production	299.8	146.3	1932

3.2.2.1 Impact of large point sources (LPS)

In each of the six regions, emissions of one large point source were reduced. Note that these point sources are both surface emissions (4) and high stack (2) ammonia emissions. With these emission reductions, a model calculation and evaluation based the methodology described in Chapter 2 was performed. In Figure 32 and Figure 33, the impact on deposition of nitrogen compounds is shown. For all point sources, reductions of the NH_x, deposition were found, albeit a small increase of NO_y deposition was observed due to the different chemical composition in air.

For the individual sources, the impact is shown as a function of distance to the source in Figure 34 and Figure 35. For an intersect through the fixed latitude of this source, impact on deposition of this source is shown up to a range of 60 km. The simulation at 2x2 km^2 show significant larger impact close to the source with respect to the simulation at 6x6 km^2. But for distances further than 10 km for the source, both simulations show similar impacts.

To quantify the impact on the deposition independent of absolute reductions, depositions are calculated relative to the emission reduction. In Figure 36, the cumulative deposited NH_x up to a given distance to the source is shown as a fraction of the reduced emissions. For the surface sources, about 18-22 % of the emitted mass is deposited within a radius of 20 km from the source. No dependency on NH_3 background level is obvious. Hence, for surface emissions a rule of thumb of 20 % within 20 km can be taken from these simulations. For the stack sources in Warendorf and Wittenberg, the reduction of NH_x deposition within 20 km of the point source is close to 5 % of the emission reduction. Therefore, for both stack sources, the impact on the direct surrounding is relatively small.

Note that the absolute emission reduction in Ludwigslust-Parchim was very limited, in comparison to those of the others. Although the distances to the location of the other point sources is large, the impacts of the other point sources were significant with respect to those of Ludwigslust-Parchim itself. Therefore, the distance dependency for Ludwigslust-Parchim is not shown here. Furthermore, these simulations should be repeated with single sources in a single simulation to extend the range above 60 km.

Figure 32: **Impact on total modelled nitrogen deposition as a result of emission reductions for the selected large point sources in Warendorf (top), Schwäbisch Hall (middle) and Landshut (bottom). Left: Absolute change, right: Relative change.**

Source: TNO

Figure 33: **Impact on total modelled nitrogen deposition as a result of emission reductions for the selected large point sources in Ludwigslust-Parchim (top), Harz (middle) and Wittenberg (bottom). Left: Absolute change, right: Relative change.**

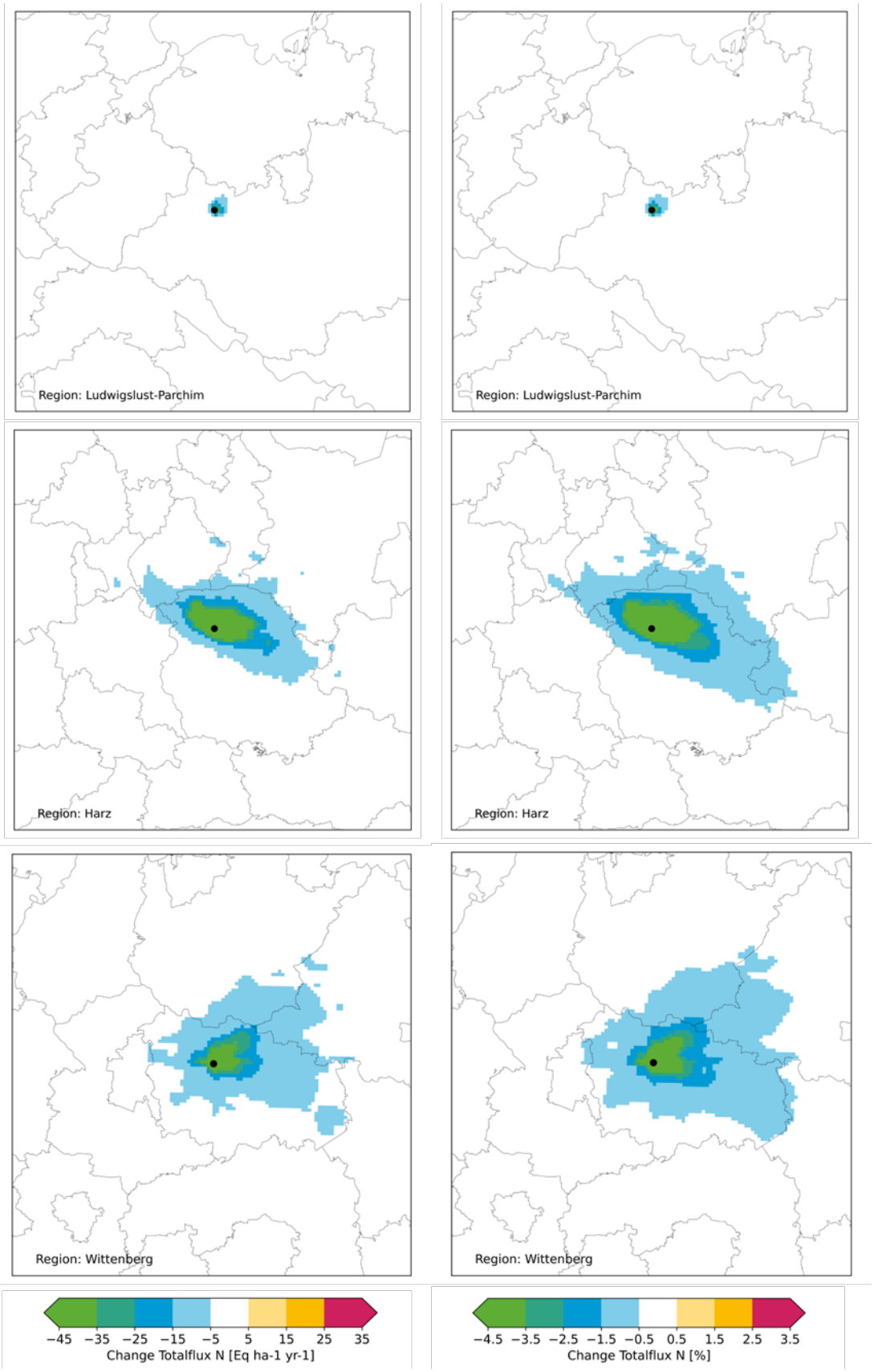

Source: TNO

Figure 34: **Impact on NH_x deposition at a fixed latitude intersect through the large point source in Warendorf, Schwäbisch Hall and Landshut. Impacts are shown for both runs on ~6x6 km² and ~2x2 km² resolution as a function of distance to the source.**

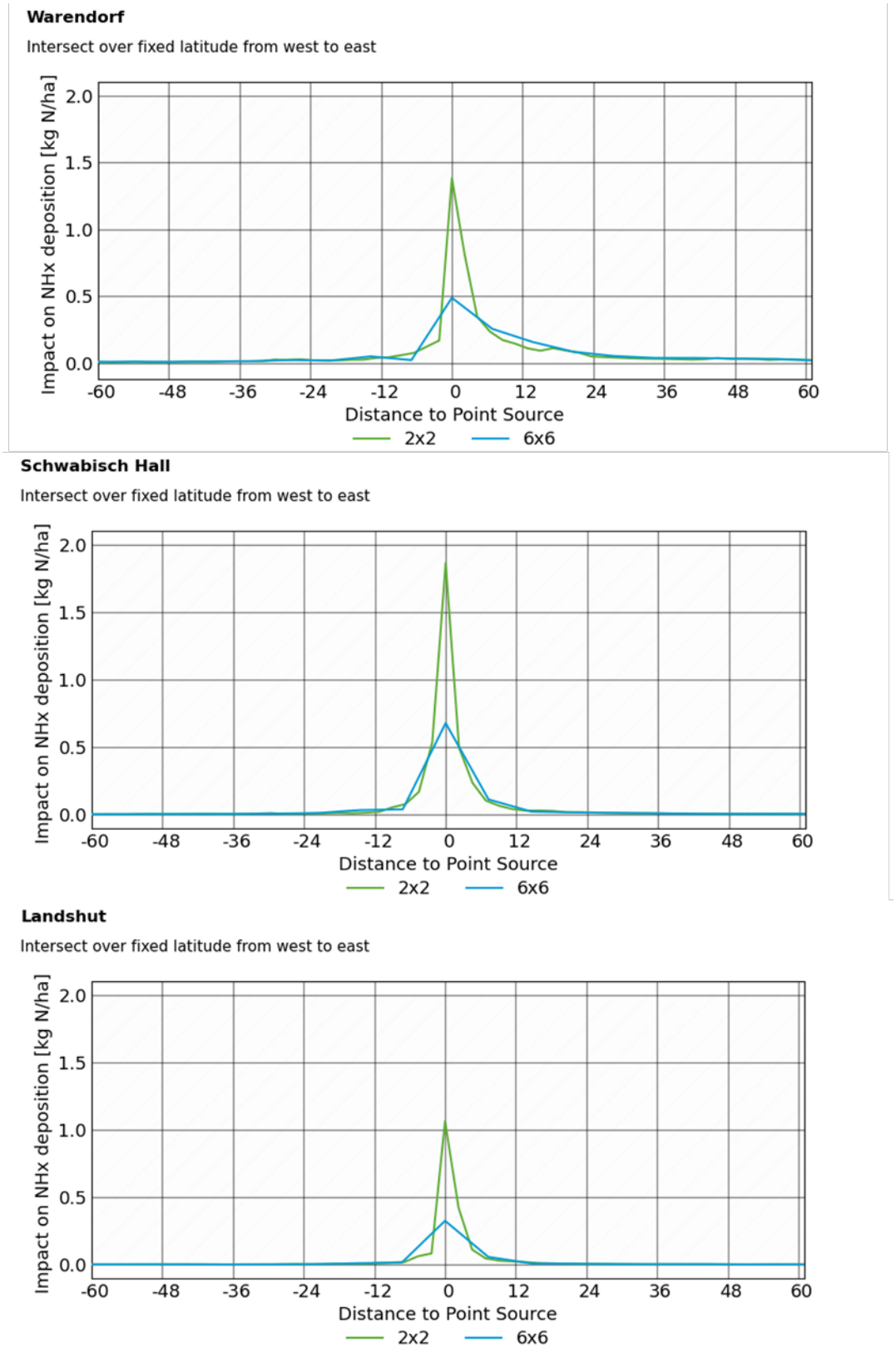

Source: TNO

Figure 35: Impact on NH_x deposition at a fixed latitude intersect through the large point source in Ludwigslust-Parching, Harz and Wittenberg. Impacts are shown for both runs on ~6x6 km² and ~2x2 km² resolution as a function of distance to the source.

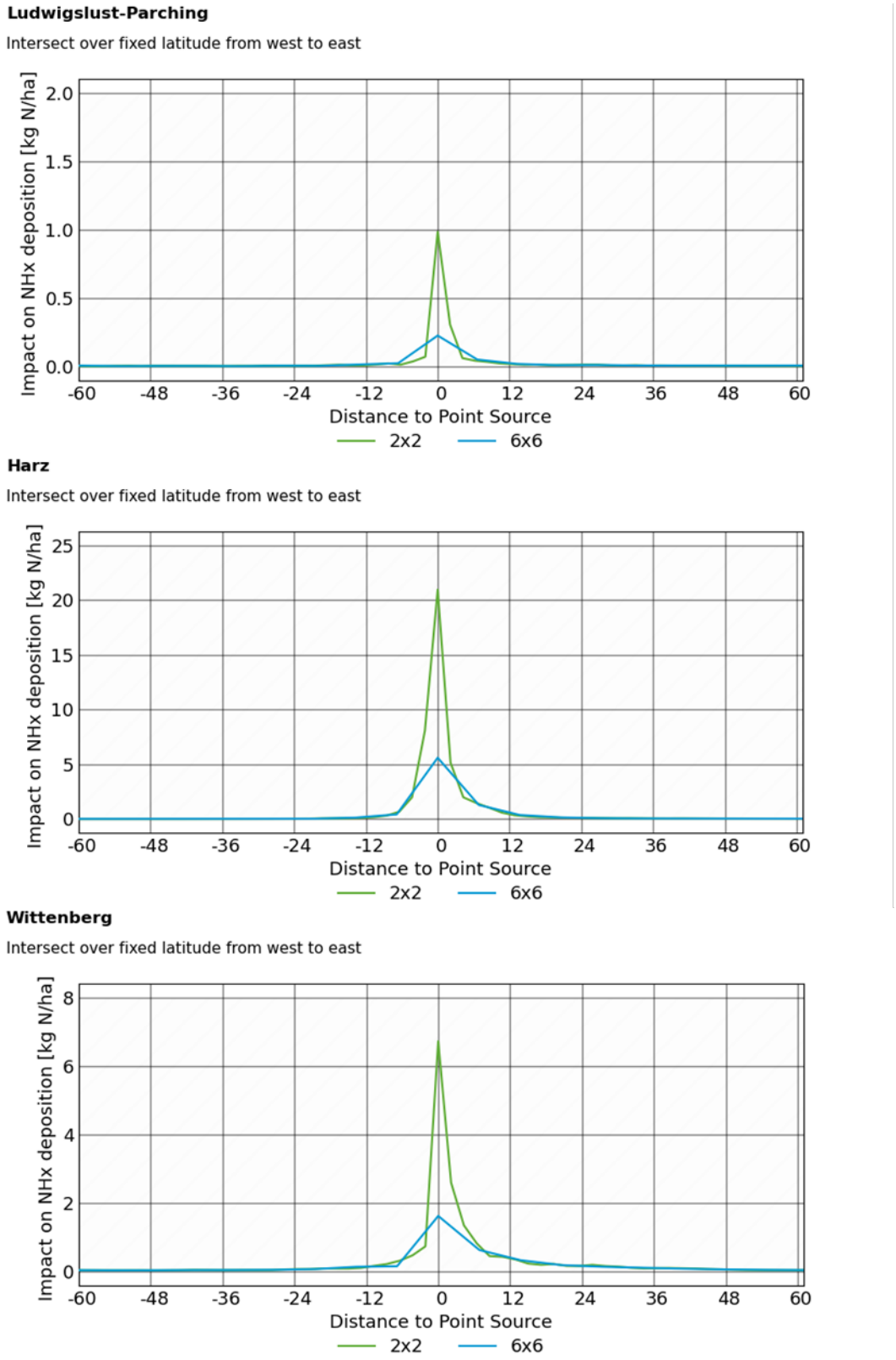

Source: TNO

Figure 36: Distance dependent cumulative deposited fraction of NH_x as a result of NH_3 emission change for each of the point sources (2x2 km²).

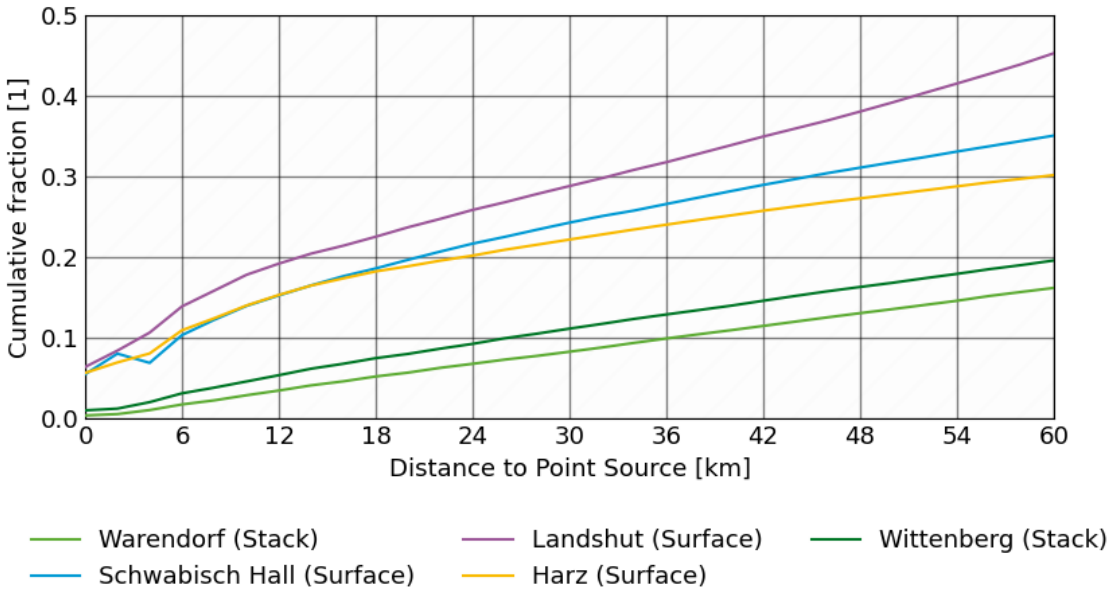

Source: TNO

3.2.2.2 Impact reduction scenarios

For the same counties, four model calculations were performed with reductions for different emission sources (animal housing, fertilizer application, grazing and road transport). For each source, all NH_3 and NO_x emissions were set to zero in those counties. Emission reductions are listed in Table 16 (NH_3) and Table 17 (NO_x) for each of these six regions and four scenarios. Reductions are given in ton N, note that for animal housing, Fertilizer application and Grazing, largest reductions are applied on NH_3, while road transport has largest reductions for NO_x emissions.

Table 16: Emission reduction of NH_3 [ton N] for six regions and four scenarios.

Region	Animal housing	Fertilizer appl.	Grazing	Road transport
Warendorf	3270.7	1446.8	52.0	24.4
Schwäbisch Hall	1949.4	1431.0	31.0	23.4
Landshut	1737.3	1355.3	15.2	20.0
Ludwigslust-Parchim	1067.9	1856.2	73.1	37.6
Harz	562.6	642.2	14.3	17.3
Wittenberg	703.0	779.1	22.8	16.0

Table 17: Emission reduction of NO_x [ton N] for six regions and four scenarios.

Region	Animal housing	Fertilizer appl.	Grazing	Road transport
Warendorf	4.3	160.4	7.3	404.7
Schwäbisch Hall	3.3	156.1	4.3	363.3
Landshut	3.5	147.2	2.1	291.1
Ludwigslust-Parchim	2.1	306.2	10.2	597.6
Harz	0.7	131.9	2.0	332.1
Wittenberg	1.4	120.4	3.1	280.1

In Figure 37, differences for simulated depositions, with respect to the reference simulation [%], are shown for the different emission sources (animal housing, fertilizer application, grazing and road transport). Because emissions reductions are applied on complete districts, impacts are visible in complete regions and its close surroundings.

In Table 18 to Table 23, the relative influences (in %) of the four emission categories on the total deposition are listed for all six counties and their neighbouring counties (regions marked with a * contain both the county itself and an independent city in the county). Emission reductions for the grazing scenario are the smallest, and typically contribute with less than 1 % to the total deposition. For the road transport scenario, N emissions are mostly in the form of NO_x . Because transport distances of oxidized nitrogen are larger, the impact on deposition in the region is also limited (around 1 % in own region and much lower in neighbouring regions). Both animal housing and fertilizer application have larger reductions of NH_3 emissions, which result in larger impact on regional depositions (5-20 % in own counties, and up to 5 % in neighbouring regions)

Table 24 shows how much of the emissions from different emission categories are deposited in the counties themselves. For example, only 16 % of the housing emissions in Warendorf are deposited in Warendorf itself. Overall, one can see that for scenarios dominated by the reduction of NH_3 emissions (animal housing, fertilizer application, grazing), the reduction of the deposition is about 15-20 % of the reduced emissions of that sector. For scenario dominated by the reduction of NO_x-emissions (road transport), this reduction is about 5 %. Again, these differences are due to the different lifetimes of reduced and oxidized nitrogen.

Figure 37: Impact on total (modelled) nitrogen deposition for emission reductions of animal housing (top left), fertilizer (top right), grazing (bottom left) and road transport (bottom right) on six different locations across Germany.

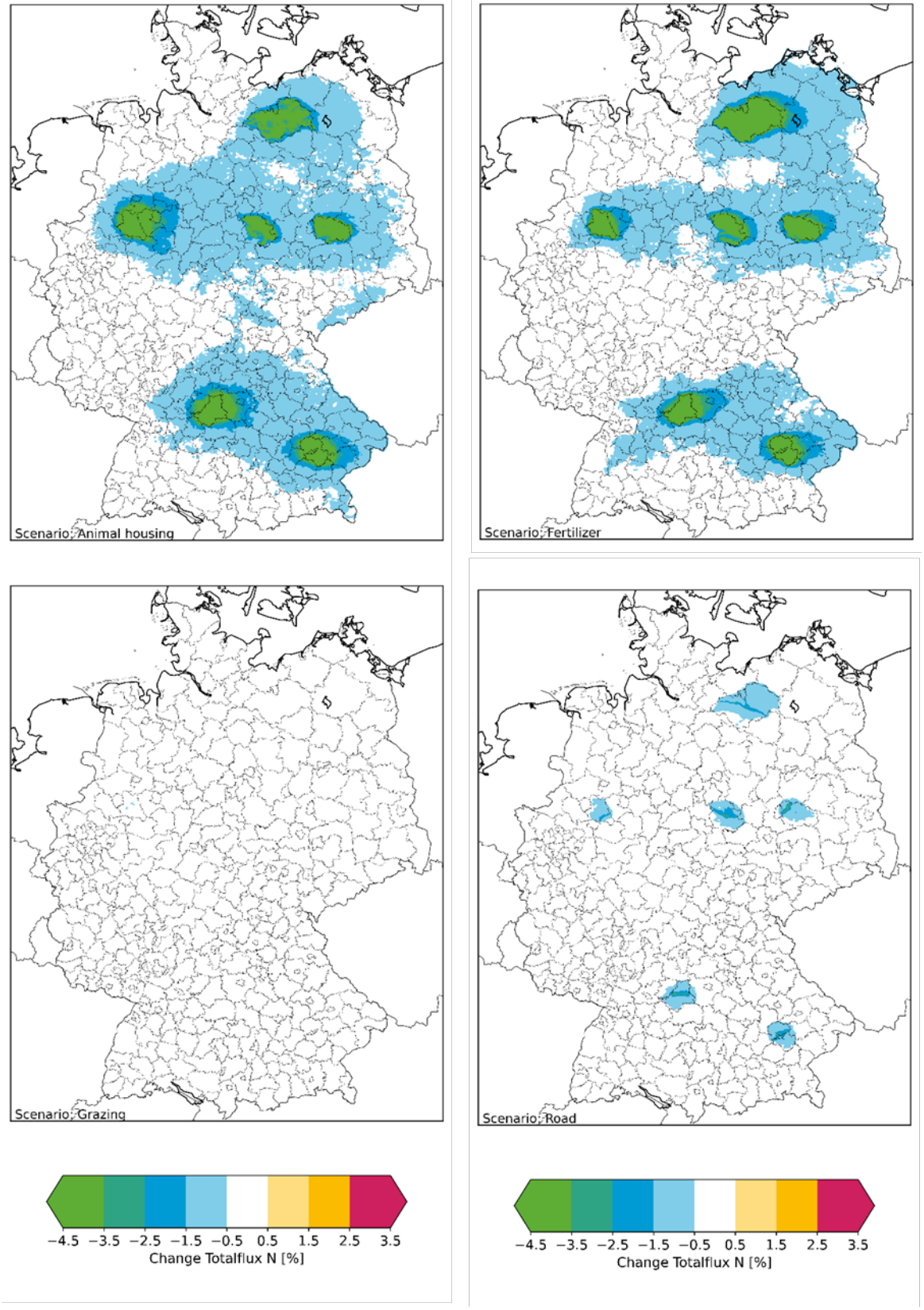

Source: TNO

Table 18: Reductions of total nitrogen deposition [%] in Warendorf itself and in neighbouring counties by removing the emissions from four different sources in Warendorf.

Warendorf	Reference deposition (ton N)	Animal housing	Fertilizer appl.	Grazing	Road transport
Warendorf	2584	20.4	9.9	0.36	0.68
Coesfeld	2323	1.0	0.7	0.03	0.06
Gütersloh	1967	6.9	3.4	0.13	0.27
Hamm	447	2.1	1.6	0.06	0.14
Munster	626	4.9	2.2	0.08	0.16
Osnabrück *	4867	2.0	0.8	0.03	0.07
Soest	2094	2.0	1.0	0.03	0.07
Steinfurt	3888	1.5	0.7	0.03	0.07

Table 19: Reductions of total nitrogen deposition [%] in Schwäbisch Hall itself and in neighbouring counties by removing the emissions from four different sources in Schwäbisch Hall.

Schwäbisch Hall	Reference deposition (ton N)	Animal housing	Fertilizer appl.	Grazing	Road transport
Schwäbisch Hall	2167	18.0	11.0	0.24	1.08
Ansbach *	2558	4.0	3.2	0.07	0.30
Heilbronn *	1397	1.2	1.0	0.02	0.14
Höhenlohekreis	1069	4.0	2.5	0.06	0.44
Main-Tauber-Kreis	1410	2.0	1.2	0.03	0.19
Ostalbkreis	1934	1.8	1.3	0.03	0.16
Rems-Murr-Kreis	1170	1.5	1.3	0.03	0.15

Table 20: Reductions of total nitrogen deposition [%] in Landshut itself and in neighbouring counties by removing the emissions from four different sources in Landshut.

Landshut	Reference deposition (ton N)	Animal housing	Fertilizer appl.	Grazing	Road transport
Landshut *	1994	16.6	10.6	0.12	1.03

Landshut	Reference deposition (ton N)	Animal housing	Fertilizer appl.	Grazing	Road transport
Dingolfing-Landau	1147	4.2	3.7	0.05	0.35
Erding	1349	1.7	1.0	0.02	0.11
Freising	1011	2.3	1.6	0.02	0.20
Kelheim	1194	1.7	1.5	0.02	0.22
Mühldorf am Inn	1236	1.9	1.2	0.02	0.12
Regensburg *	1605	0.9	0.6	0.01	0.12
Straubing-Bogen *	1437	1.7	1.4	0.02	0.16

Table 21: Reductions of total nitrogen deposition [%] in Harz itself and in neighbouring counties by removing the emissions from four different sources in Harz.

Harz	Reference deposition (ton N)	Animal housing	Fertilizer appl.	Grazing	Road transport
Harz	2082	5.4	5.8	0.13	0.93
Börde	2500	1.0	1.3	0.03	0.21
Goslar	1228	0.8	0.8	0.02	0.15
Helmstedt	751	1.0	1.0	0.03	0.18
Mansfeld-Südharz	1276	0.9	1.1	0.03	0.22
Nordhausen	666	0.6	0.6	0.02	0.12
Salzlandkreis	1347	1.4	2.1	0.05	0.29
Wolfenbüttel	788	1.2	1.9	0.03	0.21

Table 22: Reductions of total nitrogen deposition [%] in Wittenberg itself and in neighbouring counties by removing the emissions from four different sources in Wittenberg.

Wittenberg	Reference deposition (ton N)	Animal housing	Fertilizer appl.	Grazing	Road transport
Wittenberg	2066	7.4	7.9	0.23	0.77
Anhalt-Bitterfeld	1513	0.8	1.1	0.03	0.20
Dessau-Roßlau	277	1.4	1.6	0.04	0.40
Elbe-Elster	1999	1.1	1.3	0.04	0.17
Nordsachsen	1973	0.9	0.9	0.03	0.14

Wittenberg	Reference deposition (ton N)	Animal housing	Fertilizer appl.	Grazing	Road transport
Potsdam-Mittelmark	2765	1.0	1.1	0.03	0.26
Teltow-Fläming	2213	1.3	1.9	0.05	0.21

Table 23: Reductions of total nitrogen deposition [%] in Ludwigslust-Parchim itself and in neighbouring counties by removing the emissions from four different sources in Ludwigslust-Parchim.

Ludwigslust-Parchim	Reference deposition (ton N)	Animal housing	Fertilizer appl.	Grazing	Road transport
Ludwigslust-Parchim	5399	4.9	7.7	0.31	0.78
Herzogtum Lauenburg	2027	0.5	0.7	0.03	0.14
Lüchow-Dannenberg	1419	0.7	0.8	0.03	0.14
Lüneburg	1836	0.6	0.8	0.03	0.11
Mecklenburg-ische Seenplatte	4996	0.9	1.6	0.06	0.19
Nordwestmeck-lenburg	2627	0.9	1.4	0.05	0.24
Prignitz	2274	1.0	1.4	0.05	0.22
Rostock *	3918	0.8	1.5	0.05	0.19
Schwerin	159	3.1	5.2	0.21	0.72

Table 24: Reduced amount of deposition [ton N] in each of the six counties. Percentages with respect to the total (NO_x + NH_3) reduced emissions are given between brackets.

Region	Animal housing	Fertilizer appl.	Grazing	Road transport
Warendorf	528 (16 %)	256 (16 %)	9 (16 %)	18 (4 %)
Schwäbisch Hall	390 (20 %)	237 (15 %)	5 (15 %)	24 (6 %)
Landshut	330 (19 %)	211 (14 %)	3 (14 %)	21 (7 %)
Harz	112 (20 %)	120 (16 %)	3 (17 %)	19 (6 %)
Wittenberg	152 (22 %)	163 (18 %)	5 (19 %)	16 (5 %)
Ludwigslust-Parchim	262 (25 %)	417 (19 %)	17 (20 %)	42 (7 %)

4 Mapping of depositions across Germany: Extension of time series 2015-2019 including pillar years 2000, 2005 and 2010

To create annual deposition maps for nitrogen and sulphur over Germany for 2015-2019, model calculations are performed with improved model settings described and evaluated in Section 2.2. After that, the kriging method described in Section 2.1.2 is used to derive wet deposition fields and after that occult depositions are calculated. For this, a set of wet deposition observations is provided by UBA. In Figure 38, the number of available stations for each year is shown, together with the number of stations which are used in the kriging procedure. For 2018, 2019 significant lower amount of stations are flagged as valid. Especially in Saarland and Bayern, stations are flagged as invalid. One reason for this is that 2018 and 2019 were very dry years, which makes it difficult to have enough observations with significant amount of rain. However, the overall coverage of valid observations over Germany is still high, so it is not expected that this has a large impact on calculated country total depositions.

An example of kriging procedure and results for NH_4 in 2019 is given in Figure 39. Most patterns are covered well by the model. Areas in Niedersachsen and the south of Germany with higher deposition levels are captured by the model. However, in the eastern part of Germany, the model underestimates wet depositions, thus results are pulled “upwards” by the kriging procedure.

In Section 4.1 and 4.2, calculations of dry, wet and occult depositions are shown for 2015-2019. Calculations of effective deposition velocities are shown in Section 4.3. Comparison and continuation of timeseries from PINETI-3 are discussed in Section 4.4. Therefore, also data availability for 2000, 2005 and 2010 are also shown in Figure 38. Finally, the resulting critical load exceedances are discussed in Section 4.5.

Figure 38: Number of available stations with wet deposition observations, which are used for application of the kriging method.

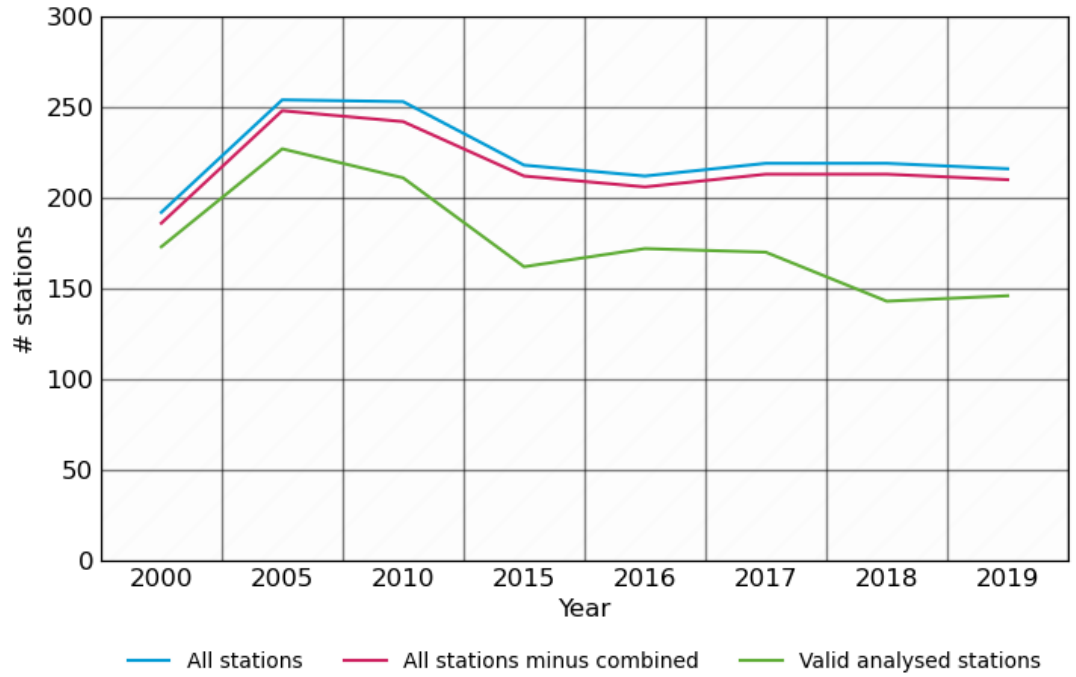

Source: TNO

Figure 39: **Mapping of kriging procedure. Modelled concentration of NH_4 in rain water (upper left), result of kriging approach (upper right). Rain amount on high resolution (lower left), combined result for wet deposition flux on high resolution (lower left).**

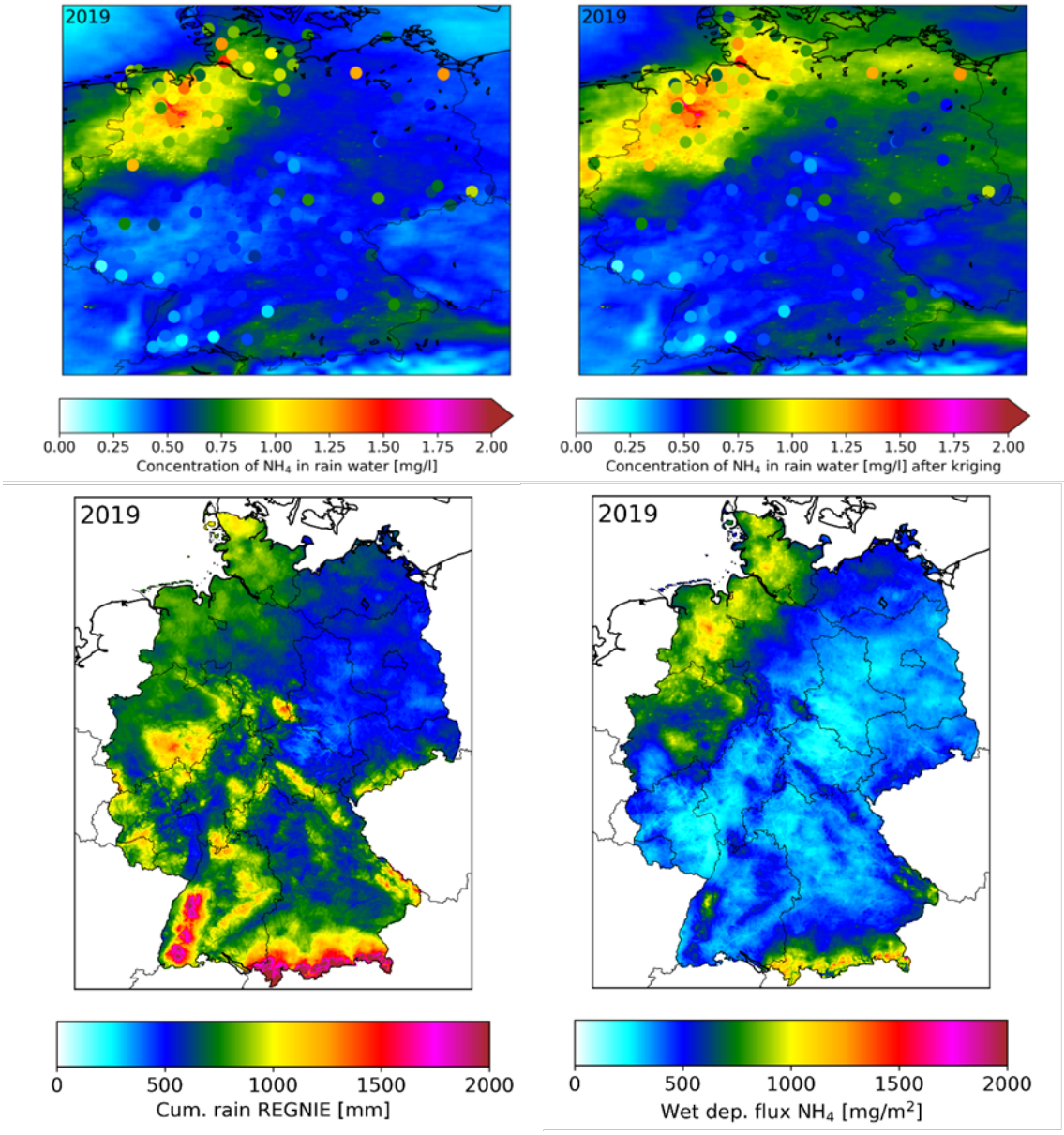

Source: TNO

4.1 Timeseries

Annual average depositions of nitrogen for 2015 until 2019 are shown in Figure 40. For 2015 to 2017 total deposition increases from 15.1 kg N ha^{-1} yr^{-1} to 16.2 kg N ha^{-1} yr^{-1} (1080 eq ha^{-1} yr^{-1} to 1160 eq ha^{-1} yr^{-1}), while 2018 and 2019 show a decrease to values around 14 kg N ha^{-1} yr^{-1} (1000 eq ha^{-1} yr^{-1}). The timeseries show specified values for dry, wet and occult deposition for both NH_x and NO_y. NH_x contributes approximately 60 % to the total N deposition, while NO_y contributes for 40 %. For NH_x, dry deposition is the most important pathway (~60 %), while dry and wet depositions for NO_y have an equal share. Occult deposition has a small contribution for both NH_x and NO_y. Looking at the trend, 2018 and 2019 have a significant lower total deposition

with respect to the first three years. As shown in Section 2.2.2.1, emissions are the lowest for 2018 and 2019, but also meteorological circumstances with significant less precipitation in those years contribute to lower depositions. Also, for deposition of SO_x (Figure 41), 2018 and 2019 show significant lower depositions with respect to previous years. Identical to nitrogen, wet deposition is mostly decreased in those years. In the following section, spatial dependencies are discussed for both nitrogen and sulphur deposition in Germany.

Figure 40: Timeseries of annual average nitrogen deposition over Germany for 2015-2019.

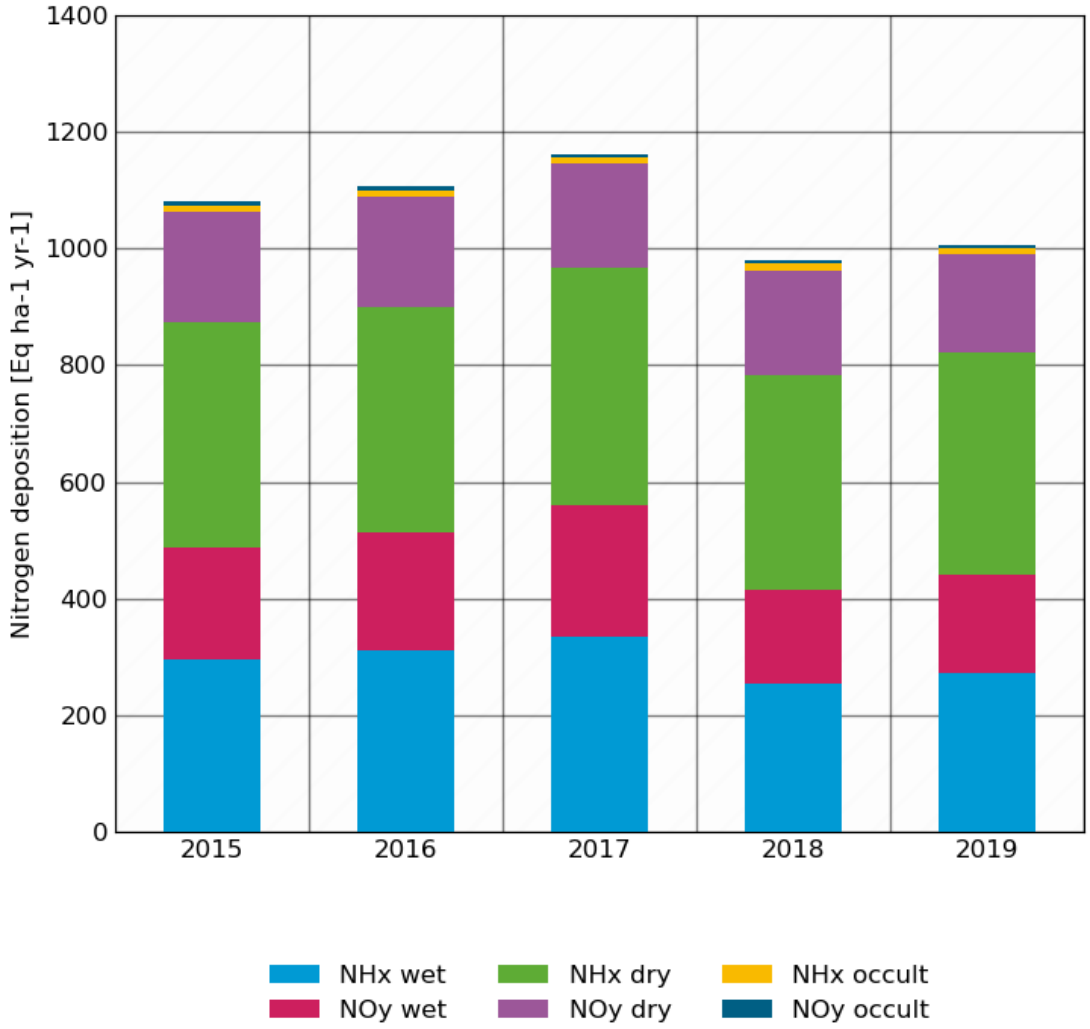

Source: TNO

Figure 41: Timeseries of annual average sulphur deposition over Germany for 2015-2019.

Source: TNO

4.2 Maps

As shown in the timeseries above, 2018 and 2019 have significant lower values compared to previous years. In Figure 42, annual average nitrogen deposition fields are shown for 2015-2019. From this, one can observe a country-wide decrease in deposition, which cannot be attributed to specific regions. Looking at specified maps for dry and wet depositions (Figure 43 and Figure 44), the decrease in 2018 and 2019 is driven by wet deposition. As a consequence, next to lower emissions in those years, dry circumstances cause lower wet depositions (and lower total deposition) in these years. For sulphur depositions (total in Figure 45, dry in Figure 46, and wet in Figure 47), we see similar patterns with reductions in 2018 and 2019 driven by lower wet depositions.

Figure 42: Maps with annual average total nitrogen deposition over Germany for 2015-2019.

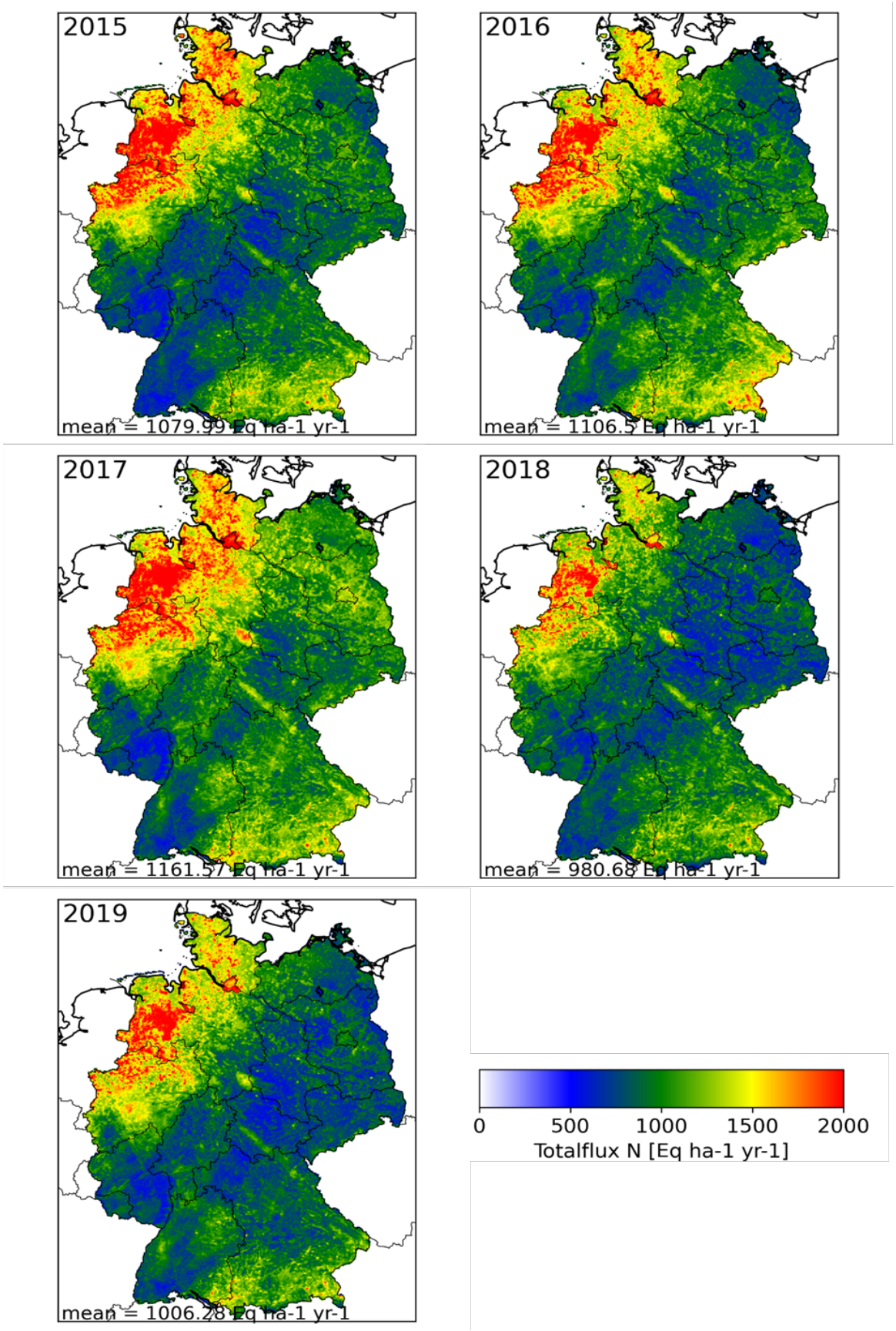

Source: TNO

Figure 43: Maps with annual average total nitrogen dry deposition over Germany for 2015-2019.

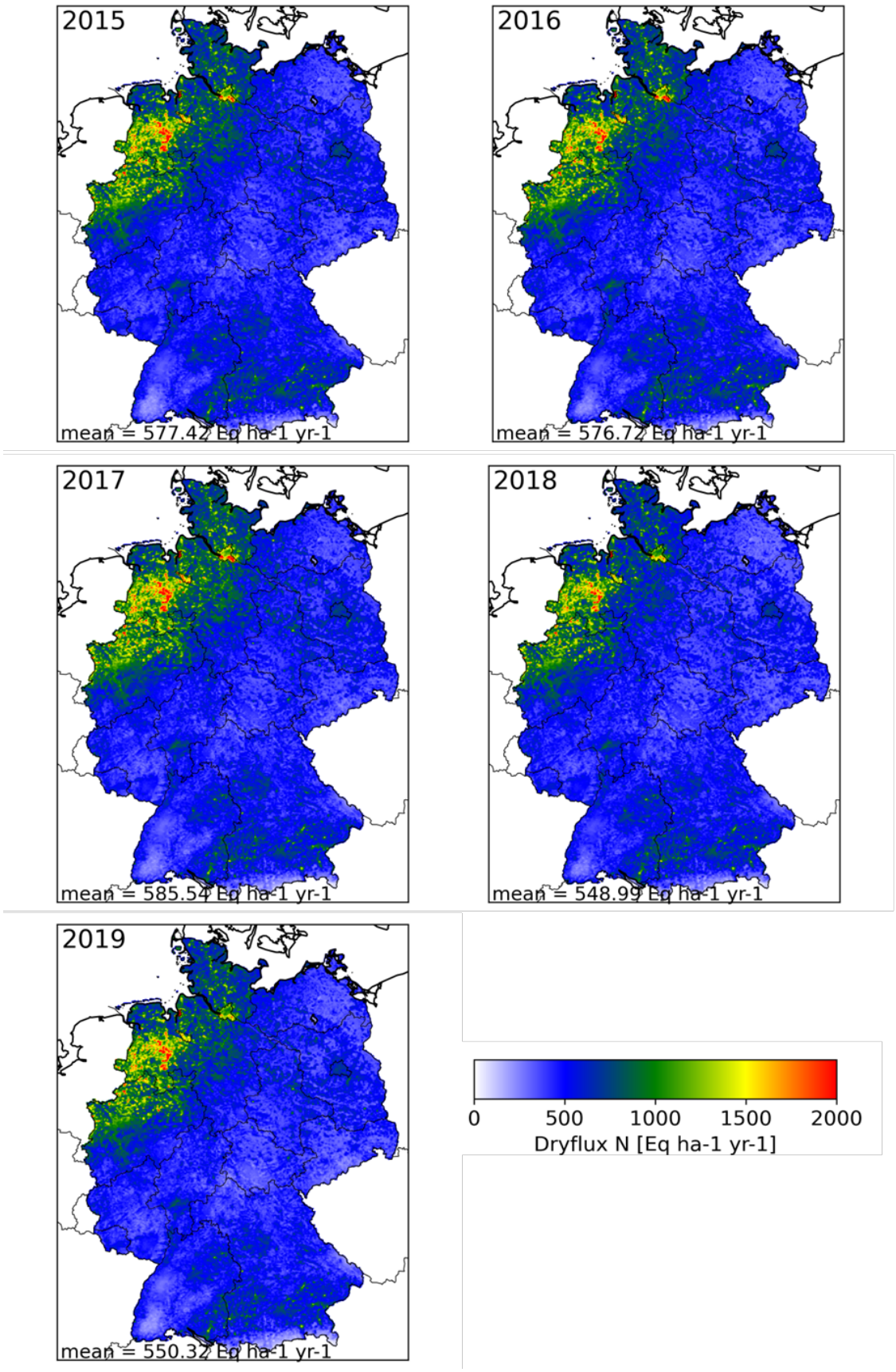

Source: TNO

Figure 44: Maps with annual average total nitrogen wet deposition over Germany for 2015-2019.

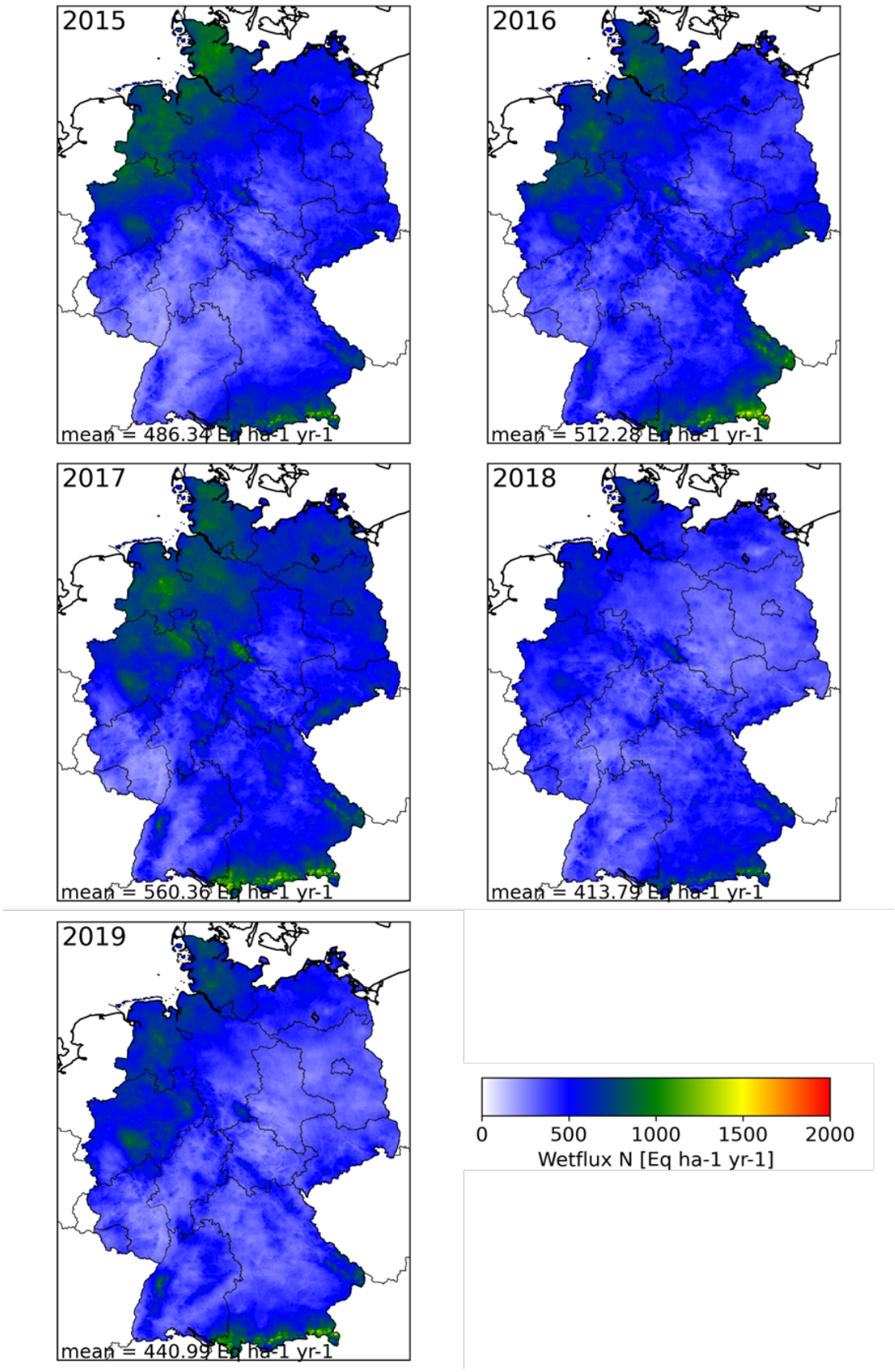

Source: TNO

Figure 45: Maps with annual average total sulphur deposition over Germany for 2015-2019.

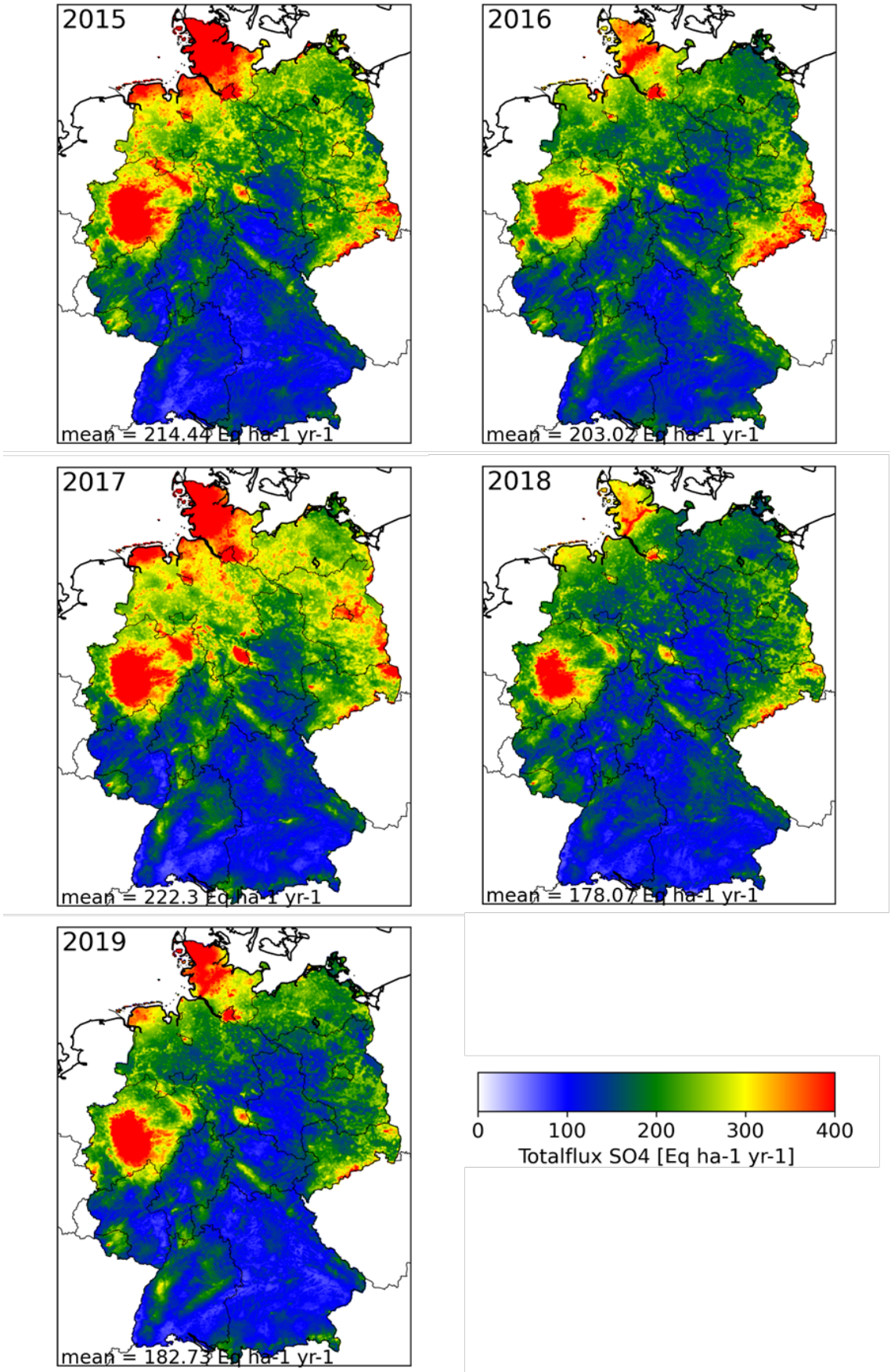

Source: TNO

Figure 46: Maps with annual average total sulphur dry deposition over Germany for 2015-2019.

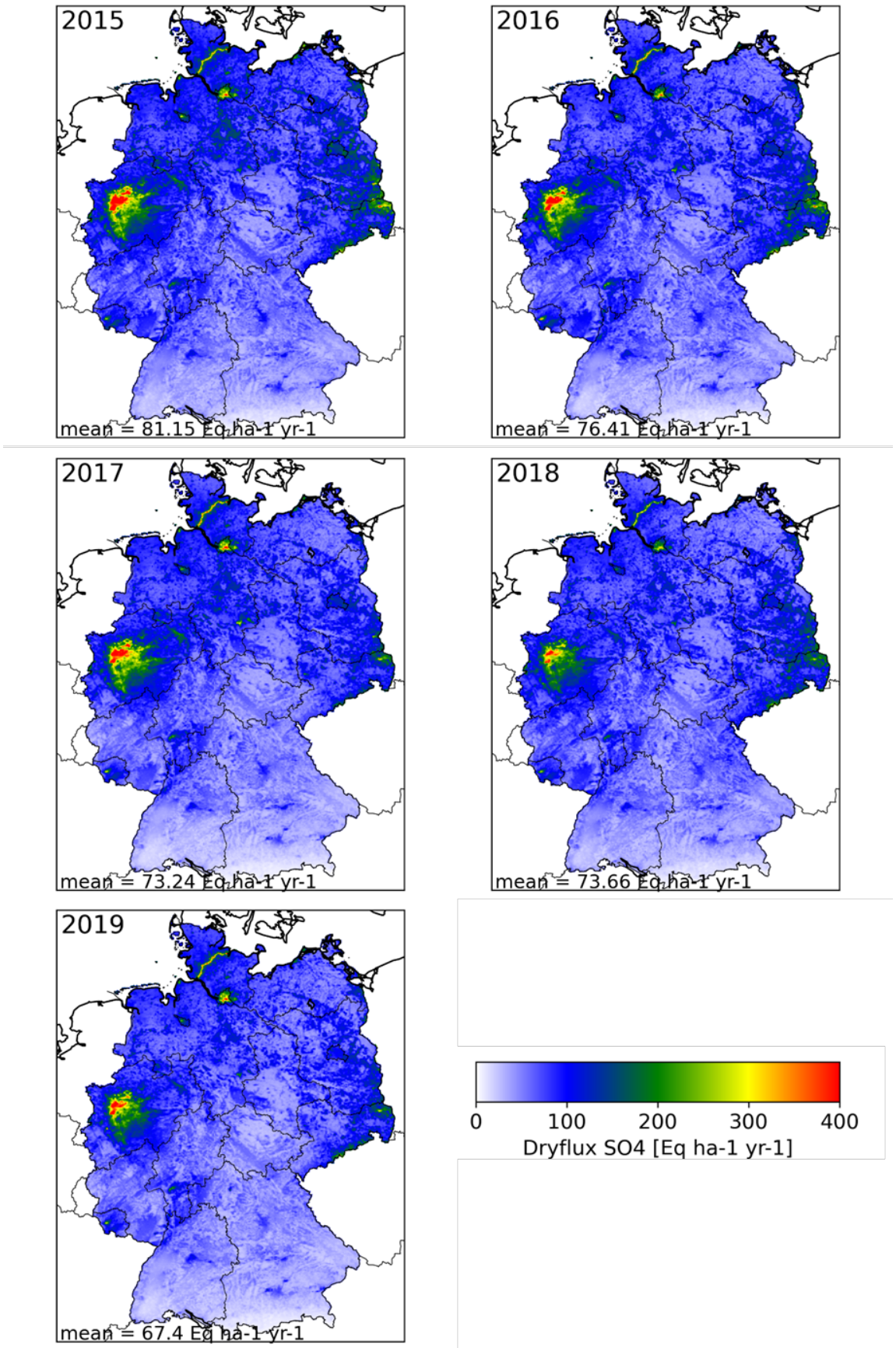

Source: TNO

Figure 47: Maps with annual average total sulphur wet deposition over Germany for 2015-2019.

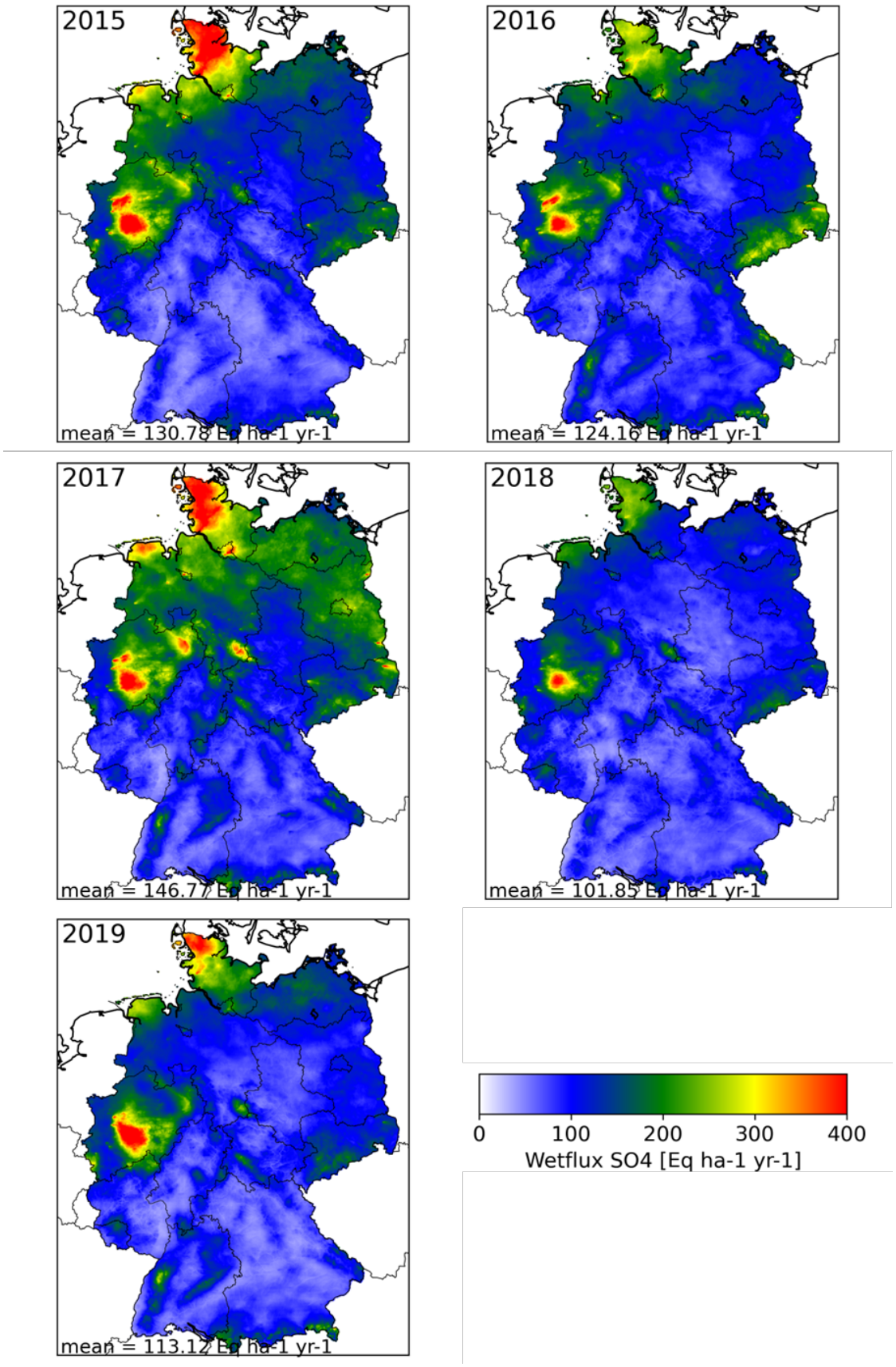

Source: TNO

4.3 Effective deposition velocities

Table 25 shows the average values of the calculated effective deposition speeds in the years 2017 to 2019 for all gases that contain nitrogen or sulphur atoms. The deposition rate is higher for land use classes with larger roughness (e.g. trees instead of grass) and is not the same for all species. The rate of deposition depends on the chemical properties, such as whether the species are water-soluble or react when they hit the surface. For example, the deposition of NH_3 in coniferous forests is two times higher than in arable land. There are also differences in overall deposition between the land use classes, but since wet deposition does not depend on land use, these are relatively smaller than with dry deposition.

Table 25: Effective deposition velocities on each land use category.

species	ara	cnf	crp	dec	mix	grs	oth	sem	urb	wai	wat
HNO_3	1.10	1.71	1.53	1.71	1.71	1.18	0.80	1.33	3.44	0.68	0.78
N_2O_5	0.45	0.82	0.70	0.82	0.82	0.58	0.41	0.64	1.45	0.35	0.40
NH_3	0.53	1.18	0.74	0.87	1.02	0.54	0.45	0.59	0.99	0.49	0.54
NO	0.02	0.02	0.02	0.02	0.02	0.02	0.04	0.02	0.08	0.04	0.04
NO_2	0.09	0.16	0.13	0.13	0.14	0.08	0.07	0.08	0.07	0.04	0.04
SO_2	0.12	0.34	0.30	0.33	0.33	0.25	0.07	0.26	0.17	0.26	0.29
Particles	0.64	0.94	0.36	0.34	0.64	0.26	0.25	1.61	0.27	0.25	0.29

4.4 Continuation of PINETI-3 timeseries

The timeseries shown in Section 4.1 represent 2015-2019 with the latest model version, including emission updates (see Section 1.4). This timeseries extends the series derived in PINETI-3, which represents 2000-2015. To quantify the impacts of model and emission updates, the model run and kriging procedure are also performed for three so-called pillar years (2000, 2005 and 2010). In Figure 48, results of the pillar years and the series for 2015-2019 are shown together with the PINETI-3 timeseries. In general, higher total depositions are found with the updated model version. This is mainly driven by higher values for dry deposition, which is caused by increasing the vertical resolution of the model (see Section 2.2.1). Wet depositions remain similar because the kriging procedure is applied on the same wet deposition observations.

Figure 48: Extension of PINETI-3 timeseries, including recalculation of pillar years 2000,2005 and 2010 (averaged value over Germany in eq ha^{-1} yr^{-1}). PINETI-4 results in solid bars, PINETI-3 results in dashed bars.

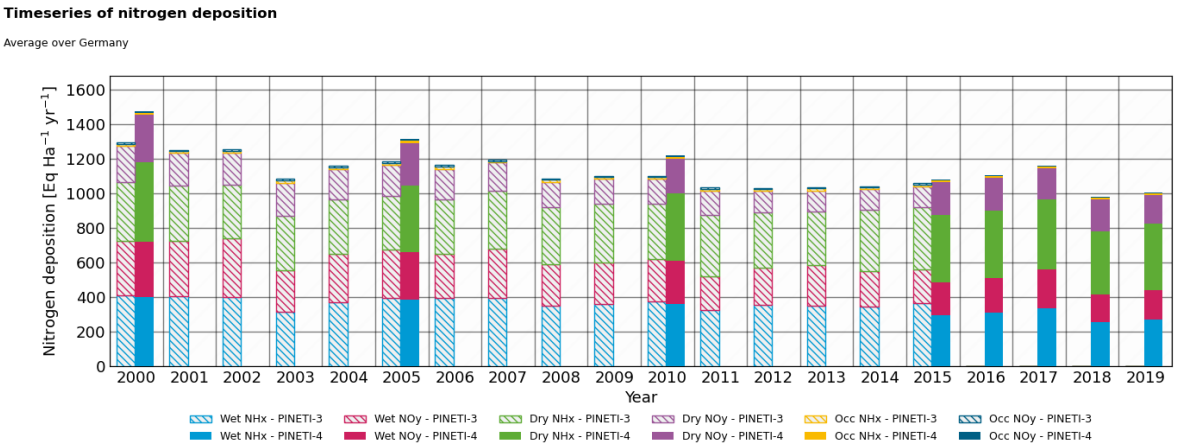

Source: TNO

4.5 Critical load exceedances

4.5.1 Critical Load concept and background

With the entry into force of the Geneva Convention on Long-range Transboundary Air Pollution (CLRTAP) in 1983 and its implementation in the associated protocols, a close relationship was established between air pollutants and their effects on humans and the environment. Thus, in addition to the exhaustion of all technical possibilities (best available technology), the measures for air pollution control should above all be oriented to the avoidance of negative effects (effect-based activities). For environmental effects, it was postulated that the inputs of air pollutants should not exceed critical ecological thresholds. According to current knowledge, compliance with or undercutting of such critical loads provides a guarantee that a selected protected good, the ecological receptor, will not be damaged either acutely or in the long term. The definition of critical load is:

"A quantitative estimate of an exposure to one or more pollutants below which significant harmful effects on specified sensitive elements of the environment do not occur according to present knowledge." (Nilsson & Grennfelt, 1988).

Generally, there are two different methods to access critical loads for air borne nitrogen and/or sulphur inputs for natural or semi-natural ecosystems. One way is to estimate the critical load on basis of empirical field data or gradient studies. For this approach a large number of studies are needed and the resulting thresholds should be discussed with a maximum of ecological experts in order to provide the necessary reliability. Last time the so called empirical critical loads were updated within the framework of the CLRTAP was in the year 2022 and the resulting numbers are published in Bobbink et al. (2022). In this report, ranges of empirical critical loads for nitrogen deposition are defined for more than 60 ecosystems. It also contains an extensive description about the included methods and literature. However, this method was not used in order to calculate the critical load exceedance described in this chapter. The used method is called Simple Mass Balance (SMB) approach which is described in the Mapping Manual of the ICP Modelling and Mapping (https://www.umweltbundesamt.de/en/cce-manual). The basic idea of this approach is to estimate the potential of natural or semi-natural ecosystems to handle certain air pollutants (nitrogen and/or sulphur) under so-called steady state conditions. This

includes the estimation of the potential to safely store and/or buffer nitrogen and sulphur deposition via naturally occurring processes like uptake in the vegetation and buffer mechanisms via the available Acid Neutralization Capacity (ANC) of the soil. Additionally, the maximum allowed discharge of nitrogen and ANC needs to be estimated as well. Steady state condition in this context means that the potential of the described processes shall be estimated under the prerequisite of no alteration of or no negative impact on the ecosystem and its properties. Naturally, the potential of an ecosystem to compensate for harmful inputs depends on site factors like soil type, vegetation type and climatic condition. Therefore, data from various sources needs to be integrated in to a modelling framework in order to calculate SMB critical loads. The last time this was done for Germany was within the framework of the ICP Modelling and Mapping in the year 2018 (Schaap et al., 2018). This report includes a detailed description about methods and data used in order to create a policy relevant critical load dataset which is also used on European level in order to validate to qualify abatement success of the implementation of emission reduction policies. Latest findings regarding the application of this dataset within the framework of the CLRTAP can also be found here in the CCE Status Report 2022 (Geupel et al., 2022).

4.5.2 Exceedance of critical loads for acidification

According to the SMB method of estimating the critical load for acidification, nitrogen and sulphur needs to be acknowledged. For this a two-dimensional linear function needs to be established using estimations for a maximum of sulphur deposition ($CL_{max}S$) and a maximum for nitrogen deposition ($CL_{max}N$). This function is additionally adapted by including a threshold marking an estimation for naturally needed nitrogen ($CL_{min}N$) of the ecosystem. A reduction of nitrogen deposition below the $CL_{min}N$ is within the mindset of a steady-state model not needed and therefor the function is altered accordingly. In order to calculate the total exceedance of the critical load for acidification, the paired information of nitrogen and sulphur deposition needs to be compared with the critical load function. In order to calculate the shortest path to the function which represents the space with no critical load exceedance, the exceedance region needs to be identified first. After that, the shortest path to the critical load function can be calculated and the shares for exceedance by nitrogen and sulphur are summarized in order to get the total critical load exceedance. This method is described in more detail in the Mapping Manual (CCE 2017) and the final report of the PINETI-3 project (Schaap et al., 2018).

Figure 49: Time series of exceedance of critical loads for acidification.

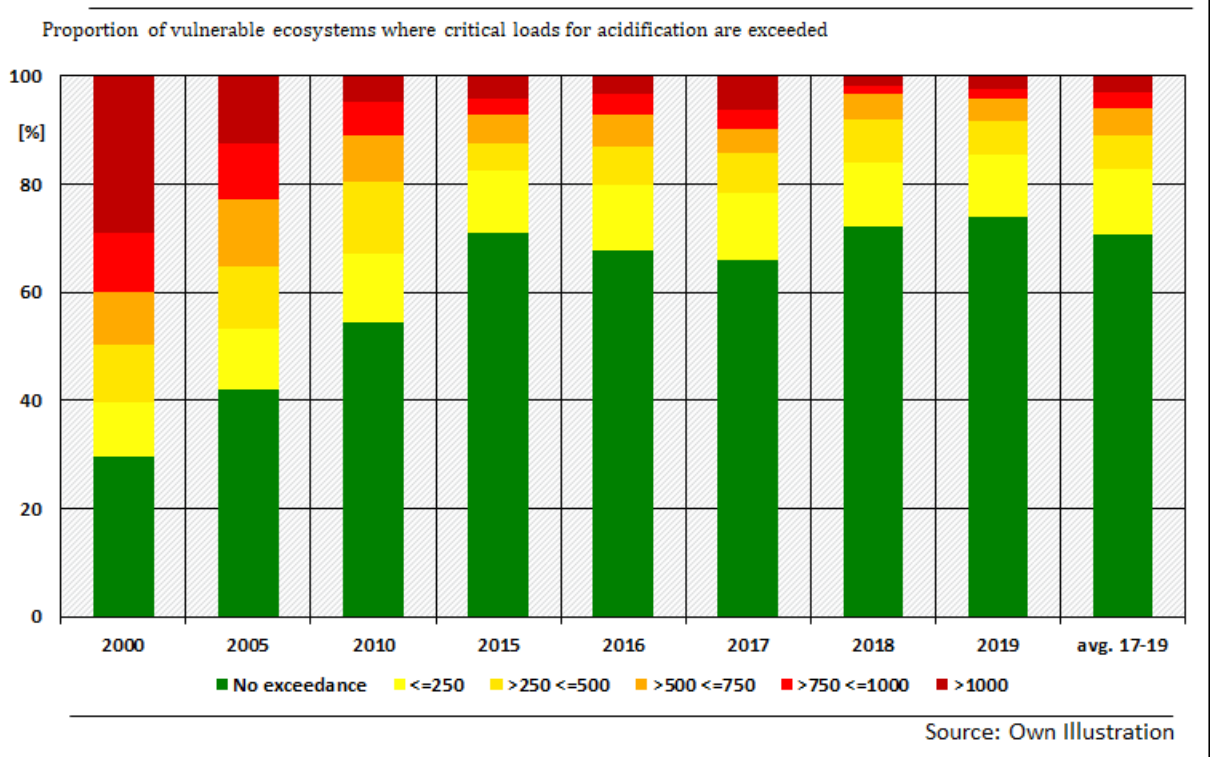

As described above, the latest available CL dataset was used for the CL exceedance calculation. These CL were compared with the model output of this project for the years listed in Figure 49. Additionally, a deposition average of the years 2017, 2018 and 2019 was calculated and used for the exceedance calculation as well. As displayed in Figure 49, there is a rather steady decrease of the share of receptors with CL exceedance from the year 2000 (70 %) till 2015 (29 %). After some years with a rising share of ecosystems threatened by acidification, the number finally dropped to 26 % in the year 2019. The result for the calculated average (2017-19) fit in to the time series and gives the expected results.

The Figure 50 shows the spatial distribution of the calculation of the CL exceedance for acidifying deposition on basis of the calculated average deposition for the years 2017-19. There is no very clear trend visible, however, it appears that in southern regions of Germany are dominated by areas with no or low exceedances. In eastern parts of Germany CL exceedance seems to be more prominent and on higher levels. However, the regions in North-West of Germany have areas with highest levels of CL exceedances.

Since the effects of high or low levels of nitrogen and sulphur deposition are overlaid with the estimated sensitivity of the ecosystems, an interpretation of the results is not trivial. However, it is obvious that highest levels of CL exceedances occur in North-West Germany which is a region with a big proportion of intensive agriculture with high levels of NH_3 emissions. The temporal trend appears promising even if 26 % of the receptor area still has exceedances for critical load for acidification.

Figure 50: The spatial distribution of the CL exceedance for acidifying deposition.

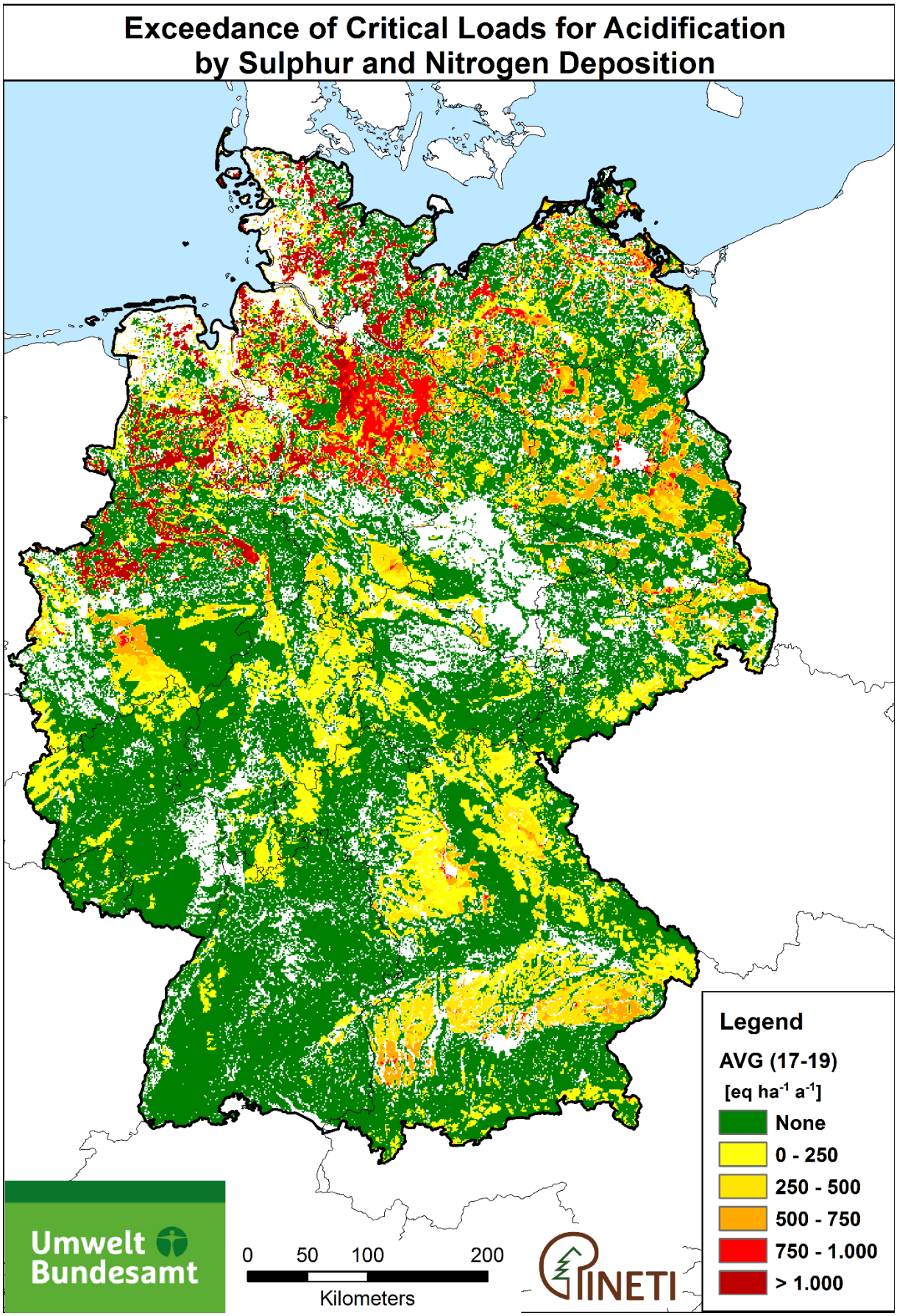

4.5.3 Exceedance of critical load for eutrophication

Figure 51: Time series for exceedance of critical loads for eutrophication.

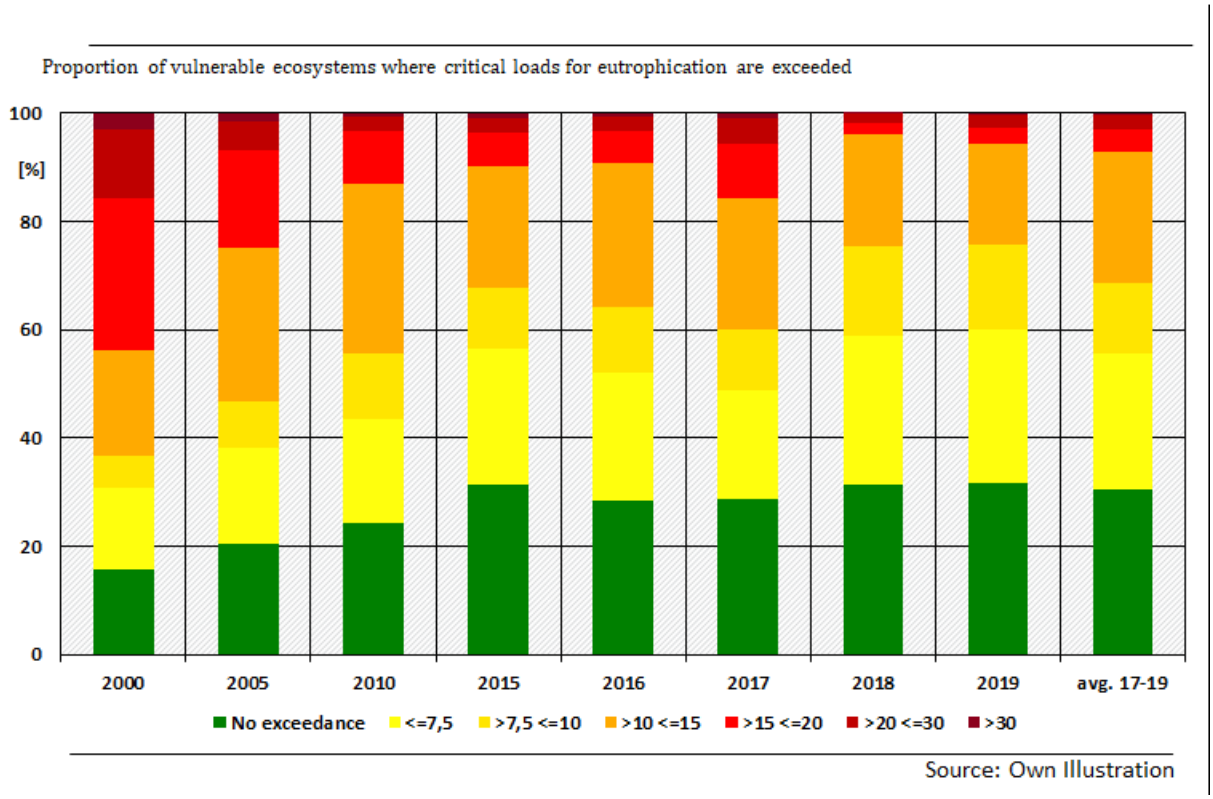

Compared to the exceedance calculation of the acidification, the calculations for the eutrophication is rather simple. Since there is only nitrogen responsible for eutrophication, only one threshold ($CL_{eut}N$) is described in the estimation of the sensitivity of the ecosystems. Therefore only the modelled deposition of nitrogen needs to be compared with the $CL_{eut}N$.

Figure 51 shows the trend of the share of ecosystems with exceedance of critical load for eutrophication. This trend looks less positive than the trend for acidification. First of all, the decrease in the years 2000 (84 %) till 2015 (69 %) is less prominent than for the acidification. Secondly, also the last modelled years and the additionally calculated average (2017-19) end up with a rather high share of ecosystems threatened by eutrophying nitrogen deposition. However, the spatial trend displayed in Figure 52 shows a clearer distribution of the areas with CL exceedances. The central and southern regions of Germany are dominated by no or low levels of exceedances. Only a small share has medium levels (up to 15 kg ha^{-1} yr^{-1}) of exceedances. The region of North-East Germany is dominated by medium and elevated (up to 20 kg ha^{-1} yr^{-1}) exceedances while the highest numbers (up to 30 kg ha^{-1} yr^{-1} and above) can be found in the North-West of Germany.

Figure 52: The spatial distribution of the CL exceedance for eutrophying deposition.

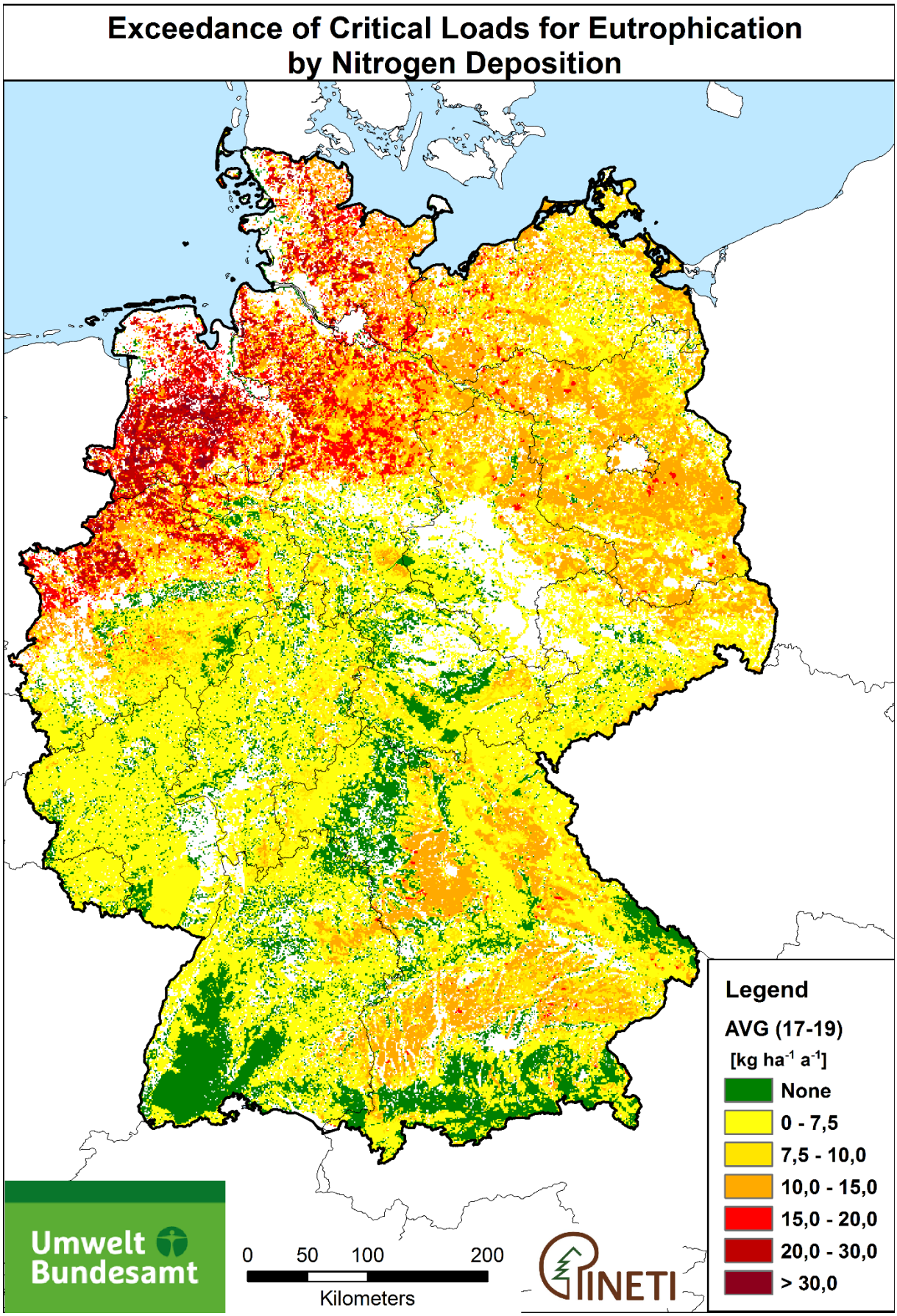

5 Synthesis

5.1 Conclusions

The main objective of the project was to extend the time series of nitrogen and sulphur deposition in Germany for the period 2015-2019 using an updated methodology that further improved the quality of the deposition estimates. For this, individual assessments for the dry, wet and occult deposition were combined to arrive at high resolution, land use specific maps of total nitrogen and sulphur deposition. The new estimates yield national mean total nitrogen deposition fluxes between 1000 and 1160 eq ha^{-1} yr^{-1}. From 2015 to 2017 total N-deposition increases from 1080 to 1160 eq ha^{-1} yr^{-1}, while the lowest values around 1000 eq ha^{-1} yr^{-1} were estimated for 2018 and 2019. The latter is driven by lower (observed) wet deposition fluxes due to significantly less precipitation in 2018 and 2019 in comparison to earlier years and especially 2017. On average, NH_x contributes approximately 60 % to the total N deposition, while NO_y contributes for 40 %. Looking at the spatial distribution, largest depositions of nitrogen are mapped in the agricultural regions in the north-west of the country as well as in the southern part of Bavaria. For sulphur, also largest values are found in the north-west of Germany, but also regions bordering the Czech Republic have significant deposition. Sulphur deposition estimates show a similar behaviour with larger national mean values (200-225 eq ha^{-1} yr^{-1}) for 2015 to 2017 and lower values (175 eq ha^{-1} yr^{-1}) for 2018 and 2019. This is also driven by lower wet deposition. The resulting maps replace the PINETI-3 maps in the high-resolution (1x1 km^2) and nation-wide UBA GIS service.

The mapping procedure applied in PINETI-4 was improved compared to the procedure used in PINETI-3 through updates in the LOTOS-EUROS modelling. The simulations were improved by including the newest available emission information (i.e. totals and spatial distributions; most notably for the agricultural sector), by incorporation of dynamic emission time profiles and by considerably increasing the horizontal and vertical model resolutions of the model. Due to a lack of (consistent) meteorological data at this resolution, the implementation of high-resolution meteorological data needed to be postponed. For 2015, it was shown that these updates have generally a positive impact on the model performance. Temporal and spatial correlations for all gaseous tracers increased or remained almost unchanged. For example, for annual mean NO_2 concentrations the spatial correlation increased from 0.57 to 0.64, whereas the average temporal correlation over all stations increased from 0.50 to 0.54. Also, the model-measurement biases and RMSE were improved for air concentrations. Largest impact was found for ozone with a mean overestimate by the model reduced from 18 µg m^{-3} to less than 5 µg m^{-3}. The systematic underestimation of wet deposition was slightly increased for NO_y and SO_x, whereas the spatial correlations increased for both. Overall, we conclude that model quality increased in comparison to PINETI-3. Nonetheless, the process of implementing and testing potential improvements of the modelling and mapping procedure is a continuous and ongoing process and ongoing activities are listed in the outlook.

Given the update in the mapping procedure, re-assessments were performed for the pillar years 2000, 2005 and 2010 using the PINETI-4 methodology and input data. On average, depositions are 12 % larger for total nitrogen and 9 % larger for total sulphur compared to the results from the previous study (PINETI-3). The differences are mainly driven by larger modelled fluxes for dry deposition, as a result of the updates in the emission information and the model's vertical resolution.

The decline of critical loads exceedances for acidification shows a positive trend, as the area without exceedance developed from around 29.6 % (2000) to around 73.9 % (2019). In the case of critical loads for eutrophication, a positive trend is observed as well, however, the proportion of ecosystems with critical load exceedance is still high. The proportion of ecosystems without exceedances increased from around 15.7 % (2000) to around 31.5 % (2019). This means that about 68.5 % of the ecosystems analysed were still threatened by eutrophication in 2019.

By applying the source apportionment functionality of LOTOS-EUROS, we established a source attribution at state level for the first time. Hamburg and Bremen have the largest average nitrogen depositions in Germany, followed by Niedersachsen, Nordrhein-Westfalen and Schleswig-Holstein. Both Hamburg and Bremen are small city states with relatively high NO_x emission densities and are surrounded by agricultural regions. The local emissions in these states only play a limited role in the local deposition (approx. 20 %), due to their small size. Niedersachsen and Schleswig-Holstein have higher values due to their prominent agricultural sector that emits large amounts of ammonia. Even for Nordrhein-Westfalen with large emitters of nitrogen oxides deposition is dominated by NH_x. In general, an average domestic contribution of 40 % is found for these states. For all other states modelled domestic contributions are approximately 20 %. Not surprisingly, a feature with elevated contributions by neighbouring states in the east-west direction is noticed, due to preferred westerly winds. Further, considerable contributions from neighbouring countries is found, especially from countries west of Germany. The Netherlands contribute mainly to Bremen, Hamburg, Niedersachsen, Nordrhein-Westfalen and Schleswig-Holstein, while France contributes to Saarland and Baden-Wurttemberg. Contributions of Poland and Czech Republic to eastern states are more limited due to the preferential westerly winds. The result outlined above indicate that national and international efforts are required to lower the nitrogen deposition across Germany. Targeting ammonia is the most effective route to ensure domestic deposition reductions.

To assess the effect of a reduction of specific local emission sources on the nitrogen deposition on the new model resolution, additional scenario calculations were performed. In six counties, the emissions of a specific large point source of ammonia were reduced. Four of these sources are surface emissions and two sources have a high stack. Obviously, the reduction in the modelled deposition in the grid cell containing the source itself was considerably larger at the 2x2 km^2 resolution than at 7x7 km^2 resolution (a factor 4-5). Still, the differences are mainly present within the 7x7 km^2 cell as after 10 km the impact of the emission reductions was almost equal. These simulations also allowed to address the fraction of the ammonia emission deposited within a given distance to a source. To quantify the impact on the deposition independent of absolute reductions, depositions were calculated relative to the emission reduction. For the surface sources, about 18-22 % of the emitted mass is deposited within a radius of 20 km from the source. For the stack sources, the fraction of the emission deposited 20 km of the point source was calculated to be close to 5 %. Hence, for surface emissions a rule of thumb of 20 % within 20 km can be taken from these simulations, while for stack sources, this number is a factor 4 lower.

5.2 Outlook

This study described the successful extension of the PINETI time series with a higher underlying resolution of the modelling efforts. As the modelling of nitrogen and sulphur deposition is complex and systematic differences to (variability in) observed concentrations and fluxes are observed, directions for improvement are continuously explored. Here we list ongoing and unfinished development activities, which may be implemented in the operational PINETI mapping procedure in the future when proven to be of added value:

- Detailing the spatial and temporal emission variability for agriculture. Spatial allocation of emission inventories are generally using two main proxies, animal numbers and land use types. Hence, within a country, state or county all agricultural land of the same type receives an equal amount of ammonia emission, although the intensity of the agricultural praxis, crop distributions, applied techniques, and housing type may vary substantially within such an area. Hence, a large part of the intrinsic variability of ammonia emissions is not accounted for. The same applies for the temporal variability of the emissions. Hence, efforts are made to improve the representation of the agricultural ammonia and NO_x emissions (Ge et al., 2020; Ge, Schaap, Dammers, et al., 2023; Ge, Schaap, & de Vries, 2023).
- Detailing the spatial and temporal emission variability for combustion emissions (NO_x). Several projects are dedicated to improve the emissions estimates for sectors as road traffic, transport through shipping (international and national inland and sea going vessels), etc. which could be consolidated in the future in GRETA or temporal emission modelling frameworks.
- During recent years the spatial-temporal coverage of satellite observations of (i.e.) NO_x, NH_3 and SO_2 have stepwise improved making them increasingly useful to constrain emissions. Germany has been the subject of several studies, both for NH_3 and NO_2, using various methodologies (Dammers et al., 2022; Valks, 2022). These studies provide general confidence in the German inventories, but also hint at areas to improve.
- The interface for ICON-DE in LOTOS-EUROS was developed and tested, allowing to further refine and test the use of high-resolution meteorological data from the DWD.
- A flexible module to expand the number of vegetation types for which the dry deposition is calculated is under development. For example, arable land is one category, but in reality reflects a wide range of crops. Further, satellite observations are tested to better prescribe vegetation height, roughness length (z_0) and leaf area index (LAI) (van der Graaf et al., 2022).
- Model intercomparisons for deposition modelling are ongoing within AQMEII and CAMS. Feedback on LOTOS-EUROS results in comparison to other model systems may yield best practices to incorporate.
- Model evaluation of the DEPAC module to novel flux measurements in Germany and The Netherlands are ongoing.
- Incorporation of global boundary conditions from ECMWF-IFS (Inness et al., 2019; Remy & Bock, 2018) may largely solve the underestimation of sulphur wet deposition as found in all PINETI projects. The open question is in how far this sulphur is contributing to acid deposition. This relates to the release of HCl from sea salt, which we recommend to investigate.

6 List of references

Banzhaf, S., Schaap, M., Kerschbaumer, A., Reimer, E., Stern, R., van der Swaluw, E., & Builtjes, P. (2012). Implementation and evaluation of pH-dependent cloud chemistry and wet deposition in the chemical transport model REM-Calgrid. *Atmospheric Environment*, *49*, 378–390. https://doi.org/10.1016/j.atmosenv.2011.10.069

Banzhaf, S., Schaap, M., Kranenburg, R., Manders, A. M. M., Segers, A. J., Visschedijk, A. J. H., Denier van der Gon, H. a. C., Kuenen, J. J. P., van Meijgaard, E., van Ulft, L. H., Cofala, J., & Builtjes, P. J. H. (2015). Dynamic model evaluation for secondary inorganic aerosol and its precursors over Europe between 1990 and 2009. *Geoscientific Model Development*, *8*(4), Article 4. https://doi.org/10.5194/gmd-8-1047-2015

Beltman, J. B., Hendriks, C., Tum, M., & Schaap, M. (2013). The impact of large scale biomass production on ozone air pollution in Europe. *Atmospheric Environment*, *71*, 352–363. Scopus. https://doi.org/10.1016/j.atmosenv.2013.02.019

Bender, J., Bergmann, E., Weigel, H.-J., Grünhage, L., Schröder, M., Builtjes, P. J. H., Schaap, M., Kranenburg, R., Wichink Kruit, R. J., Stern, R., Baumgarten, M., & Matyssek, R. (2015). Anwendung und Überprüfung neuer Methoden zur flächenhaften Bewertung der Auswirkung von bodennahem Ozon auf die Biodiversität terrestrischer Ökosysteme—Teil I. UBA-Texte 70/2015. *UBA-Texte*, *70/2015*, http://www.umweltbundesamt.de/publikationen/anwendung-ueberpruefung.

Bobbink, R., Hicks, K., Galloway, J., Spranger, T., Alkemade, R., Ashmore, M., Bustamante, M., Cinderby, S., Davidson, E., Dentener, F., Emmett, B., Erisman, J.-W., Fenn, M., Gilliam, F., Nordin, A., Pardo, L., & De Vries, W. (2010). Global assessment of nitrogen deposition effects on terrestrial plant diversity: A synthesis. *Ecological Applications*, *20*(1), 30–59. Scopus. https://doi.org/10.1890/08-1140.1

Bobbink, R., Loran, C., & Tomassen, H. (2022). *Review and revision of empirical critical loads of nitrogen for Europe* (110/2022). UBA. https://www.umweltbundesamt.de/sites/default/files/medien/1410/publikationen/2022-10-12_texte_110-2022_review_revision_empirical_critical_loads.pdf

Builtjes, P. J. H., Hendriks, E., Koenen, M., Schaap, M., Banzhaf, S., Kerschbaumer, A., Gauger, T., Nagel, H. D., Scheuschner, T., & Schlutow, A. (2011). *Erfassung, Prognose und Bewertung von Stoffeinträgen und ihren Wirkungen in Deutschland Zusammenfassender Abschlussbericht*. UBA, Dessau-Rosslau. https://www.umweltbundesamt.de/publikationen/erfassung-prognose-bewertung-von-stoffeintraegen

Curier, R. L., Kranenburg, R., Segers, A. J. S., Timmermans, R. M. A., & Schaap, M. (2014). Synergistic use of OMI NO2 tropospheric columns and LOTOS-EUROS to evaluate the NOx emission trends across Europe. *Remote Sensing of Environment*, *149*, 58–69. Scopus. https://doi.org/10.1016/j.rse.2014.03.032

Curier, R. L., Timmermans, R., Calabretta-Jongen, S., Eskes, H., Segers, A., Swart, D., & Schaap, M. (2012). Improving ozone forecasts over Europe by synergistic use of the LOTOS-EUROS chemical transport model and in-situ measurements. *Atmospheric Environment*, *60*, 217–226. Scopus. https://doi.org/10.1016/j.atmosenv.2012.06.017

Damgaard, C., Jensen, L., Frohn, L. M., Borchsenius, F., Nielsen, K. E., Ejrnæs, R., & Stevens, C. J. (2011). The effect of nitrogen deposition on the species richness of acid grasslands in Denmark: A comparison with a study performed on a European scale. *Environmental Pollution*, *159*(7), 1778–1782. Scopus. https://doi.org/10.1016/j.envpol.2011.04.003

Dammers, E., Shephard, M., Griffin, D., Chow, E., White, E., Hickman, J., Tokaya, J., Lutsch, E., Kharol, S., van der Graaf, S., Cady-Pereira, K., Bittman, S., Mclinden, C., Erisman, J. W., & Schaap, M. (2022). *County-level ammonia emissions monitored worldwide*. https://doi.org/10.21203/rs.3.rs-1752718/v1

Dise, N. B., Ashmore, M., Belyazid, S., Bleeker, A., Bobbink, R., de Vries, W., Erisman, J. W., Spranger, T., Stevens, C. J., & van den Berg, L. (2011). Nitrogen as a threat to European terrestrial biodiversity. In A. Bleeker, B. Grizzetti, C. M. Howard, G. Billen, H. van Grinsven, J. W. Erisman, M. A. Sutton, & P. Grennfelt (Eds.), *The European Nitrogen Assessment: Sources, Effects and Policy Perspectives* (pp. 463–494). Cambridge University Press; Cambridge Core. https://doi.org/10.1017/CBO9780511976988.023

Dore, C., Adams, M., & Saarinen, K. (2019). *ISSN 1977-8449EMEP/EEA air pollutant emission inventory guidebook 2019Technical guidance to prepare national emission inventories* (13/2019). https://www.eea.europa.eu/publications/emep-eea-guidebook-2019

Erisman, J. W., Galloway, J., Seitzinger, S., Bleeker, A., & Butterbach-Bahl, K. (2011). Reactive nitrogen in the environment and its effect on climate change. *Current Opinion in Environmental Sustainability*, *3*(5), 281–290. Scopus. https://doi.org/10.1016/j.cosust.2011.08.012

Erisman, J. W., Möls, H., Fonteijn, P., Geusebroek, M., Draaijers, G., Bleeker, A., & Van Der Veen, D. (2003). Field intercomparison of precipitation measurements performed within the framework of the Pan European Intensive Monitoring Program of EU/ICP Forest. *Environmental Pollution*, *125*(2), 139–155. Scopus. https://doi.org/10.1016/S0269-7491(03)00082-4

Erisman, J. W., & Schaap, M. (2004). The need for ammonia abatement with respect to secondary PM reductions in Europe. *Environmental Pollution*, *129*(1), Article 1. https://doi.org/10.1016/j.envpol.2003.08.042

Escudero, M., Segers, A., Kranenburg, R., Querol, X., Alastuey, A., Borge, R., De La Paz, D., Gangoiti, G., & Schaap, M. (2019). Analysis of summer O3 in the Madrid air basin with the LOTOS-EUROS chemical transport model. *Atmospheric Chemistry and Physics*, *19*(22), 14211–14232. Scopus. https://doi.org/10.5194/acp-19-14211-2019

Fountoukis, C., & Nenes, A. (2007). ISORROPIA II: A computationally efficient thermodynamic equilibrium model for K^+ - Ca^{2+} - Mg^{2+} - NH_4^+ - Na^+ - SO_4^{2-} - NO_3^- - Cl^- - H_2O aerosols. *Atmospheric Chemistry and Physics*, *7*(17), Article 17. https://doi.org/10.5194/acp-7-4639-2007

Fowler, D., Coyle, M., Skiba, U., Sutton, M. A., Cape, J. N., Reis, S., Sheppard, L. J., Jenkins, A., Grizzetti, B., Galloway, J. N., Vitousek, P., Leach, A., Bouwman, A. F., Butterbach-Bahl, K., Dentener, F., Stevenson, D., Amann, M., & Voss, M. (2013). The global nitrogen cycle in the Twentyfirst century. *Philosophical Transactions of the Royal Society B: Biological Sciences*, *368*(1621). Scopus. https://doi.org/10.1098/rstb.2013.0164

Fowler, D., Sutton, M. A., Flechard, C., Cape, J. N., Storeton-West, R., Coyle, M., & Smith, R. I. (2001). The Control of SO2 Dry Deposition on to Natural Surfaces by NH3 and its Effects on Regional Deposition. *Water, Air and Soil Pollution: Focus*, *1*(5), Article 5. https://doi.org/10.1023/A:1013161912231

Galloway, J. N., Aber, J. D., Erisman, J. W., Seitzinger, S. P., Howarth, R. W., Cowling, E. B., & Cosby, B. J. (2003). The nitrogen cascade. *BioScience*, *53*(4), 341–356. Scopus. https://doi.org/10.1641/0006-3568(2003)053[0341:TNC]2.0.CO;2

Gauger, T., Haenel, H. D., Rosemann, C., Dammgen, U., Bleeker, A., Erisman, J. W., Vermeulen, A. T., Schaap, M., Timmermans, R. M. A., Builtjes, P. J. H., & Duyzer, J. H. (2008). *National Implementation of the UNECE Convention on Long-range Transboundary Air Pollution (Effects) Part 1: Deposition Loads: Methods, modelling and mapping results, trends*. UBA, Dessau-Rosslau. https://www.umweltbundesamt.de/en/publikationen/national-implementation-of-unece-convention-on-long

Ge, X., Schaap, M., Dammers, E., Shephard, M., & de Vries, W. (2023). Impact of interannual weather variation on ammonia emissions and concentrations in Germany. *Agricultural and Forest Meteorology*, *334*, 109432. https://doi.org/10.1016/j.agrformet.2023.109432

Ge, X., Schaap, M., & de Vries, W. (2023). Improving spatial and temporal variation of ammonia emissions for the Netherlands using livestock housing information and a Sentinel-2-derived crop map. *Atmospheric Environment: X*, *17*. Scopus. https://doi.org/10.1016/j.aeaoa.2023.100207

Ge, X., Schaap, M., Kranenburg, R., Segers, A., Jan Reinds, G., Kros, H., & De Vries, W. (2020). Modeling atmospheric ammonia using agricultural emissions with improved spatial variability and temporal dynamics. *Atmospheric Chemistry and Physics*, *20*(24), 16055–16087. Scopus. https://doi.org/10.5194/acp-20-16055-2020

Gery, M. W., Whitten, G. Z., & Killus, J. P. (1988). *Development and testing of the CBM-IV (Carbon-Bond Mechanism) for urban and regional modeling. Final report, July 1985-June 1987* (PB-88-180039/XAB; Issue PB-88-180039/XAB). Systems Applications, Inc., San Rafael, CA (USA). https://www.osti.gov/biblio/5212670

Geupel, M., Heldstab, J., Schäppi, B., Reutimann, J., Bach, M., Häussermann, U., Knoll, L., Klement, L., & Breuer, L. (2021). A National Nitrogen Target for Germany. *Sustainability*, *13*, 1121. https://doi.org/10.3390/su13031121

Geupel, M., Loran, C., Scheuschner, T., & Wohlgemuth, L. (2022). *CCE Status Report 2022 Coordination Centre for Effects (CCE)* (135/2022). UBA. https://www.umweltbundesamt.de/en/publikationen/cce-status-report-2022

Grubbs, F. E. (1969). Procedures for Detecting Outlying Observations in Samples. *Technometrics*, *11*(1), 1–21. Scopus. https://doi.org/10.1080/00401706.1969.10490657

Häußermann, U., Bach, M., Fuchs, S., Geupel, M., Heldstab, J., Klement, L., Knoll, L., Reutimann, J., Schäppi, B., Weber, T., & Breuer, L. (2021). National nitrogen budget for Germany. *Environmental Research Communications*, *3*(9), 095004. https://doi.org/10.1088/2515-7620/ac23e5

Hendriks, C., Kranenburg, R., Kuenen, J. J. P., Van den Bril, B., Verguts, V., & Schaap, M. (2016). Ammonia emission time profiles based on manure transport data improve ammonia modelling across north western Europe. *Atmospheric Environment*, *131*, 83–96. Scopus. https://doi.org/10.1016/j.atmosenv.2016.01.043

Hendriks, C., Kranenburg, R., Kuenen, J., van Gijlswijk, R., Wichink Kruit, R., Segers, A., Denier van der Gon, H., & Schaap, M. (2013). The origin of ambient particulate matter concentrations in the Netherlands. *Atmospheric Environment*, *69*, 289–303. Scopus. https://doi.org/10.1016/j.atmosenv.2012.12.017

Hettelingh, J.-P., Posch, M., De Smet, P. A. M., & Downing, R. J. (1995). The use of critical loads in emission reduction agreements in Europe. *Water, Air, & Soil Pollution*, *85*(4), 2381–2388. Scopus. https://doi.org/10.1007/BF01186190

Inness, A., Ades, M., Agustí-Panareda, A., Barré, J., Benedictow, A., Blechschmidt, A.-M., Dominguez, J. J., Engelen, R., Eskes, H., Flemming, J., Huijnen, V., Jones, L., Kipling, Z., Massart, S., Parrington, M., Peuch, V.-H., Razinger, M., Remy, S., Schulz, M., & Suttie, M. (2019). The CAMS reanalysis of atmospheric composition. *Atmospheric Chemistry and Physics*, *19*(6), 3515–3556. https://doi.org/10.5194/acp-19-3515-2019

Katata, G., Kajino, M., Hiraki, T., Aikawa, M., Kobayashi, T., & Nagai, H. (2011). A method for simple and accurate estimation of fog deposition in a mountain forest using a meteorological model. *Journal of Geophysical Research Atmospheres*, *116*(20). Scopus. https://doi.org/10.1029/2010JD015552

Katata, G., Nagai, H., Wrzesinsky, T., Klemm, O., Eugster, W., & Burkard, R. (2008). Development of a land surface model including cloud water deposition on vegetation. *Journal of Applied Meteorology and Climatology*, *47*(8), 2129–2146. Scopus. https://doi.org/10.1175/2008JAMC1758.1

Klemm, O., & Wrzesinsky, T. (2007). Fog deposition fluxes of water and ions to a mountainous site in Central Europe. *Tellus, Series B: Chemical and Physical Meteorology*, *59*(4), 705–714. Scopus. https://doi.org/10.1111/j.1600-0889.2007.00287.x

Kranenburg, R., Segers, A. J., Hendriks, C., & Schaap, M. (2013). Source apportionment using LOTOS-EUROS: Module description and evaluation. *Geoscientific Model Development*, *6*(3), Article 3. https://doi.org/10.5194/gmd-6-721-2013

Manders, A. M. M., Builtjes, P. J. H., Curier, L., Denier van der Gon, H. A. C., Hendriks, C., Jonkers, S., Kranenburg, R., Kuenen, J. J. P., Segers, A. J., Timmermans, R. M. A., Visschedijk, A. J. H., Wichink Kruit, R. J., van Pul, W. A. J., Sauter, F. J., van der Swaluw, E., Swart, D. P. J., Douros, J., Eskes, H., van Meijgaard, E., … Schaap, M. (2017). Curriculum vitae of the LOTOS–EUROS (v2.0) chemistry transport model. *Geoscientific Model Development*, *10*(11), Article 11. https://doi.org/10.5194/gmd-10-4145-2017

Manders, A. M. M., Schaap, M., & Hoogerbrugge, R. (2009). Testing the capability of the chemistry transport model LOTOS-EUROS to forecast PM10 levels in the Netherlands. *Atmospheric Environment*, *43*(26), 4050–4059. Scopus. https://doi.org/10.1016/j.atmosenv.2009.05.006

Manders, A. M. M., Schaap, M., Querol, X., Albert, M. F. M. A., Vercauteren, J., Kuhlbusch, T. A. J., & Hoogerbrugge, R. (2010). Sea salt concentrations across the European continent. *Atmospheric Environment*, *44*(20), 2434–2442. Scopus. https://doi.org/10.1016/j.atmosenv.2010.03.028

Massad, R. S., Loubet, B., Tuzet, A., & Cellier, P. (2008). Relationship between ammonia stomatal compensation point and nitrogen metabolism in arable crops: Current status of knowledge and potential modelling approaches. *Environmental Pollution*, *154*(3), Article 3. https://doi.org/10.1016/j.envpol.2008.01.022

Meng, C., Tian, D., Zeng, H., Li, Z., Yi, C., & Niu, S. (2019). Global soil acidification impacts on belowground processes. *Environmental Research Letters*, *14*(7), 074003. https://doi.org/10.1088/1748-9326/ab239c

Mills, G. E., & Harmens, H. (2011). *Ozone pollution: A hidden threat to food security*.

Mues, A., Kuenen, J., Hendriks, C., Manders, A., Segers, A., Scholz, Y., Hueglin, C., Builtjes, P., & Schaap, M. (2014). Sensitivity of air pollution simulations with LOTOS-EUROS to the temporal distribution of anthropogenic emissions. *Atmospheric Chemistry and Physics*, *14*(2), Article 2. https://doi.org/10.5194/acp-14-939-2014

Nemitz, E., Sutton, M. A., Schjoerring, J. K., Husted, S., & Paul Wyers, G. (2000). *Resistance modelling of ammonia exchange over oilseed rape*. *105*(4), 405–425. Scopus. https://doi.org/10.1016/S0168-1923(00)00206-9

Nilsson, J. (1988). Critical Loads for Sulphur and Nitrogen. In P. Mathy (Ed.), *Air Pollution and Ecosystems* (pp. 85–91). Springer Netherlands.

Nilsson, J., & Grennfelt, P. (1988). Critical Loads for Sulphur and Nitrogen. In P. Mathy (Ed.), *Air Pollution and Ecosystems* (pp. 85–91). Springer Netherlands.

Rauthe, M., Steiner, H., Riediger, U., Mazurkiewicz, A., & Gratzki, A. (2013). A Central European precipitation climatology—Part I: Generation and validation of a high-resolution gridded daily data set (HYRAS). *Meteorologische Zeitschrift*, *22*(3), 235–256. Scopus. https://doi.org/10.1127/0941-2948/2013/0436

Remy, S., & Bock, J. (2018). *Improvement of the SO2 to SO4 conversion processes in IFS-AER and IFS-GLOMAP* (Deliverable report for D43.1.1.1). https://atmosphere.copernicus.eu/sites/default/files/publications/CAMS43_20217SC2_D43.1.1.1_201710_Sulphate.pdf

Rockström, J., Steffen, W., Noone, K., Persson, A., Chapin III, F. S., Lambin, E., Lenton, T. M., Scheffer, M., Folke, C., Schellnhuber, H. J., Nykvist, B., de Wit, C. A., Hughes, T., van der Leeuw, S., Rodhe, H., Sörlin, S., Snyder, P. K., Costanza, R., Svedin, U., … Foley, J. (2009). Planetary boundaries: Exploring the safe operating space for humanity. *Ecology and Society*, *14*(2). Scopus. https://doi.org/10.5751/ES-03180-140232

Salomon, M., Schmid, E., Volkens, A., Hey, C., Holm-Müller, K., & Foth, H. (2016). Towards an integrated nitrogen strategy for Germany. *Environmental Science and Policy*, *55*, 158–166. Scopus. https://doi.org/10.1016/j.envsci.2015.10.003

Schaap, M., Cuvelier, C., Hendriks, C., Bessagnet, B., Baldasano, J. M., Colette, A., Thunis, P., Karam, D., Fagerli, H., Graff, A., Kranenburg, R., Nyiri, A., Pay, M. T., Rouïl, L., Schulz, M., Simpson, D., Stern, R., Terrenoire, E., & Wind, P. (2015). Performance of European chemistry transport models as function of horizontal resolution. *Atmospheric Environment*, *112*, 90–105. Scopus. https://doi.org/10.1016/j.atmosenv.2015.04.003

Schaap, M., Hendriks, C., Kranenburg, R., Kuenen, J. J. P., Segers, A. J., Schlutow, A., Nagel, H. D., Ritter, A., & Banzhaf, S. (2018). *PINETI-3: Modellierung atmosphärischer Stoffeinträge von 2000 bis 2015 Zur Bewertung der ökosystem-spezifischen Gefährdung von Biodiversität durch Luftschadstoffe in Deutschland.* Texte | 79/2018, p. 149, Umweltbundesamt, Dessau-Rosslau. https://doi.org/10.60810/OPENUMWELT-5590

Schaap, M., Kranenburg, R., Curier, L., Jozwicka, M., Dammers, E., & Timmermans, R. (2013). Assessing the sensitivity of the OMI-NO2 product to emission changes across europe. *Remote Sensing*, *5*(9), 4187–4208. Scopus. https://doi.org/10.3390/rs5094187

Schaap, M., Otjes, R. P., & Weijers, E. P. (2011). Illustrating the benefit of using hourly monitoring data on secondary inorganic aerosol and its precursors for model evaluation. *Atmospheric Chemistry and Physics*, *11*(21), 11041–11053. Scopus. https://doi.org/10.5194/acp-11-11041-2011

Schaap, M., van Loon, M., ten Brink, H. M., Dentener, F. J., & Builtjes, P. J. H. (2004). Secondary inorganic aerosol simulations for Europe with special attention to nitrate. *Atmospheric Chemistry and Physics*, *4*(3), Article 3. https://doi.org/10.5194/acp-4-857-2004

Schaap, M., Wichink Kruit, R. J., Hendriks, C., Kranenburg, R., Segers, A. J., Builtjes, P., & Banzhaf, S. (2017). *Modelling and assessment of acidifying and eutrophying atmospheric deposition to terrestrial ecosystems* (FKZ 3712 63 240 1). Texte | 62/2017, p. 98, Umweltbundesamt, Dessau-Rosslau. https://doi.org/10.60810/OPENUMWELT-5590

Schlutow, A., & Huebener, P. (2004). *The Bern Model: Bioindication for Ecosystem Regeneration towards Natural conditions* (Research Report 200 85 221). Texte | 22/2004, p. 56, Umweltbundesamt, Dessau-Rosslau.

Skjøth, C. A., Geels, C., Berge, H., Gyldenkaerne, S., Fagerli, H., Ellermann, T., Frohn, L. M., Christensen, J., Hansen, K. M., Hansen, K., & Hertel, O. (2011). Spatial and temporal variations in ammonia emissions ĝ€" a freely accessible model code for Europe. *Atmospheric Chemistry and Physics*, *11*(11), 5221–5236. Scopus. https://doi.org/10.5194/acp-11-5221-2011

Steffen, W., Richardson, K., Rockström, J., Cornell, S. E., Fetzer, I., Bennett, E. M., Biggs, R., Carpenter, S. R., de Vries, W., de Wit, C. A., Folke, C., Gerten, D., Heinke, J., Mace, G. M., Persson, L. M., Ramanathan, V., Reyers, B., & Sörlin, S. (2015). Planetary boundaries: Guiding human development on a changing planet. *Science*, *347*(6223), 1259855. https://doi.org/10.1126/science.1259855

Ströher, H., Roth, K., Erdmann, K.-H., Schell, C., & Engels, B. (2016). *Daten zur Natur 2016*. Bundesamt für Naturschutz (BfN). https://www.bfn.de/sites/default/files/2021-09/Daten_zur_Natur_2016_BfN%20%282%29.pdf

Sutton, M., Howard, C., & Erisman, J. W. (2011). *The European Nitrogen Assessment: Sources, Effects and Policy Perspectives*. https://doi.org/10.1017/CBO9780511976988

Thürkow, M., Banzhaf, S., Butler, T., Pültz, J., & Schaap, M. (2023). Source attribution of nitrogen oxides across Germany: Comparing the labelling approach and brute force technique with LOTOS-EUROS. *Atmospheric Environment*, *292*. Scopus. https://doi.org/10.1016/j.atmosenv.2022.119412

Thürkow, M., Kirchner, I., Kranenburg, R., Timmermans, R. M. A., & Schaap, M. (2021). A multi-meteorological comparison for episodes of PM10 concentrations in the Berlin agglomeration area in Germany with the LOTOS-EUROS CTM. *Atmospheric Environment*, *244*. Scopus. https://doi.org/10.1016/j.atmosenv.2020.117946

Timmermans, R., van Pinxteren, D., Kranenburg, R., Hendriks, C., Fomba, K. W., Herrmann, H., & Schaap, M. (2022). Evaluation of modelled LOTOS-EUROS with observational based PM10 source attribution. *Atmospheric Environment: X*, *14*, 100173. https://doi.org/10.1016/j.aeaoa.2022.100173

Valks, P. (2022, February 16). *Sentinel-basierte Atmosphärenprodukte zur Bewertung des Einflusses von Verkehrsemissionen auf die Luftqualität in Deutschland (S-VELD)*. https://atmos.eoc.dlr.de/sveld/doc/S-VELD_Abschlussveranstaltung_20220216.pdf

Van Damme, M., Wichink Kruit, R. J., Schaap, M., Clarisse, L., Clerbaux, C., Coheur, P.-F., Dammers, E., Dolman, A. J., & Erisman, J. W. (2014). Evaluating 4 years of atmospheric ammonia (NH3) over Europe using IASI satellite observations and LOTOS-EUROS model results. *Journal of Geophysical Research*, *119*(15), 9549–9566. Scopus. https://doi.org/10.1002/2014JD021911

van der Graaf, S., Dammers, E., Segers, A., Kranenburg, R., Schaap, M., Shephard, M. W., & Erisman, J. W. (2022). Data assimilation of CrIS NH3 satellite observations for improving spatiotemporal NH3 distributions in LOTOS-EUROS. *Atmos. Chem. Phys.*, *22*(2), 951–972. https://doi.org/10.5194/acp-22-951-2022

Van Zanten, M. C., Wichink Kruit, R. J., van Jaarsveld, H. A., & van Pul, W. A. J. (2010). *Description of the DEPAC module: Dry deposition modelling with DEPAC_GCN2010* [Report]. Rijksinstituut voor Volksgezondheid en Milieu RIVM. https://rivm.openrepository.com/handle/10029/256555

Wichink Kruit, R. J., Schaap, M., Sauter, F. J., van Zanten, M. C., & van Pul, W. a. J. (2012). Modeling the distribution of ammonia across Europe including bi-directional surface–atmosphere exchange. *Biogeosciences*, *9*(12), Article 12. https://doi.org/10.5194/bg-9-5261-2012

Wichink Kruit, R. J., Schaap, M., Segers, A. J., Heslinga, D., Builtjes, P. J. H., Banzhaf, S., & Scheuschner, T. (2014). *Modelling and mapping of atmospheric nitrogen and sulphur deposition and critical loads for ecosystem specific assessment of threats to biodiversity in Germany – PINETI (Pollutant INput and EcosysTem Impact)*. UBA, Dessau-Rosslau. https://www.umweltbundesamt.de/en/publikationen/modelling-mapping-of-atmospheric-nitrogen-sulphur

Wintjen, P., Schrader, F., Schaap, M., Beudert, B., Kranenburg, R., & Brümmer, C. (2022). Forest-atmosphere exchange of reactive nitrogen in a remote region—Part II: Modeling annual budgets. *Biogeosciences*, *19*(22), 5287–5311. Scopus. https://doi.org/10.5194/bg-19-5287-2022

A Source receptor matrices for nitrogen deposition

A.1 Source receptor matrix of dry nitrogen deposition.

Table 26: Contributions to dry nitrogen deposition [kg N ha^{-1} yr^{-1}] for each state (Bundesland) (source areas in rows, receiving states in columns).

	BB	BE	BW	BY	HB	HE	HH	MV
DE-BB	**2.1**	**1.9**	0.0	0.0	0.0	0.0	0.1	0.3
DE-BE	0.1	**2.1**	0.0	0.0	0.0	0.0	0.0	0.0
DE-BW	0.1	0.1	**3.6**	0.5	0.0	0.2	0.0	0.0
DE-BY	0.1	0.1	0.7	**4.2**	0.0	0.3	0.0	0.1
DE-HB	0.0	0.0	0.0	0.0	**3.4**	0.0	0.1	0.0
DE-HE	0.1	0.1	0.1	0.1	0.1	**2.6**	0.1	0.0
DE-HH	0.0	0.0	0.0	0.0	0.1	0.0	**5.7**	0.1
DE-MV	0.1	0.1	0.0	0.0	0.1	0.0	0.2	**1.8**
DE-NI	0.5	0.6	0.0	0.1	**11.0**	0.2	5.5	0.7
DE-NW	0.3	0.3	0.1	0.1	0.7	0.6	0.5	0.2
DE-RP	0.0	0.0	0.1	0.1	0.0	0.4	0.0	0.0
DE-SL	0.0	0.0	0.0	0.0	0.0	0.0	0.0	0.0
DE-SH	0.1	0.2	0.0	0.0	0.2	0.0	**1.7**	0.6
DE-SN	0.2	0.1	0.0	0.0	0.0	0.0	0.0	0.0
DE-ST	0.5	0.4	0.0	0.0	0.1	0.0	0.1	0.1
DE-TH	0.1	0.1	0.0	0.1	0.0	0.1	0.0	0.0
NLD	0.2	0.3	0.1	0.1	**1.0**	0.2	0.6	0.3
BEL	0.1	0.1	0.1	0.0	0.2	0.1	0.2	0.1
LUX	0.0	0.0	0.0	0.0	0.0	0.0	0.0	0.0
FRA	0.2	0.3	0.7	0.3	0.4	0.6	0.3	0.2
CHE	0.0	0.0	0.4	0.2	0.0	0.1	0.0	0.0
AUT	0.1	0.1	0.1	0.3	0.0	0.1	0.0	0.0
CZE	0.1	0.1	0.1	0.1	0.0	0.1	0.1	0.1
POL	0.5	0.5	0.1	0.1	0.1	0.1	0.2	0.3
DNK	0.1	0.1	0.0	0.0	0.0	0.0	0.1	0.1
W-EUR	0.2	0.2	0.1	0.1	0.4	0.2	0.4	0.2
S-EUR	0.1	0.1	0.2	0.1	0.0	0.1	0.0	0.0
E-EUR	0.1	0.2	0.0	0.1	0.1	0.1	0.1	0.1
N-EUR	0.0	0.0	0.0	0.0	0.0	0.0	0.0	0.0
Int-Ship	0.2	0.2	0.1	0.1	0.4	0.1	0.5	0.3

	BB	BE	BW	BY	HB	HE	HH	MV
Nat	0.2	0.2	0.2	0.2	0.2	0.2	0.2	0.2
BC	0.1	0.2	0.2	0.1	0.1	0.1	0.1	0.1
Total	**6.6**	**8.7**	**6.8**	**6.8**	**18.9**	**6.6**	**16.9**	**6.2**

Table 27: Table 26 - continued

	NI	NW	RP	SL	SH	SN	ST	TH
DE-BB	0.1	0.0	0.0	0.0	0.0	0.1	0.2	0.0
DE-BE	0.0	0.0	0.0	0.0	0.0	0.0	0.0	0.0
DE-BW	0.0	0.1	0.2	0.2	0.0	0.1	0.1	0.1
DE-BY	0.1	0.1	0.2	0.2	0.0	0.3	0.1	0.4
DE-HB	0.1	0.0	0.0	0.0	0.0	0.0	0.0	0.0
DE-HE	0.1	0.2	0.2	0.1	0.0	0.1	0.1	0.3
DE-HH	0.1	0.0	0.0	0.0	0.3	0.0	0.0	0.0
DE-MV	0.1	0.0	0.0	0.0	0.2	0.0	0.0	0.0
DE-NI	**6.7**	0.6	0.1	0.1	**1.2**	0.2	0.8	0.3
DE-NW	**1.0**	**6.0**	0.4	0.2	0.2	0.2	0.4	0.3
DE-RP	0.0	0.2	**2.0**	0.4	0.0	0.0	0.1	0.1
DE-SL	0.0	0.0	0.1	**1.6**	0.0	0.0	0.0	0.0
DE-SH	0.1	0.0	0.0	0.0	**5.9**	0.0	0.1	0.0
DE-SN	0.0	0.0	0.0	0.0	0.0	**1.6**	0.1	0.1
DE-ST	0.1	0.0	0.0	0.0	0.0	0.3	**2.5**	0.2
DE-TH	0.0	0.0	0.0	0.0	0.0	0.3	0.3	**1.9**
NLD	0.9	**1.2**	0.2	0.1	0.4	0.1	0.2	0.2
BEL	0.2	0.5	0.3	0.2	0.1	0.1	0.1	0.1
LUX	0.0	0.0	0.2	0.1	0.0	0.0	0.0	0.0
FRA	0.3	0.6	**1.1**	**2.0**	0.2	0.2	0.3	0.3
CHE	0.0	0.0	0.1	0.1	0.0	0.0	0.0	0.0
AUT	0.0	0.0	0.0	0.0	0.0	0.1	0.0	0.1
CZE	0.0	0.1	0.1	0.0	0.0	0.5	0.1	0.1
POL	0.1	0.1	0.1	0.1	0.1	0.3	0.2	0.1
DNK	0.0	0.0	0.0	0.0	0.2	0.0	0.0	0.0
W-EUR	0.3	0.3	0.2	0.2	0.4	0.1	0.2	0.1
S-EUR	0.0	0.1	0.1	0.1	0.0	0.1	0.1	0.1
E-EUR	0.1	0.0	0.0	0.0	0.1	0.2	0.1	0.1
N-EUR	0.0	0.0	0.0	0.0	0.0	0.0	0.0	0.0
Int-Ship	0.3	0.2	0.1	0.1	0.7	0.1	0.2	0.1

	NI	NW	RP	SL	SH	SN	ST	TH
Nat	0.2	0.2	0.2	0.2	0.1	0.2	0.2	0.2
BC	0.1	0.1	0.2	0.2	0.1	0.2	0.1	0.1
Total	**11.3**	**10.8**	**6.2**	**6.3**	**10.6**	**5.4**	**6.7**	**5.4**

A.2 Source receptor matrix for wet nitrogen deposition

Table 28: Contributions to wet nitrogen deposition [kg N ha^{-1} yr^{-1}] for each state (Bundesland) (source areas in rows, receiving states in columns).

	BB	BE	BW	BY	HB	HE	HH	MV
DE-BB	0.3	0.2	0.0	0.0	0.0	0.0	0.0	0.1
DE-BE	0.0	0.1	0.0	0.0	0.0	0.0	0.0	0.0
DE-BW	0.1	0.0	**1.1**	0.6	0.1	0.2	0.0	0.0
DE-BY	0.1	0.1	0.5	**1.7**	0.1	0.2	0.1	0.1
DE-HB	0.0	0.0	0.0	0.0	0.3	0.0	0.0	0.0
DE-HE	0.1	0.1	0.1	0.1	0.1	0.4	0.1	0.1
DE-HH	0.0	0.0	0.0	0.0	0.0	0.0	0.5	0.0
DE-MV	0.0	0.0	0.0	0.0	0.0	0.0	0.1	0.3
DE-NI	0.4	0.3	0.1	0.1	**3.1**	0.1	**2.0**	0.6
DE-NW	0.2	0.2	0.2	0.2	0.6	0.3	0.4	0.3
DE-RP	0.0	0.0	0.1	0.1	0.0	0.2	0.0	0.0
DE-SL	0.0	0.0	0.0	0.0	0.0	0.0	0.0	0.0
DE-SH	0.1	0.1	0.0	0.0	0.1	0.0	0.4	0.2
DE-SN	0.1	0.0	0.0	0.0	0.0	0.0	0.0	0.0
DE-ST	0.2	0.2	0.0	0.0	0.0	0.0	0.1	0.1
DE-TH	0.1	0.0	0.0	0.0	0.0	0.0	0.0	0.0
NLD	0.2	0.2	0.1	0.1	0.7	0.2	0.5	0.3
BEL	0.1	0.1	0.2	0.1	0.2	0.2	0.2	0.1
LUX	0.0	0.0	0.0	0.0	0.0	0.0	0.0	0.0
FRA	0.3	0.3	**1.3**	0.8	0.6	0.8	0.5	0.3
CHE	0.0	0.0	0.3	0.3	0.0	0.1	0.0	0.0
AUT	0.1	0.1	0.1	0.2	0.0	0.1	0.0	0.1
CZE	0.1	0.1	0.1	0.1	0.1	0.1	0.1	0.1
POL	0.2	0.2	0.2	0.1	0.1	0.1	0.2	0.2
DNK	0.0	0.0	0.0	0.0	0.0	0.0	0.1	0.1
W-EUR	0.2	0.2	0.2	0.2	0.5	0.3	0.5	0.3
S-EUR	0.1	0.1	0.4	0.4	0.1	0.2	0.1	0.1

	BB	BE	BW	BY	HB	HE	HH	MV
E-EUR	0.2	0.2	0.1	0.2	0.1	0.1	0.2	0.2
N-EUR	0.0	0.0	0.0	0.0	0.0	0.0	0.0	0.0
Int-Ship	0.2	0.2	0.2	0.2	0.3	0.2	0.3	0.3
Nat	0.1	0.1	0.1	0.1	0.1	0.1	0.1	0.1
BC	0.2	0.2	0.4	0.4	0.2	0.3	0.3	0.2
Total	**3.6**	**3.3**	**6.0**	**6.3**	**7.6**	**4.4**	**6.7**	**4.2**

Table 29: Table 28 - continued

	NI	NW	RP	SL	SH	SN	ST	TH
DE-BB	0.0	0.0	0.0	0.0	0.0	0.1	0.1	0.0
DE-BE	0.0	0.0	0.0	0.0	0.0	0.0	0.0	0.0
DE-BW	0.1	0.1	0.1	0.1	0.1	0.1	0.1	0.1
DE-BY	0.1	0.1	0.2	0.1	0.1	0.3	0.2	0.4
DE-HB	0.0	0.0	0.0	0.0	0.0	0.0	0.0	0.0
DE-HE	0.1	0.1	0.1	0.0	0.0	0.1	0.1	0.3
DE-HH	0.0	0.0	0.0	0.0	0.1	0.0	0.0	0.0
DE-MV	0.0	0.0	0.0	0.0	0.1	0.0	0.0	0.0
DE-NI	**1.9**	0.3	0.0	0.0	**1.2**	0.4	0.4	0.2
DE-NW	0.7	**1.4**	0.2	0.1	0.4	0.3	0.3	0.3
DE-RP	0.0	0.1	0.3	0.1	0.0	0.1	0.0	0.1
DE-SL	0.0	0.0	0.0	0.1	0.0	0.0	0.0	0.0
DE-SH	0.1	0.0	0.0	0.0	**1.2**	0.1	0.0	0.0
DE-SN	0.0	0.0	0.0	0.0	0.0	0.3	0.0	0.1
DE-ST	0.0	0.0	0.0	0.0	0.1	0.2	0.3	0.1
DE-TH	0.0	0.0	0.0	0.0	0.0	0.2	0.1	0.3
NLD	0.8	0.9	0.1	0.1	0.6	0.2	0.2	0.2
BEL	0.2	0.5	0.2	0.1	0.2	0.1	0.1	0.1
LUX	0.0	0.0	0.1	0.0	0.0	0.0	0.0	0.0
FRA	0.6	0.9	**1.3**	**2.2**	0.5	0.4	0.3	0.5
CHE	0.0	0.1	0.1	0.1	0.0	0.0	0.0	0.1
AUT	0.0	0.0	0.0	0.0	0.1	0.1	0.1	0.1
CZE	0.1	0.0	0.1	0.0	0.1	0.2	0.1	0.1
POL	0.1	0.1	0.1	0.1	0.2	0.2	0.1	0.1
DNK	0.0	0.0	0.0	0.0	0.1	0.1	0.0	0.0
W-EUR	0.5	0.6	0.2	0.2	0.6	0.2	0.2	0.2
S-EUR	0.2	0.2	0.2	0.3	0.2	0.1	0.1	0.2

	NI	NW	RP	SL	SH	SN	ST	TH
E-EUR	0.1	0.1	0.1	0.1	0.1	0.2	0.1	0.1
N-EUR	0.0	0.0	0.0	0.0	0.0	0.0	0.0	0.0
Int-Ship	0.3	0.3	0.2	0.2	0.4	0.2	0.2	0.2
Nat	0.1	0.1	0.1	0.1	0.1	0.1	0.1	0.1
BC	0.3	0.3	0.3	0.3	0.3	0.2	0.2	0.2
Total	**6.6**	**6.3**	**4.1**	**4.6**	**6.8**	**4.6**	**3.8**	**4.3**